CHARACTERIZATION OF INHERITED IRAK-4 DEFICIENCY IN A PATIENT WITH ACUTE HHV-6 ENCEPHALITIS

A THESIS SUBMITTED TO
THE GRADUATE SCHOOL OF ENGINEERING AND SCIENCE
OF BILKENT UNIVERSITY
IN PARTIAL FULFILLMENT OF THE REQUIREMENTS FOR
THE DEGREE OF
MASTER OF SCIENCE
IN
MOLECULAR BIOLOGY AND GENETICS

By

Zeynep Güneş Tepe Demir

July 2023

To my family,

for always loving and supporting me

CHARACTERIZATION OF INHERITED IRAK-4 DEFICIENCY IN A PATIENT WITH ACUTE HHV-6 ENCEPHALITIS

By Zeynep Güneş Tepe Demir

July 2023

We certify that we have read this thesis and that in our opinion it is fully adequate, in scope and in quality, as a thesis for the degree of Master of Science.

Serkan Belkaya (Advisor)

Ilyas Chachoua

Emel Timuçin

Approved for the Graduate School of Engineering and Science:

Orhan Arıkan

Director of the Graduate School of Engineering and Science

ABSTRACT

CHARACTERIZATION OF INHERITED IRAK-4 DEFICIENCY IN A PATIENT WITH ACUTE HHV-6 ENCEPHALITIS

Zeynep Güneş Tepe Demir
M.Sc. in Molecular Biology and Genetics
Advisor: Serkan Belkaya
July 2023

Human herpesvirus-6 (HHV-6), a ubiquitous virus among humans, typically causes acute febrile illness in children, whereas the majority remain asymptomatic. HHV-6 infection can rarely cause encephalitis, with unknown pathogenesis. We hypothesized that inborn single-gene defects may underlie susceptibility to HHV-6 encephalitis in otherwise healthy children. We performed whole-exome sequencing on genomic DNA of a male child diagnosed with acute HHV-6 encephalitis and found a novel homozygous missense variation (NM_016123.4:c.G236A:p.C79Y) in Interleukin-1 receptor-associated kinase 4 (*IRAK4*), which is involved in the Toll-Interleukin-1 receptor signaling pathway. Sanger sequencing confirmed that both parents and the sibling were heterozygotes. The p.C79Y that affected an evolutionary conserved residue was predicted to be damaging by *in silico* algorithms. We found that IRAK-4 expression was severely reduced in patient's leukocytes. There were similar levels of wild-type (WT) and mutant IRAK-4 when transiently over-expressed in HEK293 cells, however mutant IRAK-4 expression was dramatically decreased upon cycloheximide treatment, compared to the WT. This indicated that the p.C79Y might impair IRAK-4 stability. We found that patient's leukocytes had diminished innate immune responses to various stimuli inducing different

Toll-like receptors and cytosolic nucleic acid sensors, compared to the healthy controls. We also generated *IRAK4* knockout HEK293 cells by CRISPR-Cas9 genome editing. Transient expression of mutant IRAK-4 had significantly reduced NFκB-dependent luciferase activity, compared to the WT in *IRAK4* knockout cells treated with IL-18. Collectively, the p.C79Y impaired both the expression and function of IRAK-4, leading to diminished immune responses against bacterial and viral stimuli in patient's leukocytes. Overall, this was the first study demonstrating that inborn errors of immunity could underlie isolated acute HHV-6 encephalitis. Our findings also widened the known genotypic and phenotypic spectrum of inherited IRAK-4 deficiency in humans.

Key words: Human genetics, IRAK-4, Immunodeficiency, HHV-6 infection, Encephalitis

ÖZET

AKUT HHV-6 ENSEFALİTİ GÖRÜLEN BİR HASTADA KALITSAL IRAK-4 EKSİKLİĞİNİN KARAKTERİZASYONU

Zeynep Güneş Tepe Demir
Moleküler Biyoloji ve Genetik, Yüksek Lisans
Tez danışmanı: Serkan Belkaya
Temmuz 2023

İnsanlar arasında sıkça karşılaşılan bir virüs olan İnsan herpesvirüs-6 (HHV-6), genel olarak çocuklarda akut ateşli hastalığa sebep olurken çocukların çoğunluğu asemptomatik kalmaktadır. HHV-6 enfeksiyonu nadiren ensefalite yol açabilmektedir, fakat patogenezi bilinmemektedir. Doğuştan gelen tek gen bozukluklarının aksi halde sağlıklı olan çocuklarda HHV-6 ensefalitine yatkınlığa neden olabileceği hipotezini ileri sürdük. Akut HHV-6 ensefalit teşhisi konan bir erkek çocuğun genomik DNA'sında tüm ekzom dizilemesi gerçekleştirdik ve hastada Toll/İnterlökin-1 reseptörü sinyal yolağında rolü olan İnterlökin-1 reseptör-ilişkili kinaz 4 (*IRAK4*) geninde daha önce görülmemiş yanlış anlamlı bir mutasyon (NM_016123.4:c.G236A:p.C79Y) bulduk. Hastanın ebeveynleri ve sağlıklı kardeşinde bu mutasyonun heterozigot olduğu Sanger sekanslaması ile doğrulandı. Evrimsel olarak korunan bir kalıntıyı etkileyen p.C79Y'nin *in siliko* algoritmalar tarafından hasar verici olacağı tahmin edildi. Hastanın lökositlerinde IRAK-4 ekspresyonunun ciddi şekilde azaldığını bulduk. HEK293 hücrelerinde yapılan geçici aşırı ekspresyon sonucunda yabanıl (WT) ve mutant IRAK-4 düzeyleri benzerdi ancak siklohekzimid muamelesinden sonra mutant IRAK-4 ekspresyonu WT'ya kıyasla ciddi şekilde azaldı. Bu durum, p.C79Y'nin IRAK-4 stabilitesini bozabileceğini

göstermektedir. Hastanın lökositlerindeki, sağlıklı kontrollere kıyasla farklı Toll-benzeri reseptörler ve sitozolik nükleik asit sensörlerini indükleyen çeşitli uyaranlara karşı doğuştan gelen immün cevaplarının azaldığını bulduk. Ayrıca, CRIPSR-Cas9 genom düzenleme ile *IRAK4* nakavt HEK293 hücre hatları oluşturduk. Mutant IRAK-4 proteininin IL-18 ile muamele edilmiş *IRAK4* nakavt hücrelerdeki geçici ekspresyonu sonucunda NFκB'ye bağlı lusiferaz aktivitesini WT'ya kıyasla anlamlı derecede azalttığını gördük. Sonuç olarak, p.C79Y IRAK-4'ün hem ifadesini hem de işlevini bozarak hastanın lökositlerinde bakteriyel ve viral uyaranlara karşı azalan immün yanıtlarına sebep oldu. Bu çalışma ilk kez izole akut HHV-6 ensefalitinin altında doğuştan gelen bağışıklık kusurlarının yatabileceğini göstermiştir. Bulgularımız ayrıca insanlarda kalıtsal IRAK-4 eksikliğinin bilinen genotipik ve fenotipik spektrumunu genişletmiştir.

Anahtar kelimeler: İnsan genetiği, IRAK-4, İmmün yetersizlik, HHV-6 enfeksiyonu, Ensefalit

ACKNOWLEDGMENTS

I would like to express my sincere gratitude to my supervisor, Dr. Serkan Belkaya, for his guidance throughout my Master's studies. His unwavering commitment to achieving excellence has pushed me to my limits and helped me improve my skills. I am truly fortunate to have the opportunity to work under his supervision. His in-depth knowledge, critical insights, and meticulous attention to detail have enriched my intellectuality during my graduate studies. Additionally, I would like to extend my appreciation to Dr. Serkan Belkaya for his continuous availability and willingness to provide support whenever I needed it. Without his constant support and invaluable guidance, this thesis would not have been possible.

I would like to express my appreciation to the esteemed committee members, Dr. İlyas Chachoua and Dr. Emel Timuçin, for their invaluable contributions and helpful feedback throughout this thesis. Additionally, I would like to thank Dr. Caner Aytekin for the patient recruitment and his feedback.

I am deeply grateful to my friends Alperen Baran, Servin Bagheralmoosavi and Beste Uygur for their constant emotional support. They have been my steadfast pillars, accompanying me through both the brightest and darkest times. Without their tremendous support, I could not have survived. They have created indelible memories that will forever be etched in my heart. I cannot imagine a greater friendship than they ever provided to me. Briefly, the depth of their friendship is beyond measure, and words cannot adequately represent their true value.

I am also thankful to Yılmaz Yücehan Yazıcı, Umut Tank, Ladin Işık Köse, Aysima Atılgan and Tunahan Çalıkoğlu for sharing their knowledge and providing me with a collaborative and supportive research environment in the laboratory. They were always there to help me whenever I needed. Additionally, I would like to thank Dr. İhsan Gürsel and his laboratory members for kindly sharing their reagents.

I would like to express my deepest gratitude to my family for their continuous encouragement, understanding and patience throughout my studies. I would not be able to succeed without their contribution. I am also extremely thankful to my spouse, Ali Berk Demir, for always being on my side and for his unconditional love and support throughout my studies. His unwavering belief in my abilities has given me strength and motivation when I needed it the most.

Finally, I am thankful to the members of the Molecular Biology and Genetics Department at Bilkent University for providing a peaceful and friendly atmosphere. Their efforts in creating such an environment have contributed significantly to my overall experience during my graduate studies. Particularly, I would like to offer my special thanks to the Laboratory Manager, Pelin Makas, for her constant support and understanding.

Lastly, I would like to thank The Scientific and Technological Research Council of Turkey (TÜBİTAK) for supporting my Master's studies through BIDEB-2210/A scholarship.

ASSOCIATED PUBLICATIONS

1) Tepe ZG, Yazıcı YY, Tank U, Köse LI, Özer M, Aytekin C, Belkaya S. Inherited IRAK-4 Deficiency in Acute Human Herpesvirus-6 Encephalitis. J Clin Immunol. 2023;43(1):192-205. doi:10.1007/S10875-022-01369-4.

TABLE OF CONTENTS

LIST OF TABLES

LIST OF FIGURES

ABBREVIATIONS

APC	Allophycocyanin
APS	Ammonium persulphate
AR	Autosomal recessive
BE	Brainstem viral encephalitis
CADD	Combined annotation dependent depletion
CD46	Cluster of differentiation 46
cDNA	Complementary DNA
cGAMP	Cyclic guanosine monophosphate–adenosine monophosphate
CHX	Cycloheximide
CMV	Cytomegalovirus
CpG ODN	CpG oligodeoxynucleotide
CRISPR	Clustered regularly interspaced short palindromic repeats
CSF	Cerebrospinal fluid
DAMPs	Danger-associated molecular patterns
DBR1	Debranching enzyme 1
DD	Death domain
DENV	Dengue virus
DMEM	Dulbecco's modified Eagle medium

DNA	Deoxyribonucleic acid
DP	Depth quality
dsDNA	Double-stranded DNA
DTT	Dithiothreitol
EBV	Epstein-Barr virus
ECL	Enhanced chemiluminescence
EDTA	Ethylenediaminetetraacetic acid
FACS	Flow cytometry staining buffer
FBS	Fetal bovine serum
FITC	Fluorescein isothiocyanate
Fwd	Forward
GABA	Gamma-aminobutyric acid
GAPDH	Glyceraldehyde 3-phosphate dehydrogenase
GDI	Gene damaging index
gDNA	Genomic DNA
GFP	Green fluorescent protein
GME	Greater Middle East
gnomAD	The genome aggregation database
GQ	Genome quality
GTF3A	General Transcription Factor IIIA
HHV-6	Human herpesvirus 6
HRP	Horseradish peroxidase
HSE	Herpes simplex encephalitis

HSV	Herpes simplex virus
IFN	Interferon
IgG	Immunoglobulin G
IL	Interleukin
IL-18	Interleukin 18
IL18RAP	Interleukin 18 receptor-associated protein
IRAK-4	Interleukin 1 receptor-associated kinase 4
JEV	Japanese encephalitis virus
KD	Kinase domain
KO	Knockout
LB	Lysogeny broth
LPS	Lipopolysaccharide
MAF	Minor allele frequency
MERS-CoV	Middle east respiratory syndrome-coronavirus
MHV	Mouse hepatitis virus
MP	Map quality
MSC	Mutation significance cutoff
MyD88	Myeloid differentiation primary response protein 88
NFκB	Nuclear factor kappa B
NMDAR	N-methyl-D-aspartate receptor
ORF	Open reading frame
PAGE	Polyacrylamide gel electrophoresis
Pam3CSK4	Pam3CysSerLys4

PAMPs	Pathogen-associated molecular patterns
PBMCs	Peripheral blood mononuclear cells
dPBS	Dulbecco's phosphate-buffered saline
PCR	Polymerase chain reaction
PE	Phycoerythrin
PID	Primary immunodeficiency
PKC	Protein kinase C
pLOF	Potential loss of function
PMA	Phorbol-12-myristate-13-acetate
PolyPhen-2	Polymorphism phenotyping v2
PRR	Pattern recognition receptor
PV-B19	Parvovirus-B19
R848	Resiquimod
RABV	Rabies virus
RBC	Red blood cell
Rev	Reverse
RIPA	Radio immunoprecipitation assay buffer
RLTK	Renilla luciferase
RNA	Ribonucleic acid
RT-qPCR	Reverse transcriptase-quantitative PCR
SARS-CoV-1	Severe acute respiratory syndrome coronavirus
SDM	Site-directed mutagenesis
SDS	Sodium dodecyl sulfate

SIFT	Sorting intolerant from tolerant
snoRNA31	Small Nucleolar RNA, H/ACA Box 31
T7E1	T7 endonuclease 1
TBE	Tris borate EDTA buffer
TBEV	Tick-borne encephalitis virus
TBS	Tris-buffered saline
TEMED	N,N,N',N'-Tetramethyl ethylene diamine
TIR	Toll-Interleukin 1 receptor
TLR	Toll-like receptor
TNF	Tumor necrosis factor
UV-Vis	Ultraviolet-visible
VZV	Varicella zoster virus
WES	Whole exome sequencing
WNV	West Nile virus
WT	Wild-type
ZIKV	Zika virus

CHAPTER 1

Introduction

1.1.Encephalitis

Encephalitis is a life-threatening condition defined as the inflammation in the brain[1–3]. It is characterized by the central nervous system (CNS) inflammation in the brain parenchyma, more specifically perivenular or periventricular spaces depending on the inflammatory culprit presented[2,4]. If the CNS inflammation occurs outside of the brain parenchymal tissues, such as meninges, brain stem, spinal cord or nerve roots, they are identified as meningitis, rhombencephalitis, myelitis and radiculitis, respectively[5–8]. The onset of the disease is generally acute, whereas in some rare cases, progressive inflammation of the brain becomes chronic, particularly in children[2,3,9]. Although acute encephalitis has serious complications, chronic encephalitis develops more severely and presents with more devastating symptoms, such as epilepsy, mental deterioration and paraplegia[3,9,10].

1.1.1.Symptoms

Common clinical symptoms of encephalitis include severe headaches, high fever, nausea, vomiting and seizures[2,11,12]. In some cases, impaired function of the nervous system disturbs other physiological systems that are mainly implicated by focal or multifocal neurological signs[3]. Depending on the extent of the inflammation, alterations in the mental status can also be observed, which may even progress to loss

of consciousness[3]. If it is not diagnosed and treated on time, it can lead to coma, the collapse of the CNS and eventually death[2,3].

1.1.2.Classification

Viral infection and autoimmune reactions are the most common causes of encephalitis in humans[13–15]. Additionally, other causes, including metabolic disorders, toxins, organ failure, neoplastic formations and vascular changes can also induce encephalitis[13,16,17]. Imbalances in glucose or calcium metabolism affect the physiologic activity of the brain, which in turn can promote inflammation in the brain[10,13]. Toxin substances, such as ammonia, can disrupt neuronal signaling, which can create inflammatory responses in CNS[13,18]. Similarly, hepatic failure prevents the removal of toxins, and thus systemic transportation of toxins to the brain may promote inflammation[13,19]. Additionally, brain tumors, such as glioblastoma, could induce inflammation in the brain[10,13].

Autoimmune encephalitis is identified by the presence of autoantibodies against self-proteins on neuronal cell surfaces and synaptic receptors[20–22]. It is seen predominantly in the younger population, such as adolescents and children with a lower incidence than infectious encephalitis[20–22]. However, the number of autoimmune encephalitis cases is increasing rapidly by the identification and detection of novel autoantibodies[21–23].

The clinical diagnosis of autoimmune encephalitis relies on the presence of neurological deficits and the detection of previously identified autoantibodies in cerebrospinal fluid (CSF) or serum[11,21,22]. Since the production of autoantibodies is the main cause of the prognosis, immunotherapies are considered to be useful to suppress autoimmune responses[20,21]. Three major classes of antibodies are responsible for more than half of the cases in the general population[21,22].

Autoantibodies against N-methyl-D-aspartate receptor (NMDAR) are the most common cause of autoimmune encephalitis in the general population[20,22]. Symptoms including seizure, dyskinesia and psychiatric disorders are frequently seen during the early onset of disease in both children and adults[20,22]. In some cases, antibody production is associated with the presence of tumors, such as ovarian teratoma[20,21]. Production of antibodies against Leucine-rich Glioma Inactivated 1 (LGI1) is another cause of autoimmune encephalitis, which is generally seen in the elderly[15,21]. In the course of LGI1 encephalitis, rapid cognitive declines with drastic memory loss or high-frequency focal seizures are commonly observed in the patients[20,22]. Third common autoantibodies are produced against Gamma-aminobutyric Acid (GABA) receptors[22,23]. Anti-GABA receptor encephalitis is less studied and the clinical symptoms are not distinctive[21,22].

Infectious encephalitis is characterized by the presence of infectious agents that invade the host organism[11,12,24,25]. Immune responses against those infectious microorganisms create an inflammatory environment in the brain[11,12]. This inflammation disturbs the physiological functioning of the brain, especially when the infection persists[2,11,12]. The main etiology of infectious encephalitis is viruses, whereas bacteria, fungi and parasites could induce encephalitis to a lesser extent[7,8,11,26,27].

Infectious encephalitis can also be divided into two subcategories based on the site of infection [24,28,29]. Primary infectious encephalitis is caused by a direct infection of the CNS by the microbe [2,12,23,28]. Mostly, gray matter is affected by the inflammation[2,28]. On the other hand, post-infectious or para-infectious encephalitis does not result from an infection of a CNS itself [24,28,29]. In post-infectious encephalitis, systemic host

immune responses against infectious agents induce inflammation in the brain, particularly affecting white matter[24,28].

For primary infectious encephalitis, microorganisms must enter the brain in order to infect the neuronal tissues directly[4,25,30]. Several virus families are neurotrophic, indicating that they are capable of invading the brain and infecting the CNS cells[12,30,31]. The blood-brain barrier is an anatomic barrier that protects the brain from invading microorganism[28,31–33]. In order to evade blood-brain barrier, those neurotropic viruses evolutionarily developed various strategies[28,32–35]. Arboviruses, located in the bloodstream, can be transported to the CNS by infecting endothelial cells or they are carried as a cargo inside the cells translocating to CNS[28,33]. Moreover, herpesviruses and polioviruses are capable of entering the CNS through retrograde transportation from neurons[28,36,37]. By these mechanisms, not only the entrance into CNS, but also the avoidance of immunosurveillance can be achieved[28,36,37]. Overall, the etiopathogenesis of primary infectious encephalitis is diverse, yet other mechanisms employed by different types of viruses are not well understood[4,12,25,28,30].

In addition to viruses, bacterial, fungal and protozoal infections could induce inflammation in the brain indirectly, and subsequently cause post-infectious encephalitis in humans[12,24]. The presence of an infection throughout the organism triggers immune system robustly and may induce inflammation in the brain parenchyma[8,12,26]. Major syndromes associated with post-infectious encephalitis are acute disseminated encephalomyelitis, acute hemorrhagic leukoencephalitis and Bickerstaff's brainstem encephalitis[24,26]. Although no infectious agents from neural

tissue could be isolated in those cases, severe inflammation in the brain mimics primary encephalitis and therefore symptoms presented are similar[24,29,38].

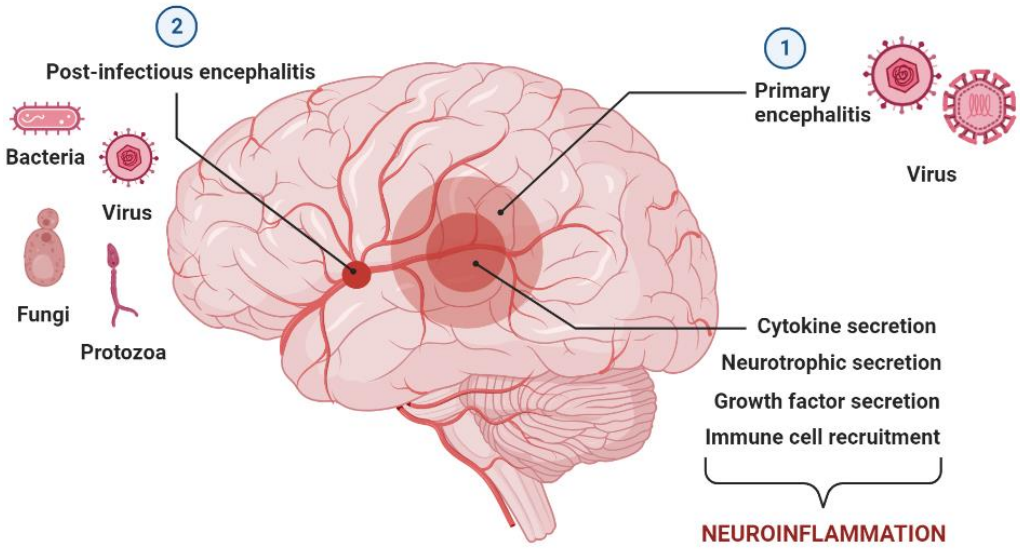

Figure 1. 1 Etiopathogenesis of infectious encephalitis (Adapted from Bohmwald K et al., 2021[15])

In the general population, encephalitis is a rare condition that can be seen in approximately every 3.5 and 7 cases per 100,000 individuals per year in Europe and USA, respectively[39,40]. However, in children, the incidence is much higher with more than 16 cases per 100,000 patients per year worldwide[4,25].

1.2.Viral encephalitis

Viral encephalitis is the most frequently seen type of encephalitis in the human population[2,25,30]. It is described by the presence of inflammation in the brain parenchyma caused by a viral agent[2,25]. This neuropathology has high morbidity and mortality rates affecting both immunocompetent and immunocompromised individuals[3,12,25,30].

1.2.1.Etiology

Various virus families are able to cause encephalitis in humans[12,25,27,39]. The most common virus families are Herpesviridae, Arboviruses, Rhabdoviridae, Picornaviridae, Retroviridae, Orthomyxoviridae, Orthopneumoviridae and Coronoviridae[12,25]. The first four families are responsible for primary viral encephalitis, whereas the latter three can spread into the CNS from their original sites of infection, such as respiratory system[12,25,27].

Herpesviruses are the most common viruses causing viral encephalitis in the human population, particularly Herpes Simplex Virus-1 (HSV-1)[12,41]. Most clinically relevant strains of the Herpesviridae are HSV-1, HSV-2, Varicella Zoster Virus (VZV), Epstein-Barr Virus (EBV), Cytomegalovirus (CMV), Human Herpesvirus-6 (HHV-6) and Human Herpesvirus-7 (HHV-7)[29,42–44]. Herpesviruses are accountable for approximately half of the cases of viral encephalitis in the human population[12,25,42,45]. In the general population, HSV encephalitis (HSE) is diagnosed in approximately every 1 to 2 cases per 500,000 people per year in Europe, predominantly in children under the age of 3[46]. Since individuals in early childhood are more susceptible to encephalitis, primary infection of HSV is considered as the cause of the inflammation[29,44,47]. HHV-6 and HHV-7 show similar characteristics and clinical presentations in humans[48–50]. HHV-7 has the ability to invade the brain, but primary infection with HHV-7 rarely leads to encephalitis in children[44,48]. When the immune system is compromised, reactivation of HHV-7 can lead to severe CNS diseases, such as encephalitis[49,50]. Furthermore, HHV-7 infection can also activate other viruses, such as HHV-6 and

human parvovirus B19[49–51]. In some patients with myalgic encephalitis, co-infection of HHV-6, HHV-7, and Parvovirus-B19 (PV-B19) were observed[51,52].

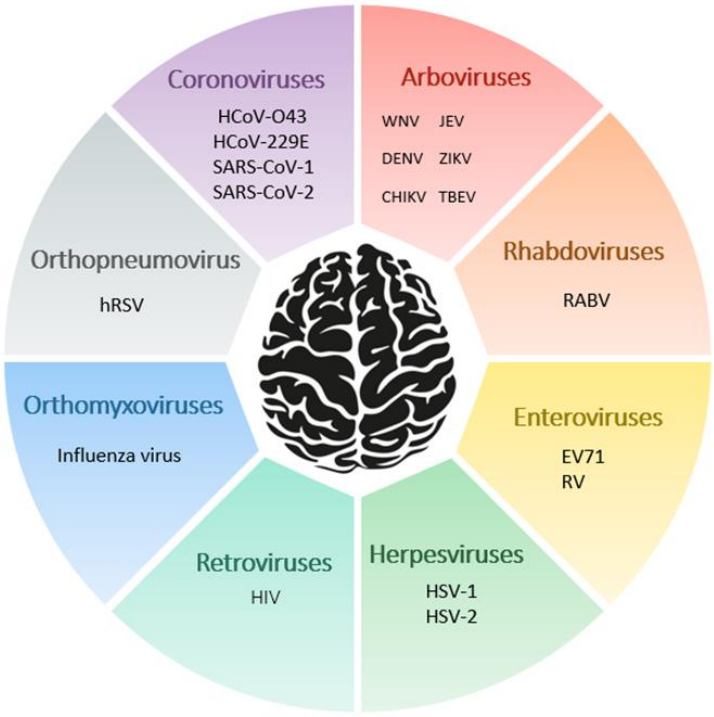

Figure 1. 2 Virus families and strains causing viral encephalitis in humans (Adapted from Bohmwald K et al., 2021[12])

Arboviruses, Rhabdoviruses, Orthomyxoviruses and Coronaviruses are the zoonotic viral agents that can cause viral encephalitis in humans[11,12,25]. Arboviruses are transmitted through blood-feeding arthropods, such as ticks and mosquitos[25]. The most common strains of this family causing viral encephalitis are dengue virus (DENV), tick-borne encephalitis virus (TBEV), Zika virus (ZIKV), West Nile virus (WNV) and Japanese encephalitis virus (JEV)[11,12]. Orthomyxoviruses and Coronaviruses are respiratory viruses causing post-infectious encephalitis[12,24]. Influenza viruses (IV) belonging to Orthomyxoviridae target respiratory tissues as sites of infection[24,25].

However, the infection could spread to the CNS in severe cases and the induced inflammation is described as influenza-associated encephalitis[25,53]. Similarly, human coronaviruses target respiratory and enteric tissues as sites of infection[14,25]. Middle East respiratory syndrome coronavirus (MERS-CoV), severe acute respiratory coronavirus-1 (SARS- CoV-1) and SARS-CoV-2 can cause post-infectious encephalitis in cases with poor prognosis[12,25].

1.2.2.Epidemiology

Viral encephalitis is observed in the human population at an annual incidence of 7 cases per 100,000 people in USA[23,40]. On the other hand, in some European countries, such as England and France, lower incidence rates of viral encephalitis are observed ranging from 1.5 to 2.2 per 100,000 people[53,54]. The total number of reported viral encephalitis cases remain similar, but incidence rates of certain viral causes are continuously changing over time[12,25,38,53]. For instance, cases of measles and mumps-associated encephalitis have decreased in the last decades thanks to the application of national vaccination programs, particularly in Europe[25,55]. On the other hand, the cases of CMV and EBV-associated encephalitis have increased in the human population due to an increase in the number of immunocompromised individuals, such as transplant recipients, cancer patients, and patients with acquired immunodeficiency syndrome (AIDS)[38,53]. Additionally, seasonal, geographical and climate-related changes are important factors affecting the epidemiology of viral encephalitis[38,53,56,57]. For instance, arboviruses are transmitted via mosquitoes, and therefore arbovirus-associated encephalitis cases increase in summer seasons when mosquitoes are more abundant[38,53]. Although there are no age limitations, viral encephalitis is more

prominent in the pediatric population[12,25]. Likewise, both genders are affected similarly, whereas a slight disposition is observed in males[12,25].

1.2.3.Pathophysiology

Viral neuroinvasion can be accomplished by two major pathways, which are direct neuronal transport and transportation via hematogenous route[33,38,58,59]. Neuronal transport is mostly employed by rabies viruses and HSV[38,59]. For instance, HSV spread among neuronal cells through cell junctions or extracellular spaces upon CNS invasion[38,60]. If the spread is restricted by neuronal cells, they can also reside in the infected tissue in a quiescent state waiting for reactivation[38,60]. What determines the restriction of HSV spread is still unknown[38]. The hematogenous route is typically employed by viruses transmitted with arthropod-borne infection, such as arboviruses[11,61]. For instance, TBEV invades the skin of the host organism through the tick bites and they replicate under subcutaneous tissues[11,61]. Unless primary viremia was kept in the subcutaneous tissues, TBEV infection can spread into other organs through transport via bloodstream, including CNS[11,61].

1.3.HHV-6 encephalitis

1.3.1.HHV-6

HHV-6 is a lymphotropic double-strand DNA (dsDNA) virus, which was isolated from patients suffering from lymphoproliferative disorders and characterized for the first time in 1986[48,62,63]. Later, it was recognized as a medical condition for the first time by its association with roseola infantum, a childhood disease presented with high fever and rash[64]. It was found to have a wide tropism for not only hematopoietic cells, but also CNS cells[65–67].

HHV-6 belongs to the β-human Herpesviridae, where they share linearized dsDNA and an outer envelope[48,68,69]. They have relatively small genome size when compared with other virus families, which is approximately 150 kilobases[68,69]. The most distinguished characteristic of β-human Herpesviridae is their tendency to become latent in immune cells[63,68,69]. Similar to other herpesviruses, HHV-6 can reside in the host in a latent state after primary infection[68,69]. This persistence can be presented as no or low-level viral replication[63,68]. After the acute phase of HHV-6 infection in immune cells, the virus enters a quiescent state where it ceases replication and resides silently in the immune cells[63,68]. The most common sites for latency of HHV-6 are hematopoietic stem cells in bone marrow, brain parenchyma and salivary glands[63,64,69,70].

Cellular entry of HHV-6 is accomplished by the interaction with the CD46 receptor on the nucleated cells and further induction of the membrane fusion[69,71]. CD46 is a surface receptor responsible for the suppression of complement system activation against the host cells[69,71]. It was shown that the human CD46 receptor on leukocytes recognizes gH-gL-gQ glycoprotein complex on HHV-6 and this interaction initiates HHV-6 envelope fusion with the leukocyte membrane[70,71]. Following fusion, transportation of the nucleocapsid from the cytoplasm to the nucleus facilitates with the help of microtubule network of the host cells[63,69,71]. HHV-6 dsDNA enters nucleus, where it starts to replicate itself and integrates into the host genome[69,70,72].

Up to now, two variants of HHV-6, HHV-6A and HHV-6B, are identified based on their genomic differences and cell tropism[48,52,64]. They have structural differences in their genome, particularly in IE-1 region, which is believed to responsible for the functional differences between HHV-6 variants[64]. Additionally, there are some splicing differences in the U97-U100 region in the genome of both of the variants that could

affect their CD46 interactions and possibly cell tropisms[64]. *In vitro* studies demonstrated that although both HHV-6A and HHV-6B are lymphotropic viruses, HHV-6A is the only variant capable of infecting $CD8^+$ cytotoxic T cells, gamma/delta T cells and natural killer cells efficiently[48,52,69]. Additionally, only HHV-6A was found to persist in CSF after acute infection, suggesting that HHV-6A latency was more common than HHV-6B[48,73]. Therefore, HHV-6B is thought to be the dominant variant for primary infection[49,74,75].

1.3.2.Pathophysiology

Active HHV-6 infection can occur in a host in one of the three possible ways, which are primary acute infection of the virus, reactivation of a prior quiescent infection, and activation of the chromosomally integrated HHV-6[72,75,76]. In either ways; active HHV-6 infects target cells, primarily mature $CD4^+$ T cells, through receptor mediated endocytosis via CD46 receptors on the surface of lymphocytes[69,71,77]. After lymphocyte infection, virus replicates itself using the host cellular machinery[63,70,77]. Through inducing expression of CD4 receptors, other lymphocyte populations, such as $CD8^+$ cytotoxic T cell, gamma/delta T cells and natural killer cells were shown to sustain and induce HHV-6 replication and proliferation[77,78]. Therefore, CD4 expression is thought to be crucial for the targeting and replication of HHV-6[69,77,78]. On host lymphocytes, the replicated virus causes cytopathogenic effects, particularly a phenomenon called ballooning degeneration characterized by swollen lymphocytes[77,78].

After primary HHV-6 infection, various host immune responses were observed in individuals[63,79]. Regarding interferons (IFNs), only IFN-α levels were found to be increased in the plasma of patients with acute HHV-6 infection[80]. Similarly, an increase in the IFN-α production was observed in HHV-6-infected peripheral blood

mononuclear cells (PBMCs) *in vitro*[81,82]. Indeed, induced IFN-α production in infected PBMCs was shown to suppress replication of HHV-6[81,82]. Moreover, HHV-6 infection induces expression of several pro-inflammatory interleukins (ILs), such as IL-1β, IL-6, IL-8 and IL-18[69,83]. Similarly, TNF-α production was shown to be upregulated by HHV-6 infection in PBMCs[84]. It was demonstrated that the induction of IL-1β and TNF-α depends on the viral entry into the host cell rather than de-novo viral protein synthesis by host cell[75,85]. Thus, induction of those pro-inflammatory cytokines was seen during the primary HHV-6 infection[69,85]. Upon primary infection, HHV-6 also modulates the host cell immune responses through a variety of routes in order to evade the detection by immune system or create an environment advantageous for its survival[63,86,87]. It was reported that HHV-6 infection of PBMCs led to increased IL-10 but reduced IL-12 production, inducing a skewing towards T_H2 cell differentiation[88]. However, other studies revealed that IL-10 production was decreased in HHV-6-infected T cells and IL-6 production was increased in HHV-6-infected monocytes[83,89]. Collectively, HHV-6 modulate cytokine production with respect to the cell type it infects[89]. Furthermore, HHV-6 could induce the expression of human leukocyte antigen (HLA) class I and II molecules on immature dendritic cells while impairing the antigen presentation and processing[90]. Without antigen presentation to T cells, HHV-6 could survive, replicate and spread more easily in the host organism[69,90].

It was demonstrated that upon HHV-6 infection of activated lymphocytes, virus replication impaired proliferation of T cells, resulting in immunosuppression of the host organism[91]. Likewise, reduced IFN-γ production contributed to the suppression of T cell responses upon HHV-6 infection[81]. As a result of immune suppression, HHV-6 might be able to persist in the host[69,81,91].

After the course of primary infection, viral DNA of HHV-6 might persist inside the lymphocytes and can become integrated into the host genome, which is known as chromosomal integration of HHV-6[92,93]. In dividing cells, integrated viral DNA is subsequently passed on to the daughter cells, resulting in a substantial number of lymphocytes having the integrated viral DNA[72]. After integration into the host genome, viral DNA remains dormant, where no viral replication or infectious viral particle production was seen[72,94]. Although the virus is not active, the presence of the virus could still be detected by molecular testing[49,72]. Clinical presentations of chromosomally integrated HHV-6 (ciHHV-6) and its significance are still not well understood[72,75,94]. In most cases, individuals with ciHHV-6 remain asymptomatic, yet several cases of infertility, autoimmune or hematological disorders have been associated with ciHHV-6[74,95]. Under immunosuppression, ciHHV-6 could become activated, leading to the production of infectious virions in the affected individuals[72,95]. The ciHHV-6 represents a hallmark of HHV-6 biology, with that its long-term effects could impact on the host immunity and overall health of affected individuals[72,75,94].

1.3.3.Epidemiology

Although HHV-6 is a ubiquitous virus found in the human population worldwide, frequency of encephalitis upon primary HHV-6 infection is extremely low, particularly in children[29,64,74,75]. While primary infection with HHV-6 is more commonly seen during childhood, HHV-6 reactivation is more prevalent in immunocompromised adults, such as cancer patients[70,74]. Since HHV-6 is also neurotropic, it was reported that HHV-6 DNA was detected in 85% of post-mortem brain biopsies from patients with no viral or CNS-related diseases[68,96]. It could be deduced from the high incidence of both peripheral and neuronal positivity of HHV-6 that life-threatening complications

are rare and vast majority of infected people remain asymptomatic[64,97]. On the other hand, only 1% of the human population was found to have ciHHV-6, which is relatively low compared with its seropositivity[72,75].

1.3.4.Clinical presentations

Primary HHV-6 infection occurs mainly during childhood mostly without any accompanying symptoms[48,64,75]. Others commonly experience acute febrile illness, and a distinctive phenotype called as roseola infantum, which is characterized by high temperature followed by rashes all over the body[48,50,98]. In a previous study, early immune responses to primary HHV-6 infection were assessed by measuring IFN levels during the acute and recovery phases in patients presenting roseola infantum[80]. Only plasma IFN-α levels were elevated significantly in acute phases when compared to the recovery period[80]. No significant change was observed in other interferons[80]. Moreover, they reported that IFN-α and IFN-β inhibited the replication of HHV-6 in cord blood mononuclear cells[80]. Therefore, induction of IFN-α production and its anti-viral activity was thought to be crucial for the acute phases of roseola infantum in children[80].

Acute febrile illness is another common symptom seen in children with primary HHV-6 infection[87,99,100]. The presence of high temperature in children is generally accompanied by seizure episodes during the acute phase of HHV-6 infection[87,99]. Primary HHV-6 infection frequently manifests as a febrile disease with no rash[101]. Occasionally, the rash appears shortly after the fever has passed[101]. Additionally, in rare cases, acute encephalitis can occur during childhood[49,64,75,102]. Other associated symptoms of primary HHV-6 infection can include hepatitis and idiopathic thrombocytopenic purpura[103–105].

After the primary infection, HHV-6 can enter a latent status, which can reactivate in immunocompromised individuals, such as individuals undergoing transplantation, cancer patients and individuals with AIDS[48,63,75,87]. Commonly, patients remained asymptomatic upon HHV-6 reactivation after bone marrow transplantations[49,106]. However, there were some cases reporting that HHV-6 reactivation could lead to bone marrow suppression, encephalitis and pneumonitis[107–110]. In liver transplant recipients, HHV-6 infection can cause severe febrile illnesses characterized by thrombocytopenia, encephalopathies, and skin rashes due to post-operative immunosuppression[111–113]. It was reported that only suppressed memory responses against HHV-6 may contribute to the progression of HHV-6 reactivation in those patients[112,113]. In another study, HHV-6 infection has been associated with hepatitis and pyrexia after liver transplantation[51,63].

1.4.Human inborn errors of immunity and viral encephalitis

The occurrence of viral infection affecting the CNS is approximately 1 in 100,000 people annually[12,39,45,57]. As mentioned above, encephalitis can be caused by several viruses, such as HSV, IV and DENV[12,25,55]. Surprisingly, many of these viruses are typically self-limited and rarely lead to encephalitis in otherwise healthy individuals[43,67,114]. On the other hand, primary infection of the CNS with viruses occurs predominantly during childhood, which results in high mortality rates and severe long-term complications[27,30,114]. It was unclear why only some children develop viral encephalitis, whereas vast majority remain asymptomatic despite being exposed to same viruses[43,45,114]. However, several studies demonstrated that isolated cases of HSE could result from monogenic inborn defects of innate immunity[46,115–119]. Previously,

inherited deficiencies of genes involved in IFN-α/β immunity, such as X-linked NEMO deficiency and autosomal recessive STAT1 deficiency, were associated with HSE in children[117,120,121]. Furthermore, mono-allelic and bi-allelic defects in genes involved in Toll-like receptor 3 (TLR3)/IFN signaling cascade were identified in patients presented with isolated forebrain HSE[46,115,119,122,123]. Inborn genetic lesions in *TLR3*, *UNC93B1*, *TRIF*, *TRAF3*, *TBK1* and *IRF3* were found to underlie HSE in otherwise healthy children[115–117,121–123] (Figure 1.3). All these human genetic studies of children with HSE revealed that TLR3-dependent IFN-α/β immunity is critical for primary HSV-1 infection in the CNS[119,121,124–126]. Interestingly, PBMCs from TLR3-deficient children with HSE demonstrated normal IFN production upon HSV-1 infection as healthy controls[127,128]. However, impaired IFN production upon HSV-1 infection was observed in the fibroblasts, induced pluripotent stem cell (iPSC)-derived cortical neurons and oligodendrocytes from TLR3-deficient children with HSE[128,129]. Therefore, TLR3 signaling was suggested to generate protective cell-intrinsic immune responses in the CNS against HSV-1[128,129]. Strikingly, HSE resulting from congenital defects of TLR3 signaling exhibited brain lesions confined to the frontal and temporal lobes, suggesting that impaired cellular immunity within the forebrain contributes to the development of HSE in these children[114]. Similarly, HSE usually affects children who do not show any susceptibility to other manifestations of HSV-1. Indeed, viral dissemination to other tissues was not observed in those children with HSE[43,130].

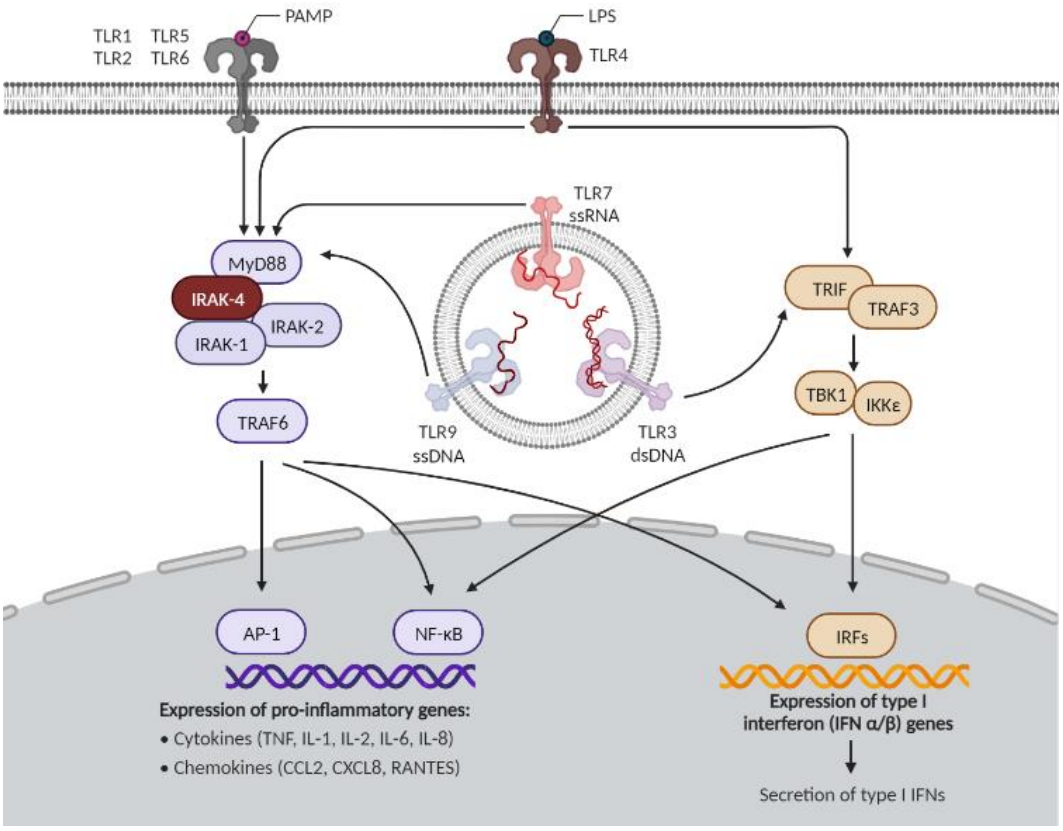

Figure 1.3 TLR signaling pathway in innate immune cells**.** Pathogen-associated molecular patterns: PAMPs, Lipopolysaccharide: LPS, IkB kinase-ε: IKKε, Interferon regulatory factors: IRF. Adapted from Duan T. et al., 2022[125] Created in BioRender.

Additionally, in a study including 5 patients with forebrain HSE, 4 rare heterozygous variants of Small Nucleolar RNA, H/ACA Box 31 (*SNORA31)* were identified[131]. snoRNA31 directs the conversion of uridine residues to pseudouridine in ribosomal RNA[132]. *SNORA31* knockout (KO) in iPSC-derived cortical neurons induced susceptibility to HSV-1 infection[131]. The analysis of gene expression patterns at the transcriptome level in *SNORA31* KO neurons revealed impaired responses to HSV-1 infection, whereas normal responses were seen upon induction of TLR3 and IFNα/β[131]. However, the exact molecular mechanism underlying the role of snoRNA31 in controlling HSV-1 infection in neurons is still unknown and requires further

investigation[124,131]. Furthermore, in children with brainstem viral encephalitis (BVE) upon infection with different viruses including HSV-1, IV and NV, partial Debranching enzyme 1 (DBR1) deficiency was discovered[114]. DBR1, which is an enzyme responsible for removing specific RNA structures called lariats in humans, is highly abundant in brainstem-resident cells[133,134]. DBR1-deficient fibroblasts showed high susceptibility to HSV-1 infection with higher level accumulation of RNA lariats compared to the controls[114]. Similar to snoRNA31, the precise molecular mechanisms underlying the connection between DBR1 deficiency and susceptibility to viral infection remain unclear[114,124]. It was suggested that cell-intrinsic anti-viral immune responses were compromised because of the impaired virus recognition upon accumulation of RNA lariats[114,124]. Finally, it was recently demonstrated that inherited General Transcription Factor IIIA (GTF3A) deficiency could lead to HSE. *GFT3A* encodes transcription factor IIIA[135,136]. GTF3A deficiency impaired the production of RNA5SP141, activator of the immune receptor RIG-I, thereby attenuated the innate immune response against HSV-1 infection[135]. This study revealed that inborn genetic lesions in *GTF3A* resulted in compromised innate immune responses against HSV-1, thereby leading to encephalitis[135].

HHV-6 is a widely prevalent virus in the human population, where 70% to 95% of individuals older than 2 years are seropositive for HHV-6[137–139]. Most individuals remain asymptomatic during the acute infection and severe outcomes, such as encephalitis, are exceedingly rare[44,63,76,121]. Although reactivation of HHV-6 is a common occurrence upon immunosuppression, just a small number of infected individuals develops encephalitis[49,140,141]. In rare cases, individuals with specific immunodeficiencies have presented severe symptoms like hemophagocytic

lymphohistiocytosis (HLH), colitis and hepatitis upon HHV-6 infection[121]. In one report, reactivation of the ciHHV-6 was associated with HLH in a patient with X-linked SCID[72]. Additionally, colitis and hepatitis were reported in a patient with ICOS deficiency, who was found to be PCR-positive for HHV-6 DNA in his intestines[142]. Recently, anti-NMDAR encephalitis followed by HHV-6 reactivation was reported in a child with autosomal recessive (AR) Interluekin-1 receptor associated kinase-4 (IRAK-4) deficiency[143]. IRAK-4 is a kinase that involves in the signaling pathway triggered by the activation of TLRs and interleukin-1 receptors (IL-1Rs), which are crucial to recognize and initiate immune responses against various pathogens[126,144]. Upon stimulation, IRAK-4 forms a complex with IRAK-2 and they are recruited to the receptor via adaptor molecule, myeloid differentiating factor 88 (MyD88)[126,144]. Following the recruitment of the IRAK complex, IRAK-4 undergoes autophosphorylation, leading to its activation[126,144]. IRAK-4 then phosphorylates and activates IRAK-1, another downstream molecule, initiating a cascade of events, leading to the activation of nuclear factor kappa B (NF-κB) and activator protein 1 (AP-1)[126,144] (Figure 1.3). AR IRAK-4 deficiency in humans confers predisposition to life-threatening recurrent pyogenic bacterial infections due to defective Toll-Interleukin-1 receptor (TIR) signaling[145–147]. Furthermore, severe encephalitis associated with HHV-6 or HHV-7 has also been reported in otherwise healthy individuals, indicating the involvement of host genetic factors underlying susceptibility to life-threatening diseases upon infection with these viruses[76,102,143]. Intriguingly, there has not been any report of isolated acute HHV-6 encephalitis in an inherited primary immunodeficiency[121].

1.5.Aim of the Study

Although HHV-6 is a ubiquitous virus in human population , acute HHV-6 encephalitis is an extremely rare condition in children[64,137–139]. Why only some children develop encephalitis upon primary infection with HHV-6 is still unclear[75,76]. Inborn errors of immunity are known to predispose otherwise healthy children to severe infectious diseases, including viral encephalitis[121,124,148–151]. Particularly, single-gene defects of tissue-intrinsic anti-viral innate immunity were shown to cause HSE in children[115,119,122,123,131,135,152]. Therefore, we hypothesized that monogenic defects might underlie inter-individual variability among children in susceptibility to HHV-6 encephalitis. In this study, we investigated a child who was diagnosed with isolated acute HHV-6 encephalitis and who was homozygous for a novel missense mutation in *IRAK4*, identified by whole-exome sequencing. We tested the damaging impact of this mutation *in vitro* by biochemical and functional assays utilizing cell lines and patient's cells.

The work presented in this thesis was originally published as "Tepe ZG, Yazıcı YY, Tank U, Köse LI, Özer M, Aytekin C, Belkaya S. Inherited IRAK-4 Deficiency in Acute Human Herpesvirus-6 Encephalitis. J Clin Immunol. 2023;43(1):192-205. doi:10.1007/S10875-022-01369-4." and reproduced with permission from Springer Nature (Appendix E).

CHAPTER 2

Materials and Methods

2.1.Materials

All materials used in this study are declared in the sections below.

2.1.1.Cell culture media and solutions

Table 2. 1. Cell culture media and solutions

Liquid consumable	Catalog #	Manufacturer
DMEM High Glucose w/stable glutamine wo/Sodium pyruvate	L0107-500	Biowest, USA
RPMI 1640 w/stable glutamine	L0498-500	Biowest, USA
Fetal Bovine Serum, European Grade, South America origin	BI0-007-1A	Biological Industries, Israel
Trypsin-EDTA Solution	03-050-1B	Biological Industries, Israel
Dulbecco's PBS (dPBS) w/o Ca^{2+} & Mg^{2+}	02-023-1A	Biological Industries, Israel
EDTA solution	SE3976102	Serva, USA
Dimethyl sulphoxide	A3672-0100	AppliChem, USA
Cell Culture Water Pyrogen free	L0970-500	Biowest, USA
Opti-MEM™ I Reduced Serum Medium	31985062	Thermo Scientific, USA
Lymphoprep™ Density Gradient Medium, Sterile, pH 6.3 - 7.3, Liquid	07801	STEMCELL Technologies, USA
RBC Lysis solution	01-888-1B	Biological Industries, Israel

2.1.2.Contents of buffers

Table 2. 2 Contents of buffers

Buffer	Contents	Amount
10X TBS	1M Tris HCl pH 7.5 5M NaCl ddH_2O	100 mL 300 mL 600 mL
1X TBS-T	10X TBS Tween-20 ddH_2O	100 mL 900 mL 1 mL
10X Running buffer	Tris base Glycine 20% SDS ddH_2O	30 g 144 g 50 mL complete to 1 L
10X Transfer buffer	Tris base Glycine ddH_2O	30 g 144 g complete to 1 L
1X Transfer buffer	10X Transfer buffer %100 Methanol ddH_2O	110 mL 165 mL 825 mL
2X RIPA Lysis buffer	NaCl EDTA Triton X-100 Sodium deoxycholate SDS 1M Tris-HCl, pH 7.6 ddH_2O	0.88 g 0.15 g 1 g 1 g 0.1 g 2.5 mL complete to 100 mL
Complete RIPA Lysis buffer	2X RIPA Lysis buffer 7X Protease inhibitor 10X Phosphatase inhibitor ddH_2O	700 µL 200 µL 140 µL 360 µL
FACS buffer	dPBS solution FBS	1 L 2 mL
PBS-EDTA solution	dPBS solution EDTA solution	1 L 1 mL
1.5 M Tris-HCl pH 8.8	Tris base ddH_2O Adjust pH with HCl ddH_2O	6.06 g 60 mL … complete to 100 mL
0.5M Tris-HCl pH 6.8	Tris base ddH_2O Adjust pH with HCl ddH_2O	12.11 g 80 mL … complete to 100 mL

20% SDS solution	Sodium dodecyl sulphate ddH_2O	2 g complete to 100 mL
10% APS solution	APS ddH_2O	1 g complete to 10 mL
Mild Stripping Buffer	Glycine SDS Tween-20 ddH_2O Adjust pH to 2.2 with HCl ddH_2O	7.5 g 0.5 g 5 mL 400 mL … complete to 500 mL
5% Stacking gel	ddH_2O 40% Bis-acrylamide 0.5 M Tris-HCl pH 6.8 20% SDS 10% APS TEMED	4.2 mL 623 µL 630 µL 25 µL 50 µL 5 µL
12% Separating gel	ddH_2O 40% Bis-acrylamide 1.5 M Tris-HCl pH 8.8 20% SDS 10% APS TEMED	4.3 mL 3 mL 2.5 mL 50 µL 100 µL 4 µL
1% Agarose gel	Agarose (Biomax) 0.5X TBE buffer SafeView Classic	1 g 100 mL 5 µL
10X TBE buffer	Tris base Boric acid Na_2EDTA ddH_2O	108 g 55 g 9.3 g complete to 1 L
LB Broth Medium	NaCl Tryptone Yeast extract ddH_2O	4 g 4 g 2 g 400 mL
LB Agar Medium	NaCl Tryptone Yeast extract Agar ddH_2O 100 mg/mL Ampicillin (if applicable)	4 g 4 g 2 g 6 g 400 mL 400 µL

2.1.3.Stimulatory reagents

Table 2. 3 Reagents used for *in vitro* stimulation experiments

Ligand	Catalog #	Manufacturer	Target Pathway	Working concentration
Pam3CSK4	tlr-pms	Invivogen, USA	TLR1/TLR2	100 ng/mL
poly (I:C) LMW	tlr-picw	Invivogen, USA	TLR3	10 µg/mL 20 µg/mL
LPS-EB	tlr-3pelp	Invivogen, USA	TLR4	1 µg/mL 100 ng/mL
Flagellin	tlr-epstfl	Invivogen, USA	TLR5	100 ng/mL
R848-Resiquimod	tlr-848	Invivogen, USA	TLR7 TLR8	2 µg/mL 5 µg/mL
CpG ODN 2395	tlr-2395	Invivogen, USA	TLR9	1 µM 2.5 µM
poly (dA:dT)	tlrl-patn	Invivogen, USA	cGAS-STING AIM2 RIG-I/MAVS DAI-STING	1 µg/mL* 3 µg/mL*
2’3’-cGAMP	tlrl-nacga23	Invivogen, USA	STING	1 µg/mL* 3 µg/mL*
Phorbol-12-myristate13-acetate (PMA)	1652981	Peprotech, USA	PKC	50 ng/mL
Ionomycin Ca^{2+} salt	5608212	Peprotech, USA	Endoplasmic reticulum Ca^{2+} channels	500 ng/mL
Recombinant human IL-18	9124-IL	R&D Systems, USA	Toll-Interleukin 1 receptor (TIR)	100 ng/mL

* Stimulants were transfected with Lipofectamine 2000 reagent according to the manufacturer’s instructions.

2.1.4.Chemicals and reagents

Table 2. 4 Chemicals and reagents

Product name	Catalog #	Manufacturer
Lipofectamine 2000 reagent	11668019	Thermo Scientific, USA
X-tremeGene 9 DNA Transfection reagent	XTG9-RO	Roche, USA
Agarose (Biomax)	BHE500	Prona, USA
NaCl	31434-1KG-R	Sigma Aldrich, USA
Tryptone	48647.02	Serva, USA
Yeast extract	1.03753.0500	Merck, USA
Tween-20	777	Ambresco/VWR, USA
Trizma Base	T1503	Sigma Aldrich, USA
Glycerol	15524	Sigma Aldrich, USA
Sodium dodecyl sulphate	822050	Merck, USA
Hydrochloric acid (HCl)	30712-2.5L	Sigma Aldrich, USA
Sodium hydroxide (NaOH)	O6203	Sigma Aldrich, USA
Glycine	GLN001.1	BioShop, Canada
Ethanol	32221	Sigma Aldrich, USA
Methanol	24229-2.5L-R	Sigma Aldrich, USA
Ethylenediaminetetraacetic Acid (EDTA)	E-5134	Sigma Aldrich, USA
Bovine Serum Albumin (BSA)	BSA-1T	Capricorn, USA
Isopropanol	100995	Sigma Aldrich, USA

0.5 N Sulphiric acid	117655	Norateks, TR
Ammonium persulphate (APS)	7727-54-0	Sigma Aldrich, USA
N,N,N',N'-Tetramethyl ethylenediamine (TEMED)	1610801	BioRad, USA
Triton X-100	A1694.0250	Applichem, USA
Sodium deoxycholate	302-95-4	Sigma Aldrich, USA
SafeView Classic	G108	ABM, USA
Orange G Sodium Salt (High Purity Grade)	E783-50G	Amresco, USA
cOmplete™, Mini, EDTA-free Protease Inhibitor Cocktail	11836170001	Roche, USA
Pierce™ Phosphatase Inhibitor Mini Tablets	A32957	Thermo Scientific, USA
Ampicillin sodium salt	BP1760-25	Fisher Bioreagents, USA
Skimmed Milk	-	Pınar, TR

2.1.5.Antibodies

Table 2. 5 Antibodies

Antibody	**Clone or Catalog #**	**Manufacturer**	**Purpose**
anti-FLAG	M2	Sigma-Aldrich, USA	Immunoblotting
anti-human GAPDH	1E6D9	Proteintech, USA	Immunoblotting
anti-GFP	JL-8	Clontech, Japan	Immunoblotting
Goat anti-Mouse IgG	72-8062-M001	Tonbo Biosciences, USA	Immunoblotting
anti-human IRAK4 Alexa Fluor 647	L29-525	BD Biosciences, USA	Immunoblotting Flow cytometry
anti-human CD3 Pacific Blue	OKT3	Biolegend, USA	Flow cytometry

anti-human CD4 FITC	OKT4	Biolegend, USA	Flow cytometry
anti-human CD8 PE	HIT8a	Biolegend, USA	Flow cytometry
anti-human CD14 FITC	M5E2	Biolegend, USA	Flow cytometry
anti-human CD19 PE	HIB19	Biolegend, USA	Flow cytometry
anti-human TNF APC	MAb11	Biolegend, USA	Flow cytometry
anti-mouse IgG1 APC	MOPC-21	Biolegend, USA	Flow cytometry
anti-mouse IgG1 Alexa Fluor 647	MOPC-21	BD Biosciences, USA	Flow cytometry

2.1.6.Enzymes and enzyme buffers

Table 2. 6 Enzyme and enzyme buffers

Enzyme	**Catalog #**	**Manufacturer**
BamHI-HF	R3136S	NEB, UK
XhoI	R0146S	NEB, UK
EcoRI-HF	R3101S	NEB, UK
XbaI	R0145S	NEB, UK
HindIII-HF	R3104S	NEB, UK
BsmBI-V2	R0739S	NEB, UK
T4 DNA Ligase	M0202S	NEB, UK
AQ97 Hi-Fi DNA Polymerase	A767501	Ampliqon, Denmark
Taq DNA Polymerase	LSG-EP0406	Thermo Scientific, USA
T7 Endonuclease I	M0302S	NEB, UK

r3.1 buffer	B6003S	NEB, UK
r2.1 buffer	B6002S	NEB, UK
rCutSmart buffer	B6004S	NEB, UK
NEBuffer 2	B7002S	NEB, UK
T4 DNA Ligase Reaction Buffer	B0202S	NEB, UK

2.1.7.Plasmids

All constructed plasmid maps were shown in the Appendix B.

Table 2. 7 Plasmids

Plasmid	**Antibiotic Resistance**	**Manufacturer**
pcDNA3.1(+)	Ampicillin	Invitrogen, USA
pCI-neo-N-3xFLAG	Ampicillin	Promega, USA
pCI-neo-C-3xFLAG	Ampicillin	Promega, USA
pCMV6	Ampicillin	OriGene, USA
pLentiCRISPR.v2	Ampicillin	Addgene plasmid # 52961
pNiFty-SEAP	Ampicillin	Invivogen, USA

2.1.8.Primers

Table 2. 8 Primers

Name	**Sequence**	**Purpose**
IRAK4 gDNA Fwd	CAGAACCGTGAGCCAAATTAAC	Sanger sequencing for C79Y
IRAK4 gDNA Rev	CCTAATTGTGGACACCCTGG	Sanger sequencing for C79Y

IRAK4 WT Fwd BamHI	GACGGATCCATGGATTACAAGGATGACGACGATAAGATGAACAAACCCATAACACC	Cloning into pcDNA3.1(+)
IRAK4 WT XhoI Rev	GCATCTCGAGTTAAGAAGCTGTCATCTCTTG	Cloning into pcDNA3.1(+)
IRAK4 Seq1 Fwd	CCACCTGACTCCTCAAGTCC	Sanger sequencing of IRAK4 ORF
IRAK4 Seq2 Rev	GGACTTGAGGAGTCAGGTGG	Sanger sequencing of IRAK4 ORF
IRAK4 Seq3 Fwd	GACTAGCAGAATTGTGGGAAC	Sanger sequencing of IRAK4 ORF
IRAK4 Seq4 Rev	GTTCCCACAATTCTGCTAGTC	Sanger sequencing of IRAK4 ORF
VP1.5 Seq Fwd	CGGGACTTTCCAAAATGTCGT	Sanger sequencing of IRAK4 ORF
SV40 Seq Rev	GCATTCTAGTTGTGGTTTGTCC	Sanger sequencing of IRAK4 ORF
IRAK4 C79Y SDM Fwd	GCACCACAAATTACACAGTTGGTG	SDM in pcDNA3.1(+)
IRAK4 C79Y SDM Rev	CACCAACTGTGTAATTTGTGGTGC	SDM in pcDNA3.1(+)
IRAK4 R12C SDM Fwd	CCATCAACATATGTGTGCTGCCTC	SDM in pcDNA3.1(+)
IRAK4 R12C SDM Rev	GAGGCAGCACACATATGTTGATGG	SDM in pcDNA3.1(+)
IRAK4 SDM Fwd	CGGGACTTTCCAAAATGTCGT	SDM in pcDNA3.1(+)
IRAK4 SDM Rev	GGCACCTTCCAGGGTCAAGG	SDM in pcDNA3.1(+)
IRAK4 EcoRI N-3xFLAG Fwd	GCTGGAATTCGATGAACAAACCCATAACACC	Subcloning into pCI-neo-N-3xFLAG
IRAK4 XbaI N-3xFLAG Rev	CTTCTAGATTAAGAAGCTGTCATCTCTTGC	Subcloning into pCI-neo-N-3xFLAG

IL18RAP HindIII Fwd	ACGAAGCTTCAATGCTCTGTTTGGG CTG	Cloning into pCMV6
IL18RAP XhoI Rev	AGGGCTCGAGTCACCATTCCTTAGG CTGG	Cloning into pCMV6
IL18RAP Seq1 Fwd	CCTACTTCTTGGGAGCACTG	Sanger Sequencing of IL18RAP ORF
IL18RAP Seq2 Rev	CAGTGCTCCCAAGAAGTAGG	Sanger Sequencing of IL18RAP ORF
IL18RAP Seq3 Fwd	GAAATAGTGCTGCTGTACCG	Sanger Sequencing of IL18RAP ORF
IL18RAP Seq4 Rev	CGGTACAGCAGCACTATTTC	Sanger Sequencing of IL18RAP ORF
IRAK4 gRNA1 Fwd[153]	CACCGTATGTGCGCTGCCTCAATG	Cloning into pLentiCRISPR.v2
IRAK4 gRNA1 Rev[153]	AAACACATTGAGGCAGCGCACATAC	Cloning into pLentiCRISPR.v2
IRAK4 gRNA2 Fwd[153]	CACCGAGGCAGCGCACATATGTTGA	Cloning into pLentiCRISPR.v2
IRAK4 gRNA2 Rev[153]	AAACTCAACATATGTGCGCTGCCTC	Cloning into pLentiCRISPR.v2
IRAK4 CRISPR Out Fwd	GTGGAAAAAGGAAGCAAACC	Competitive PCR for CRISPR
IRAK4 CRISPR Out Rev	AGCAACAACTTTAAAACGTCA	Competitive PCR for CRISPR
IRAK4 CRISPR1 In Fwd (F1)	GTGCGCTGCCTCAATGT	Competitive PCR for CRISPR
IRAK4 CRISPR1 In Rev (R1)	CAGCTTCCTAATTAGTCCAACA	Competitive PCR for CRISPR
IRAK4 CRISPR2 In Fwd (F2)	GAACAAACCCATAACACCATCA	Competitive PCR for CRISPR

IRAK4 CRISPR2 In Rev (R2)	GCAGCGCACATATGTTGA	Competitive PCR for CRISPR
IRAK4 cDNA Fwd*	TGGCAAAGTGTCAACATGAAAAC	Gene expression by RT-qPCR
IRAK4 cDNA Rev*	GGTGGAGTACCATCCAAGCAA	Gene expression by RT-qPCR
HPRT1 cDNA Fwd[154]	CTGGCGTCGTGATTAGTGATGATG	Gene expression by RT-qPCR
HPRT1 cDNA Rev[154]	TTGAGCACACAGAGGGCTACAATG	Gene expression by RT-qPCR

*Primer Bank ID: 223671887c2

2.1.9.Kits

Table 2. 9 Kits

Kit	**Catalog #**	**Manufacturer**
NucleoSpin Blood, Mini kit for DNA from blood	740951.50	Macherey-Nagel, Germany
iScript™ cDNA Synthesis Kit	1708891	Bio-Rad, USA
RevertAid First Strand cDNA Synthesis Kit	K1622	Thermo Scientific, USA
NucleoSpin Gel and PCR Clean-up, Mini kit	740609.5	Macherey-Nagel, Germany
GeneJet Plasmid Miniprep Kit	K0502	Thermo Scientific, USA
GeneJET Plasmid Midiprep Kit	K0481	Thermo Scientific, USA
Phire Tissue Direct PCR Master Mix	F170S	Thermo Scientific, USA
GeneJet RNA Purification Kit	K0731	Thermo Scientific, USA
RapidOut DNA removal Kit	K2981	Thermo Scientific, USA

Secreted Alkaline Phosphatase Reporter Gene Assay Kit (Luminescence)	600260	Cayman, USA
Cyto-Fast™ Fix/Perm Buffer Set	426803	Biolegend, USA
The Dual-Glo® Luciferase Assay System	E2920	Promega, USA
FastStart Essential DNA Green Master	06402712001	Roche, USA
WesternBright ECL HRP substrate kit	K-12045-D50	Advansta, USA
LEGENDplex™ Human Anti-Virus Response Panel (13-plex) with V-bottom Plate	740349	Biolegend, USA
IL-6 ELISA MAX™ Standard ELISA Kit	430501	Biolegend, USA
IFN-α2 ELISA MAX™ Deluxe ELISA Kit	446404	Biolegend, USA

2.1.10.Equipment

Table 2. 10 Equipment

Equipment	**Model**	**Manufacturer**
The LightCycler® 96 Instrument	05 815 916 001	Roche, USA
CytoFLEX S	A00-1-1102	Beckman Coulter, USA
NovoCyte® Flow Cytometer	NovoCyte 3000	ACEA Biosciences, USA
Thermal cycler	2720 Thermal cycler	Applied Biosystems, USA
Thermal cycler	TC-512	Techne, USA
pH meter	S-610L	Peak Instruments, USA
Amersham^{TM} Luminescent Image Analyzer	Amersham^{TM} Imager 600	GE Healthcare Life Sciences, USA
2.5 Megapixel HD Microscope Camera	Leica MC120 HD	Leica Microsystems, USA

Inverted Fluorescent Microscope	DMi8 S	Leica Microsystems, USA
Eclipse Inverted Light Microscope	TS100	Nikon, USA
NanoDrop Microvolume UV-Vis Spectrophotometer	NanoDrop One	Thermo Scientific, USA
Microplate Reader	Synergy™ HT	BioTek, Tr
Liquid Nitrogen Refrigerator	LS4800	Worthington Industries, USA
Universal Orbital Shaker OS-20	BOE 8059000	BOECO, Germany

2.1.11.Other materials

Table 2. 11 Other materials

Product	**Catalog #**	**Manufacturer**
WesternBright PVDF-FL membrane roll, 0.45 µm, 26 cm x 3.3 m	L-08025-001	Advansta, USA
PageRuler™ Prestained Protein Ladder, 10 to 180 kDa	26616	Thermo Scientific, USA
GeneRuler 1 kb DNA Ladder	SM0311	Thermo Scientific, USA
Molecular Biology grade water	01-869-1B	Biological Industries, Israel
Diethyl pyrocarbonate (DEPC) water	01-852-1A	Biological Industries, Israel
IDTE, 1X TE Solution	11-01-02-05	Integrated DNA Technologies, USA
0.45µm filter	FJ25ASCCA 004FL01	GVS, Germany
1 mL syringe	70575	Ayset, Tr
10 mL syringe	70607	Ayset, Tr
Mr. Frosty™ Freezing Container	5100-0001	Thermo Scientific, USA
Cryovials, 2 mL	122263	Greiner, USA

BD Vacutainer® Heparin Tubes	367874	BD Biosciences, USA
Mini Trans-Blot® Cell	1703930	BioRad, USA
Mini-PROTEAN Tetra Handcast Systems	1658007FC	BioRad, USA
Hemacytometer Neubauer	C962010	Marienfeld Superior, Germany

2.2.Methods

2.2.1.Patient recruitment and ethics

Clinical history and biological specimens were obtained from the referring clinician, with oral and written informed consents obtained from the patient's parents and healthy donors. All the experiments involving human subjects were conducted in accordance with the institutional, local and national ethical guidelines, and approved by İhsan Doğramacı Bilkent University Ethics Committee (#2022_04_28_01).

2.2.2.Genomic DNA isolation from whole blood

2.2.2.1.Red blood cell lysis

Whole blood samples were received in Heparin containing blood collection tubes and processed immediately on the same day. Approximately 1 mL of blood samples were first transferred into 10 mL conical centrifuge tubes. 9 mL of 1X red blood cell (RBC) lysis solution was added onto the blood samples and mixed by inversion. After 20 minutes of incubation at RT, they were centrifuged at 400 g at RT for 5 minutes. Next, supernatants were removed and pellets were resuspended in 3 mL of 1X RBC lysis solution. After 10 minutes of incubation at RT, they were centrifuged at 400 g at RT for 10 minutes. Supernatants were then removed and pellets were resuspended in 1 mL of 1X RBC lysis solution. Cells were transferred into 1.5 mL centrifuge tubes and centrifuged at 13,000 rpm for 1 minute. Supernatants were removed and pellets were used immediately for genomic DNA (gDNA) isolation.

2.2.2.2.gDNA isolation

gDNA isolation was performed using NucleoSpin Blood mini kit for DNA. Pellets obtained from RBC lysis were resuspended in 200 µL of 1X dPBS. 20 µL of Proteinase K solution was added to the cells and mixed by vortexing. Immediately after that, 400

µL of Lysis solution was added and mixed thoroughly by vortexing. Samples were incubated in previously heated heat-block at 56°C for 10 minutes. Next, 200 µL of absolute ethanol was added and mixed by pipetting. Samples were transferred into a spin columns and centrifuged at 8,000 rpm for 1 minute. Flow-through in the collection tubes were discarded. 500 µL of Wash Buffer WB I was added into spin columns and centrifuged at 10,000 rpm for 1 minute. Flow-through in the collection tubes was discarded. After that, 500 µL of Wash Buffer II was added into spin columns and centrifuged at 13,000 rpm for 3 minutes. Flow-through in the collection tubes was discarded and samples were centrifuged at 13,000 rpm for 1 minute to dry out. Next, spin columns were transferred into 1.5 mL centrifuge tubes. 50 µL of Elution buffer was added into the center of spin columns and incubated at RT for 2 minutes. Samples were then centrifuged at 10,000 rpm for 1 minute. Another 50 µL of Elution buffer was added into the center of spin columns and incubated at RT for 2 minutes. Samples were centrifuged at 10,000 rpm for 1 minute. Spin columns were discarded and the concentration of purified gDNAs collected in 1.5 mL centrifuge tubes was measured using NanoDrop™ One/OneC Microvolume UV-Vis Spectrophotometer. Purified gDNAs were stored at -20°C for further use.

2.2.3.Peripheral blood mononuclear cell isolation

Whole blood was received in Heparin containing blood collection tubes in varying volumes ranging from 6 to 10 mL and processed immediately on the same day. Blood samples were transferred into 15 mL conical centrifuge tubes and diluted with pre-warmed 1x dPBS at 1:1(v/v) ratio at RT. Next, Lymphoprep™ Density Gradient Medium were added into empty 15 mL conical centrifuge tubes at final ratio of the diluted blood:Lymphoprep™ as 2:1(v/v). The diluted blood was layered on top of

Lymphoprep™ separation media, and samples were centrifuged at 800 g for 20 minutes at RT with deceleration adjusted to zero. After centrifugation, 4 distinct layers were formed (Figure 2.1). PBMCs were collected by taking up the cloudy layer using sterile Pasteur pipettes and transferred into 15 mL conical centrifuge tubes containing 3 mL Wash medium (RPMI supplemented with 2% FBS). Next, 15 mL conical centrifuge tubes were filled up to 14 mL Wash medium. Samples were centrifuged at 250 g for 10 minutes and supernatants were removed. PBMCs were washed with 8 mL Wash medium and counted using hemocytometer. Samples were centrifuged at 250 g for 10 minutes and supernatants were removed. PBMC aliquots were resuspended in Freezing medium (FBS + 10% DMSO) in a density of $5x10^6$ cell/mL and transferred into cryovials for cryopreservation using Mr. Frosty™ Freezing Container at -80°C overnight. Next day, cryovials were placed at Nitrogen tank (-196°C) for further use.

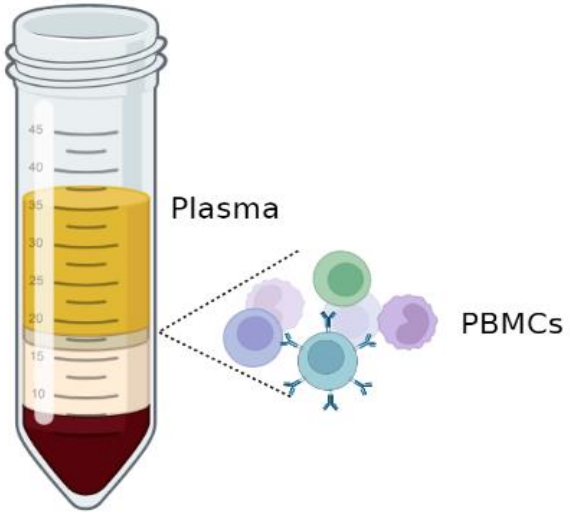

Figure 2. 1 Representative illustration of PBMC isolation from whole blood using density gradient centrifugation. The top-most yellow part is the layer of plasma. The bottom-most red part is the layer of red blood cells and granulocytes. The bottom middle colorless part is the separation media and the upper middle part is PBMCs, seen as a cloudy layer. Created in BioRender

2.2.4.Genetic analysis

2.2.4.1.Whole exome sequencing

Whole exome sequencing (WES) on isolated patient gDNA was performed by WES service provider, Genoks (Ankara, Turkey). Collection of raw sequencing data, sequence alignment to a reference human genome, refinement, variant detection and annotation were done by the service provider. Briefly, WES was performed on DNBSEQ-G400 System (MGI Tech, China) using Human Comprehensive Exome panel (Twist Bioscience, USA) together with paired-end sequencing of 150 base-paired ends. For further processing, data obtained was converted into FASTQ format using BCL2Fastq2 v2.20 conversion software. Mapping of reads in the FASTQ format were performed using two-step alignment and refinement to filter the high occurrence of mismatch pairing. The human genome reference sequence GRCh37 was used for alignments. First alignment was performed with BWA-MEM software and further refinement with Genome Analysis Toolkit was employed. For variant calling and annotations, Genome Analysis Toolkit and SnpEff were used. Additionally, allele frequencies were included in the processed data using the publicly open databases: gnomAD 2.1.1 (https://gnomad.broadinstitute.org/) including subpopulations of African, Ashkenazi Jewish, Finnish, non-Finnish European, South Asian, East Asian, and Latino, and 1000 Genomes Project (http://grch37.ensembl.org/).

2.2.4.2.Variant filtering

Initial filtering of the annotated variations on the patient's WES data was performed with the help of Yılmaz Yücehan Yazıcı. Briefly, low quality variants (identified as variants with mapping quality (MQ) <40 and genotype quality (GQ) <30) with low depth coverage (identified as variants with reads (DP) <5) were excluded. Next,

nonsynonymous variations including insertion, deletion, missense, start-lost, stop-lost and stop-gain, and essential splicing variants (located in the 2 base-pair range of exon-intron boundaries) were selected. Last, variants with minor allele frequency (MAF) higher than 1% in public databases were filtered out.

For *in silico* prediction of variant impact, gene damaging index (GDI)[155] based on the 1000 Genomes Project database, Combined annotation-dependent depletion (CADD) v1.6 (https://cadd.gs.washington.edu/score)[156], Mutation Significance Cutoff (MSC)[157], Sorting intolerant from tolerant (SIFT)[158] and Polymorphism Phenotyping v2 (PolyPhen-2)[159] tools were utilized. We also checked whether any homozygote carriers for the filtered homozygous variants in the patient were listed in the gnomAD 2.1.1 database. In addition to *in silico* damage prediction tools, expression profiles, known functions and clinical significance of the mutated genes were obtained from Human Protein Atlas (https://www.proteinatlas.org/), NCBI (https://www.ncbi.nlm.nih.gov/) and OMIM (https://www.omim.org/) databases.

2.2.5.Sanger sequencing of gDNA

Validation of the *IRAK4* mutation status in the patient and his family was performed by the amplification of around 300 bp region encompassing the target *IRAK4* mutation using gDNA samples as DNA template for the PCR reaction. Primers recognizing the indicated gDNA region were listed in the Table 2.1.8 as IRAK4 gDNA Fwd and IRAK4 gDNA Rev.

Table 2. 12 gDNA sequencing reaction

Component	**Volume (µL)**
Taq Polymerase	0.2
10x Taq Buffer	5
dNTP mix	1
IRAK4 gDNA Fwd	2
IRAK4 gDNA Rev	2
$MgCl_2$	4
Gdna	75 ng
Molecular Biology grade water	up to 50
Total volume	**50**

Table 2. 13 gDNA sequencing reaction conditions

Step	**Temperature (°C)**	**Duration (s)**	**Cycle**
Initial Denaturation	95	180	1
Denaturation	95	30	35
Annealing	60	30	
Extension	72	30	
Final extension	72	300	1
Final hold	4	-	Hold

The expected size of the PCR amplicons (303 bp) was confirmed with agarose gel electrophoresis. After confirmation of the size, PCR amplicons were purified using NucleoSpin Gel and PCR Clean-up, Mini kit. Purified amplicons were Sanger

sequenced by the service provider, Macrogen (Europe). Sequence analysis were performed by using Unipro UGENE software (Unipro, Russia).

2.2.6.Agarose gel electrophoresis

1% Agarose gel was prepared as indicated in Table 2.2. 10% (v/v) of PCR products were mixed with 10X Orange loading dye and loaded into 1% agarose gel and run at 120V for 30 minutes. Visualization was performed using Amersham™ Imager 600.

2.2.7.Cloning of *IRAK4* Constructs

2.2.7.1.Generation of cDNA template

RNA isolation of THP-1 cells was performed with GeneJet RNA isolation kit. THP-1 cell pellet was lysed with 600 µL Lysis buffer on ice and vortexed for 10 seconds. 360 µL 99% Ethanol was added onto the cell lysate and mixed with pipetting. 700 µL of the mixture was transferred into a spin column inserted into a collection tube and centrifuged at 13,000 rpm for 1 minute. Flow through was discarded and same step was applied to the remaining 260 µL of mixture. Spin column was washed with 700 µL Wash Buffer 1 and centrifuged at 13,000 rpm for 1 minute. Flow through was discarded. Spin column was washed with 700 µL Wash Buffer 2 and centrifuged at 13,000 rpm for 1 minute. This step was repeated with 250 µL Wash Buffer 2. After flow through was discarded, spin column was re-centrifuged at 13,000 rpm for 1 minute. Next, spin column was inserted into an empty 1.5 mL centrifuge tube. 50 µL Elution buffer was added into the spin column and incubated for 2 minutes at RT. It was centrifuged at 13,000 rpm for 2 minutes. Spin column was discarded and concentration of isolated total RNA was measured using NanoDrop™ One/OneC Microvolume UV-Vis Spectrophotometer. Isolated RNA samples were stored at -80°C for further use.

Next, cDNA from the isolated total RNA was synthesized using iScript™ cDNA Synthesis Kit. Generated cDNA was used immediately.

Table 2. 14 Reaction for cDNA synthesis from THP-1 RNA

Component	**Volume (µL)**
5X iScript Reaction Mix	4
iScript Reverse Transcriptase	1
Nuclease-free water	13.5
RNA template (600 ng)	1.5
Total volume	**20**

Table 2. 15 Conditions of reaction for cDNA synthesis from THP-1 RNA

Step	**Temperature (°C)**	**Duration (s)**
Priming	25	5
Reverse transcription	46	20
RT inactivation	95	1
Final hold	4	Hold

2.2.7.2.Generation of *IRAK4* open reading frame

The human canonical *IRAK4* cDNA (ENST00000613694.5, NM_016123.4) open reading frame (ORF) was obtained from THP-1 cDNA. *IRAK4* ORF was obtained using forward primer IRAK4 WT Fwd BamHI including a BamHI restriction site and a FLAG (DYKDDDDK)-tag sequence, together with the reverse primer, IRAK4 WT Rev XhoI, including a XhoI restriction site.

Table 2. 16 Reaction for generation of full length *IRAK4* ORF

Component	**Volume (µL)**
Q5 HiFi DNA Polymerase	0.5
5X Q5 Buffer	5
dNTP mix (10 µM)	1
IRAK4 WT Fwd BamHI	5
IRAK4 WT Rev XhoI	5
cDNA	5
Q5 Enhancer	10
Molecular Biology grade water	up to 50
Total volume	**50**

Table 2. 17 Reaction conditions for generation of full length *IRAK4* ORF

Step	**Temperature (°C)**	**Duration (s)**	**Cycle**
Initial Denaturation	98	45	1
Denaturation	98	10	38
Annealing	60	20	
Extension	72	45	
Final extension	72	120	1
Final hold	4	-	Hold

The expected size of the PCR product (1,427 bp) was confirmed with agarose gel electrophoresis. After that, the PCR product was extracted from agarose gel using NucleoSpin Gel and PCR Clean-up, Mini kit.

2.2.7.3.Restriction digestion of PCR products and vectors

Whole purified PCR amplicon and 700 ng of pcDNA3.1(+) mammalian expression vector were digested using BamHI and XhoI restriction enzymes for 3 hours at 37°C water bath.

Table 2. 18 Restriction enzyme digestion reaction for pcDNA3.1 vector and purified PCR products

Component	**Volume (µL)**
Purified PCR product/ plasmid DNA	700 ng
10X rCutSmart Buffer	5
XhoI	1
BamHI-HF	1
Molecular Biology grade water	up to 50
Total volume	**50**

After digestion, products were purified using NucleoSpin Gel and PCR Clean-up, Mini kit. After that, the concentration ratio of the digested products was determined with agarose gel electrophoresis.

2.2.7.4.Ligation of digested products

The digested *IRAK4* WT ORF fragment was inserted into the digested pcDNA3.1(+) mammalian expression vector using T4 DNA Ligase for 15 minutes at RT.

Table 2. 19 Ligation reaction for digested pcDNA3.1 vector and PCR products

Component	**Volume (µL)**
10X T4 DNA Ligase Buffer	0.5
Vector DNA	1.0
Insert DNA	3.0
T4 DNA Ligase	0.5
Total volume	**10**

2.2.7.5.Transformation of the ligation products

The ligation product was transformed into DH5α competent cells. Generation of DH5α competent cell stocks were described in Appendix C. First, 5 µL of ligation product was added onto 50 µL of competent cells and mixture was incubated on ice for 15 minutes. Next, heat shock was performed at 42°C for 45 seconds followed by incubation on ice for 2 minutes. After that, 800 µL LB Broth media was added and incubated in an orbital shaker incubator for 45 minutes at 37°C. After incubation, 100 µL bacteria was spread on LB Agar plates containing Ampicillin. Plates were incubated overnight at 37°C.

2.2.7.6. Colony PCR and selection of positive colonies

Single colonies of competent bacteria were selected and diluted with 50 µL Molecular Biology grade water. Colony PCR was performed by bacteria dilutions as template DNA using Taq polymerase.

Table 2. 20 Colony PCR reaction

Component	**Volume (µL)**
Taq DNA polymerase	0.1
5X Red Buffer	5
10 µM dNTP mix	0.5
VP1.5 Seq Fwd	1
SV40 Seq Rev	1
Bacterial sample	2.5
Molecular biology grade water	up to 25
Total volume	**20**

Table 2. 21 Colony PCR reaction conditions

Step	**Temperature (°C)**	**Duration (s)**	**Cycle**
Initial Denaturation	95	300	1
Denaturation	95	25	30
Annealing	60	20	
Extension	72	120	
Final extension	72	300	1
Final hold	4	-	Hold

The expected size of the bands with colonies containing the plasmid with *IRAK4* WT insert (1,730 bp) were confirmed with agarose gel electrophoresis. After confirmation, positive colonies were selected for the generation and isolation of plasmids. 3 mL LB

Broth containing ampicillin was added onto bacteria dilutions of selected colonies and incubated in an orbital shaker incubator overnight at 37°C.

2.2.7.7.Isolation of plasmid DNA

Plasmid isolation from insert-positive plasmid containing bacteria was performed using GeneJET Plasmid Miniprep kit. First, overnight incubated bacteria were centrifuged at 13,000 rpm for 1 minute in RT. Supernatant was removed and the bacteria pellet was completely resuspended in 250 µL Resuspension buffer. Bacteria solution was then transferred into a 1.5 mL centrifuge tube and 250 µL Lysis solution was added. Immediately, tube was inverted 5 times. 350 µL of Neutralization solution was added and again tube was inverted 5 times. Next, bacteria solution was centrifuged at 13,000 rpm for 5 minutes and supernatant was transferred into a GeneJET spin column. It was centrifuged at 13,000 rpm for 1 minute and flow-through was discarded. 500 µL Wash solution was added to the column and centrifuged at 13,000 rpm for 1 minute. Flow-through was discarded and wash step was repeated. Spin column was centrifuged at 13,000 rpm for 1 minute. After that, it was transferred into an empty 1.5 mL centrifuge tube. 50 µL Elution buffer was added and incubated at RT for 2 minutes. Last, plasmid DNA is eluted by centrifugation at 13,000 rpm for 1 minute. Concentration of purified plasmid DNAs were measured using NanoDrop™ One/OneC Microvolume UV-Vis Spectrophotometer and stored at -20°C for further use.

2.2.7.8.Sanger sequencing of purified plasmids

All plasmids were confirmed by Sanger Sequencing provided by the service provider, Macrogen (Europe). Primer sequences are provided in Table 2.1.8.

2.2.7.9.Site-directed mutagenesis

Site-directed mutagenesis (SDM) was used to generate *IRAK4* variants (p.C79Y and p.R12C) by performing a modified overlap-extension PCR-based method[160]. *IRAK4* p.C79Y was amplified with IRAK4 SDM Fwd/IRAK4 C79Y SDM Rev and IRAK4 C79Y SDM Fwd/IRAK SDM Rev primers in two separate reactions, using pcDNA3.1-IRAK4 WT plasmid as the template. Likewise, *IRAK4* p.R12C was amplified with IRAK4 SDM Fwd/IRAK4 R12C SDM Rev and IRAK4 R12C SDM Fwd/IRAK SDM Rev primers in two separate reactions, using pcDNA3.1-IRAK4 WT plasmid as the template.

Table 2. 22 SDM PCR reaction

Component	**Volume (µL)**
Q5 HiFi DNA Polymerase	0.5
5X Q5 Buffer	5
10 µM dNTP mix	0.5
IRAK4 SDM Fwd	2.5
IRAK4 SDM Rev	2.5
pcDNA3.1(+)-IRAK4 WT	2.5 ng
Molecular Biology grade water	up to 25
Total volume	**25**

Table 2. 23 SDM PCR reaction conditions

Step	**Temperature (°C)**	**Duration (s)**	**Cycle**
Initial Denaturation	98	30	1
Denaturation	98	10	35
Annealing	60	15	
Extension	72	30	
Final extension	72	120	1
Final hold	4	-	Hold

The expected sizes of the PCR amplicons (for p.C79Y DNA fragment 1: 480 bp, DNA fragment 2: 1,274 bp; and for p.R12C DNA fragment 1: 275 bp, DNA fragment 2: 1,479 bp) were checked with agarose gel electrophoresis. Next, amplicons were purified using NucleoSpin Gel and PCR Clean-up, Mini kit. After that, amplicons were annealed by one-step overlap extension reaction.

Table 2. 24 One-step overlap extension PCR reaction

Component	**Volume (µL)**
Q5 HiFi DNA Polymerase	1
5X Q5 Buffer	10
10 µM dNTP mix	1
DNA fragment 1	1
DNA fragment 2	1
Molecular Biology grade water	up to 40
VP1.5 Seq Fwd	5
SV40 Seq Rev	5
Total volume	**25**

Table 2. 25 Conditions for one-step overlap extension PCR reaction

Step	Temperature (°C)	Duration (s)	Cycle
Initial Denaturation	98	30	1
Annealing	50	20	1
Extension	72	30	1
Primers were added.			
Initial Denaturation	98	30	1
Denaturation	98	10	38
Annealing	60	15	
Extension	72	60	
Final extension	72	120	1
Final hold	4	-	Hold

The expected size of the PCR amplicons (1,730 bp) was confirmed with agarose gel electrophoresis. After confirmation of the size, annealed PCR products were purified using NucleoSpin Gel and PCR Clean-up, Mini kit. After that, for both mutants, restriction digestion, ligation, transformation and colony PCR were performed following the protocols as described above. All plasmids were confirmed by Sanger Sequencing.

2.2.7.10.Subcloning of *IRAK4* constructs

In order to generate constructs encoding IRAK-4 with an in-frame N-terminal 3xFLAG tag, pcDNA3.1-IRAK4 WT, pcDNA3.1-IRAK4 C79Y and pcDNA3.1-IRAK4 R12C

plasmids were then used as DNA templates and amplified by using the forward primer IRAK4 EcoRI N-3xFLAG Fwd and the reverse primer IRAK4 XbaI N-3xFLAG Rev.

Table 2. 26 PCR reaction for *IRAK4* subcloning into pCI-neo-N-3xFLAG vector

Component	**Volume (µL)**
AQ97 HiFi DNA Polymerase	0.5
5X AQ97 Buffer	10
10 µM dNTP mix	1
IRAK4 EcoRI Fwd	5
IRAK4 XbaI Rev	5
pcDNA3.1(+)-IRAK4 WT or pcDNA3.1(+)-IRAK4 C79Y or pcDNA3.1(+)-IRAK4 R12C	10 ng
Molecular Biology grade water	up to 50
Total volume	**50**

Table 2. 27 PCR reaction conditions for *IRAK4* subcloning into pCI-neo-N-3xFLAG vector

Step	Temperature (°C)	Duration (s)	Cycle
Initial Denaturation	98	120	1
Denaturation	98	20	40
Annealing	56	15	
Extension	72	60	
Final extension	72	300	1
Final hold	4	-	Hold

The expected size of the PCR amplicons (1,401 bp) was checked with agarose gel electrophoresis. After that, amplicons were purified using NucleoSpin Gel and PCR Clean-up, Mini kit.

Purified amplicons and 500 ng of empty pCI-neo-N-3xFLAG mammalian expression vectors were digested with EcoRI and XbaI restriction enzymes at 37°C for 3 hours. Next, ligation, transformation and colony PCR were performed following the protocols as described above. All plasmids, named as pCI-neo-N-3xFLAG-IRAK4 WT, pCI-neo-N-3xFLAG-IRAK4 C79Y and pCI-neo-N-3xFLAG-IRAK4 R12C, were confirmed by Sanger Sequencing.

In order to generate constructs encoding IRAK-4 without a tag, 3 µg of pCI-neo-N-3xFLAG-IRAK4 WT, pCI-neo-N-3xFLAG-IRAK4 C79Y and pCI-neo-N-3xFLAG-IRAK4 R12C plasmids and empty pCI-neo-C-3XFLAG mammalian expression vectors were digested with EcoRI and XbaI restriction enzymes at 37°C for 3 hours. Next, digested empty pCI-neo-C-3xFLAG was purified using NucleoSpin Gel and

PCR Clean-up, Mini kit. Additionally, the size of the digested *IRAK4* constructs (1394 bp) were determined by agarose gel electrophoresis. After that, *IRAK4* DNA fragments with a stop codon but no N-terminal FLAG tag (lower band, 1,394 bp) were purified from agarose gel using NucleoSpin Gel and PCR Clean-up, Mini kit. Next, ligation, transformation and colony PCR were performed following the protocols as described above. All plasmids, named as pCI-neo-No tag-IRAK4 WT, pCI-neo-No tag-IRAK4 C79Y and pCI-neo-No tag-IRAK4 R12C, were confirmed by Sanger Sequencing.

2.2.8.Cell culture

2.2.8.1.Maintenance and propagation of cell lines

Mammalian cells were maintained in an incubator supplied with 5% CO_2 at 37°C. HEK293 cells were cultured with DMEM High Glucose growth medium supplemented with 10% (v/v) FBS. *IRAK4* KO HEK293 cell lines were cultured with under selection with puromycin at a final concentration of 4 µg/mL in DMEM High Glucose growth medium supplemented with 10% (v/v) FBS. THP-1 cells were cultured with RPMI 1640 growth medium supplemented with 20% (v/v) FBS.

HEK293 cells and *IRAK4* KO HEK293 cell lines maintained in T75 culture flasks were passaged every 2 days with a 1:8 ratio (v/v). Passaging was performed by following these steps; removing the old culture media, washing by 4 mL dPBS solution, detachment by 4 mL Trypsin-EDTA solution with an incubation in the incubator for 3 minutes, collection of cells by adding 6 mL fresh culture media and final centrifugation at 300 g for 5 minutes. After centrifugation, cell pellet was resuspended in fresh culture medium and appropriate volume according to the passage ratio was transferred to the same T75 culture flask.

THP-1 cells maintained in T25 culture flasks were passaged every 3 days with 1:1.5 (v/v) ratio. Passaging was performed by adding fresh medium onto the suspension cells.

PBMCs from the patient, his healthy family members including the parents (26 and 30 years old) and his 2 years older sister, and unrelated healthy donors who were male and between 20 and 25 years of age, were cultured with RPMI 1640 medium supplemented with 10% (v/v) FBS.

2.2.8.2.Cryopreservation of cells

When adherent cells become confluent, old medium was removed and cells were washed with dPBS solution. Adherent cells were detached by Trypsin-EDTA solution. After trypsinization, cells were collected by 6 mL fresh culture media and centrifuged at 300 g for 5 minutes. After centrifugation, supernatant was discarded and cell pellets were resuspended in freezing medium composed of FBS solution with 10% (v/v) DMSO. 1 mL of cell suspension (7 million cells/mL for HEK293 cells) was transferred into each cryovial and placed at -80°C in a Mr. Frosty Cell Freezing Container overnight. THP-1 cells were collected and centrifuged at 300 g for 5 minutes. After centrifugation, the supernatant was discarded and cell pellets were resuspended in a freezing medium composed of FBS solution with 10% (v/v) DMSO. 1 mL of cell suspension (10 million cells/mL for THP-1 cell line) was transferred into each cryovial and placed at -80°C in a Mr. Frosty Cell Freezing Container overnight. Last, cryovials were transferred into liquid nitrogen for long-term storage.

2.2.8.3.Thawing of frozen cell lines

Cryovials containing frozen cells were taken from liquid nitrogen tank and rapidly thawed at 37°C water bath. Fresh growth medium was added to collect thawed cells

from cryovials. Cell suspension was transferred into a 15 mL canonical centrifuge tube and centrifuged at 300 g for 5 minutes. Supernatant was discarded and cell pellet was resuspended in fresh growth medium. Cell suspension was transferred into appropriate culture flask and maintained in an incubator supplied with 5% CO_2 at 37°C.

2.2.8.4.Transient transfection of mammalian cell lines

HEK293 cells were seeded on 24-well plates at a density of 1.5 x 10^5 cells/mL (500 µL/well) and incubated overnight at 37°C, 5% CO_2. After 16-18 hours of incubation, cells with 70%-80% confluency were transfected with a total amount of 500 ng plasmid per one well of a 24-well plate.

For transfection using Lipofectamine 2000 reagent, desired amounts of plasmids were transferred into a 1.5 mL centrifuge tube and plasmids were diluted with 25 µL Opti-MEM. In another centrifuge tube, 1.5 µL of Lipofectamine 2000 transfection reagent was diluted with 25 µL Opti-MEM. The diluted Lipofectamine-Opti-MEM mixture was added onto the diluted plasmids and mixed well by pipetting. The complete mixture was incubated at RT for 20 minutes. Next, diluted transfection complexes were added onto wells of 24-well plate drop by drop. Cells were incubated for 48 hours at 37°C, 5% CO_2 until further use.

For transfection using XtremeGene-9 reagent, desired amounts of plasmids were transferred into a centrifuge tube and plasmids were diluted with 25 µL Opti-MEM. In another centrifuge tube, 1.5 µL of XtremeGene-9 transfection reagent was diluted with 25 µL Opti-MEM. The diluted reagent-Opti-MEM mixture was added onto the diluted plasmids and mixed well by pipetting. The complete mixture was incubated at RT for 15 minutes. Next, diluted transfection complexes were added onto wells of 24-well

plate drop by drop. Cells were incubated for 48 hours at 37°C, 5% CO_2 until further use.

Transient transfection with both reagents were performed with a ratio of 1:3 (3 µL of reagent for 1 µg DNA). Total DNA amount and the volume of transfection reagent was adjusted according to the size of the cell culture plate used in the experiment.

2.2.9.Immunoblotting

Immunoblotting using the lysates from transiently transfected HEK293 cells was performed with the help of Umut Tank.

2.2.9.1.Cell lysis and protein extraction

Cells were harvested with PBS-EDTA solution and centrifuged at 13,000 rpm for 1 minute. The supernatant was discarded, and cell lysis was performed by resuspending cell pellets in ice-cold complete RIPA lysis buffer containing a protease and phosphatase inhibitor cocktail. In order to homogenize the cell lysates, they were passed through 1 mL syringes and incubated on ice for 30 minutes. Next, lysates were centrifuged at 13,000 rpm for 20 minutes at +4°C. The supernatants containing protein extracts were transferred into a new 1.5 mL centrifuge tube and stored at -20°C for further use.

2.2.9.2.Quantification of total protein

The total protein concentration of the cell lysates was determined using TaKaRa BCA Protein Assay Kit. After cell lysate samples were thawed on ice, they were diluted with Molecular Biology grade water at 1:100 (v/v) ratio. Bovine serum albumin (BSA) protein standards were prepared as shown in Table 2.28. 100 µL of diluted protein samples and diluted BSA standards were transferred into a flat bottom 96-well plate. 100 µL of Bicinchoninic acid (BCA) solution, prepared by mixing Reagent A and

Reagent B at 1:100 (v/v) ratio, were added on top of them. Plate was incubated at 37°C for 1.5 hours and absorbance values were measured with Synergy HT Microplate Reader at 620 nm. Standard curves were plotted using absorbance values of BSA protein standards and total protein concentrations of protein extracts were calculated accordingly.

Table 2. 28 Preparation of BSA standards for BCA assay

BSA (µL)	Molecular Biology grade H_2O (µL)	Concentration (µg/mL)
0	400	0
40	260	10
80	320	20
120	280	30
160	240	40
200	200	50
280	120	70
400	0	100

2.2.9.3.Preparation of protein samples for immunoblotting

Cell lysates with desired amount of protein was transferred into a 1.5 mL centrifuge tubes. 4X Laemmli sample buffer and 10X DTT were added onto the lysates. Volume adjustments were performed by completing the samples up to 30 µL using complete RIPA lysis buffer. Last, samples were boiled at 95°C for 5 minutes, and subjected to immunoblotting.

2.2.9.4.SDS/PAGE

SDS/PAGE was performed using 12% polyacrylamide gels containing SDS. Polyacrylamide gels (stacking and separating) were prepared as shown in Table 2.2 using gel casting apparatus. Following polymerization, casted polyacrylamide gels were placed into the vertical electrophoresis cells inside a western blotting tank filled with 1X Running buffer. Boiled protein samples kept at RT were loaded into polyacrylamide gels. Sample running was performed initially at 80 V for 20 minutes and then set up to 120 V for 1.5 hours.

2.2.9.5.Wet transfer of proteins onto membrane

Proteins in the polyacrylamide gels were transferred onto polyvinylidene difluoride (PVDF) membranes using Wet transfer system. Transfer sandwiches were prepared in 1X Transfer buffer containing buckets with the following order: one fiber pad, two blotting papers, PVDF membrane, polyacrylamide gel, two blotting papers and one fiber pad. The transfer sandwiches then placed into the transfer cassette in the transfer tank. The tank was filled with ice-cold 1X Transfer buffer and placed in a container filled with ice. Wet transfer was performed at 250 mA for 2 hours on ice.

Last, blotted membranes were stained with Ponceau dye for 2 minutes in order to check transfer efficiency. After staining, membranes were washed with 1X TBS for 5 minutes and blocked with 10% skimmed milk for 30 minutes at RT. After blocking, membranes were washed three times with 1X TBS-T for 5 minutes.

2.2.9.6.Protein detection

Immunoblotting was performed using primary and secondary antibodies listed in Table 2.5. Membranes were incubated with anti-FLAG or anti-human IRAK-4 Alexa Fluor 647 antibodies on an orbital shaker at +4°C overnight. As a transfection efficiency

control, membranes were incubated with anti-GFP antibody on an orbital shaker at +4°C overnight. As a loading control, membranes were incubated with anti-human GAPDH antibody on an orbital shaker at RT for 4 hours. After primary antibody incubation, membranes were washed three times with 1X TBS-T at RT for 5 minutes. Membranes were then incubated with secondary antibody on an orbital shaker at RT for 30 minutes. After secondary antibody incubation, membranes were washed three times with 1X TBS-T at RT for 5 minutes.

WesternBright® ECL Chemiluminescent HRP Substrate Kit was used for the detection of antibodies. WesternBright ECL components were mixed at a ratio of 1:1 to obtain 0.1 ml/cm^2 reagent. They were applied on membranes at RT for 2 minutes in dark. Detection was performed using the Amersham Imager 600.

2.2.9.7.Stripping and re-immunoblotting of blotted membranes

In order to sequentially analyze the blotted membranes with multiple antibodies, stripping and reprobing was performed. After detection of the first primary antibody, blotted membranes were stripped with Mild Stripping Buffer on an orbital shaker at RT for 10 minutes. Next, membranes were washed with 1X TBS-T for 5 minutes. After stripping, membranes were blocked with 10% skimmed milk for 30 minutes at RT. After blocking, membranes were washed three times with 1X TBS-T for 5 minutes. Finally, membraned were ready for re-immunoblotting following the protocol as described above.

2.2.9.8.Protein stability assay

HEK293 cells were seeded on 12-well plates at a density of 3x10^5 cells/mL (1 mL/well) and incubated overnight at 37°C, 5% CO2. After 16-18 hours, cells were transfected with total of 1 μg of desired plasmids in the presence of Lipofectamine 2000 according

to the protocol described above. At 24 hours after transfection, cell media was removed and cells were added with fresh medium containing cycloheximide (final concentration of 50 μg/mL) or 0.5% DMSO as vehicle control. Cells were then collected after 12 hours and subjected to immunoblotting as described above. ImageJ software (National Institutes of Health, USA) was used to calculate the band intensities for each lane, as described (http://rsbweb.nih.gov/ij/). The percent reduction in IRAK-4 and GFP levels was calculated by the FLAG/GAPDH and GFP/GAPDH ratios of CHX treatment to that of DMSO treatment (vehicle control), which was set to 100, respectively.

2.2.10.RNA extraction and gene expression analysis

2.2.10.1.RNA isolation

Total RNA was isolated from approximately $2x10^6$ PBMCs of patient and three healthy unrelated controls using GeneJet RNA Purification Kit according to the protocol described above (2.2.6.1).

2.2.10.2.DNase treatment

RNA samples were treated with *DNase I* in order to remove any gDNA contamination using RapidOut DNA Removal Kit. DNase treatment was performed at 37°C heat block for 30 minutes. Next, 2 μL of DNase Removal Reagent was added onto each tube and incubated at RT for 2 minutes. Samples were then centrifuged at 13,000 rpm for 2 minutes and supernatants containing pure RNA samples were immediately used.

Table 2. 29 DNase reaction for DNA removal from RNA samples

Component	**Volume (µL)**
10X DNase buffer with $MgCl_2$	1
DNase I, RNase-free	0.5
Template RNA	1 µg
DEPC water	up to 10
Total volume	**10**

2.2.10.3.cDNA synthesis

cDNA constructs were synthesized from DNase-treated RNA samples using RevertAid First Strand cDNA Synthesis Kit.

Table 2. 30 cDNA synthesis reaction for gene expression analysis

Component	**Volume (µL)**
5X Reaction Buffer	4
Oligo (dT)18 primer	1
10 mM dNTP Mix	2
RiboLock RNase Inhibitor (20 U/µL)	1
RevertAid M-MuLV RT (200 U/µL)	1
Template RNA	500 ng
DEPC water	up to 20
Total volume	**20**

Table 2. 31 cDNA synthesis reaction conditions for gene expression analysis

Step	Temperature (°C)	Duration (min)
Reverse transcription	42	60
Reverse transcription	70	5
Final hold	4	Hold

2.2.10.4.Real-time quantitative PCR

Synthesized cDNA samples were diluted with DEPC water to the concentration of 100 pg/µL. Real-time quantitative PCR (RT-qPCR) was performed using LightCycler® 480 SYBR Green I Master kit. Detection was performed in LightCycler® 96 Real-Time PCR system.

Table 2. 32 RT-qPCR reaction for gene expression analysis

Component	Volume (µL)
cDNA (100 pg/µL)	2
IRAK4 cDNA Fwd/ HPRT1 cDNA Fwd	1
IRAK4 cDNA Rev/ HPRT1 cDNA Rev	1
LightCycler® 480 SYBR Green I Master	5
DEPC water	1
Total volume	**10**

Table 2. 33 RT-qPCR reaction conditions for gene expression analysis

Step	Temperature (°C)	Ramp (°C/s)	Duration (s)	Cycle	Acquisition mode
Pre-incubation	95	4.8	600	1	None
3-step amplification	95	4.8	10	40	None
	60	2.5	20		None
	72	4.8	30		Single
Melting	95	4.8	10	1	None
	65	2.5	10		None
	97	-	60		5 readings / °C
Cooling	40	2.0	10		None

2.2.11.Luciferase reporter assay

IRAK4 KO HEK293 single cell clones (KO#1 and KO#2) were seeded on 96-well plates at a density of 2.5 x 10^5 cells/mL (100 µL/well) and incubated overnight at 37°C, 5% CO2. After 16 hours of incubation, cells with 70%-80% confluency were co-transfected with constructs encoding NFκB-dependent Firefly luciferase, RLTK (Renilla luciferase), IL-18 receptor associated protein (IL18RAP), and WT or mutant IRAK-4 by transient transfection of mammalian cell protocol mentioned above. Cells were incubated 24 hours at 37°C, 5% CO_2. After 24 hours of incubation, cells were stimulated with recombinant human IL-18 protein at a final concentration of 10 ng/mL. 12 hours after stimulation, luciferase signal was measured using Dual-Glo® Luciferase Assay System. Cells were lysed with 50 µL/well Dual-Glo® Luciferase buffer

supplemented with Dual-Glo® Luciferase Substrate for 10 minutes with constant shaking. Firefly luciferase was measured using Synergy HT Microplate Reader by luminescence signal detection with gain at 100. For cessation of Firefly luciferase and measurement of Renilla luciferase, Dual-Glo® Stop & Glo® mixture was prepared with Dual-Glo® Stop & Glo® Substrate and Dual-Glo® Stop & Glo® Buffer with a ratio of 1:100 (v/v). 50 µL/well Dual-Glo® Stop & Glo® mixture was added onto the wells and incubated for 10 minutes with constant shaking. Renilla luciferase was measured using Synergy HT Microplate Reader by luminescence signal detection with gain at 100. Relative luciferase activity was calculated as the ratio of Firefly luciferase to Renilla luciferase activity and was set for the empty plasmid as 1.

2.2.12.Staining for flow cytometry

For cell surface staining, PBMCs were washed with FACS buffer (dPBS containing %2 FBS) and resuspended at a density of $2x10^6$ cells/mL. Antibody staining was performed for 30 minutes on ice in dark in centrifuge tubes. Next, cells were washed with FACS buffer.

For intracellular staining, surface-stained cells were fixed with Fixation buffer for 30 minutes at RT. Intracellular staining was performed by indicated antibodies in Perm Buffer for 30 minutes at RT. Next, cells were washed with FACS buffer one time. After that, cells were acquired on CytoFLEX Flow Cytometer and NovoCyte® Flow Cytometer. Analysis were performed with FlowJO (BD Biosciences, USA) software.

2.2.13.*In vitro* stimulation of PBMCs

PBMCs were seeded on a round-bottom 96-well plate at a density of $3x10^6$ cells/mL (200 µL/well) in RPMI supplemented with 10% FBS. They were then stimulated with PAM3CSK4 (TLR2/TLR1 agonist), Flagellin (TLR5 agonist) and LPS (TLR4 agonist)

for 6 hours in the presence of Brefeldin A. Next, cells were harvested with FACS buffer and intracellular TNF production in $CD14^+$ monocytes was measured via flow cytometry as described above.

2.2.14.Multiplex bead-based immunoassay

PBMCs were seeded on a round-bottom 96-well plate at a density of $2x10^6$ cells/mL (200 µL/well) in RPMI supplemented with 10% FBS. Cells were stimulated with R848 (Resiquimod, TLR7 and TLR8 agonist), Poly(I:C)-LMW (TLR3 agonist), LPS (TLR4 agonist), CpG (TLR9 agonist), 2'3'-cGAMP (STING ligand) and Poly(dA:dT) (Cytosolic DNA sensor agonist). After 24 hours, culture supernatants were collected and subjected to LEGENDplex Human Anti-Virus Response Panel according to the manufacturer's instructions. Briefly, 25 µL of diluted standards and samples were added to assigned U-bottom 96 well plate. On each well, 25 µL of Assay buffer was added. Next, mixed beads were vortexed for 1 minute and 25 µL of mixed beads were added onto each well. Plate was sealed and covered with aluminum foil to prevent light exposure and incubated for 2 hours at RT in an orbital shaker. Plate was centrifuged at 250 g for 5 minutes and supernatant was discarded. On each well, 25 µL of detection antibody was added. Plate was resealed and incubated for 1 hour at RT in an orbital shaker. After that, 25 µL of SA-PE was added onto each well. Plate was resealed and incubated for 30 minutes at RT in an orbital shaker. Plate was centrifuged at 250 g for 5 minutes and supernatant was discarded. On each well, 150 µL of 1x Wash buffer was added and beads were resuspended by pipetting. After resuspension, samples were acquired using NovoCyte® Flow Cytometer with the technical help from İhsan Gürsel Lab members. Analysis was performed using LEGENDplex™ Data Analysis Software with the help of Serkan Belkaya.

2.2.15.Enzyme-linked immunosorbent assay

PBMCs were seeded on a round-bottom 96-well plate at a density of $2x10^6$ cells/mL (200 µL/well) in RPMI supplemented with 10% FBS. Cells were stimulated with R848, Poly(I:C)-LMW, CpG, 2'3'-cGAMP, poly(dA: dT) and PMA/Ionomycin. After 24 hours, culture supernatants were collected and subjected to ELISA MAX™ Standard Set Human IL-6 and ELISA MAX™ Deluxe Set Human IFN-α2 according to the manufacturer's instructions. Briefly, one day prior to the assay, 96 Well Flat Bottom High Binding ELISA Plates (Greiner, USA) were coated with 100 µL Capture antibody in Coating buffer and incubated overnight at +4°C. Capture antibodies were then discarded and plates were washed with 1X Wash buffer. In order to block non-specific bindings, wells were blocked with 1X Assay diluent for 1 hour at RT in an orbital shaker. Wells were washed with 1X Wash buffer and 100 µL of diluted standards or samples were added to assigned wells. Plate was sealed and incubated for 2 hours at RT in an orbital shaker. Wells were then washed with 1x Wash buffer and 100 µL of detection antibody was added onto each well. Plate was resealed and incubated for 1 hour at RT in an orbital shaker. Next, wells were washed with 1x Wash buffer and 100 µL of Avidin-HRP solution was added onto each well. Plate was resealed and covered with aluminum foil to prevent light exposure and incubated for 30 minutes at RT in an orbital shaker. Wells were then washed with 1X Wash buffer and 100 µL of TMB substrate solution was added onto each well. Plate was resealed and covered with aluminum foil and incubated for 15 minutes at RT. The reaction was stopped by adding 100 µL of 0.5 N Sulphiric acid solution onto each wells. Measurements were acquired in Synergy HT Microplate Reader at 450 nm and subsequently at 620 nm. Absorbance

values at 620 nm were subtracted from absorbance values at 450 nm. Data were analyzed using 4-parameter logistics curve-fitting algorithm.

2.2.16.CRISPR-Cas9 genome editing

2.2.16.1.Designing guide RNAs

Oligonucleotides for guide RNAs (gRNAs) targeting *IRAK4* exon2 (IRAK4_gRNA_CRISPR1_Fwd, IRAK4_gRNA_CRISPR1_Rev; IRAK4_gRNA_CRISPR2_Fwd, IRAK4_gRNA_CRISPR2_Rev) were utilized as previously described[153]. Oligonucleotides were purchased from Oligomer (Turkey).

2.2.16.2.Cloning of gRNAs

The cloning of gRNAs into LentiCRISPR plasmids was performed with the help of Yılmaz Yücehan Yazıcı. Briefly, pLentiCRISPR-V2 plasmid was digested using BsmBI enzyme at 55°C for 5 hours. Heat inactivation of the restriction enzyme was performed by increasing the temperature to 80°C for 20 minutes. After digestion, the size of the product (12,968 bp) was determined by agarose gel electrophoresis. Digested plasmid backbone (upper band, 12,968 bp) was extracted from agarose gel using NucleoSpin Gel and PCR Clean-up, Mini kit.

Table 2. 34 Restriction enzyme digestion reaction for pLentiCRISPR vector

Component	**Volume (µL)**
pLentiCRISPR.v2	5 µg
10X NEB Buffer 3.1	5
BsmBI	2
Molecular Biology grade water	up to 50
Total volume	**50**

Oligonucleotides were annealed at 95°C for 10 minutes on previously heated heat-block. After 10 minutes, annealed product was immediately placed in RT for 5 minutes. After that, products were inserted into linearized pLentiCRISPR-V2 plasmid at 16°C overnight.

Table 2. 35 Ligation reaction for gRNAs and digested pLentiCRISPR vector

Component	**Volume (µL)**
Linearized pLentiCRISPR.v2	100 ng
Annealed oligo duplex	1
10X T4 DNA Ligase Buffer	2
T4 DNA Ligase	1
Molecular Biology grade water	up to 20
Total volume	**20**

After ligation, ligated products were transformed into DH5α competent cells as previously described. Single colonies were screened for the presence of plasmid with

insert by colony PCR as previously described. Selected plasmids were confirmed by Sanger Sequencing by the service provider, Macrogen (Europe).

2.2.16.3.Lentivirus generation and transduction

The lentivirus generation and transduction of HEK293 cells were performed with the help of Serkan Belkaya. Briefly, for transfection, HEK293 cells were seeded on a 6-well plate at a density of 3.5 x 10^5 cells/mL (2 mL/well) and incubated overnight at 37°C, 5% CO_2 incubator. After 16 hours, they were transfected with 1.5 µg generated pLenti-CRISPR plasmids with gRNAs, 0.75 µg VSV-G envelope and 0.75 µg psPAX2 plasmids in the presence of Lipofectamine 2000 transfection reagent following the protocol as described above. At 16 hours after transfection, cell media were replaced with fresh medium and incubated for 32 hours at 37°C, 5% CO_2 incubator. At 48 and 72 hours after transfection, produced lentiviruses in the cell media were collected and centrifuged at 300 g for 5 minutes. Next, supernatants were filtered through 0.45-micron filters and concentrated with Lenti-X concentrator at 3:1 ratio (v/v). Concentrator mixture was incubated at +4°C for overnight. After 16 hours, mixture was centrifuged at 1,500 g at +4°C for 45 minutes. Supernatants were removed and virus pellets were resuspended in 500 µL medium and divided into 100 µL aliquots that stored at -80°C.

For transduction, HEK293 cells seeded on 24-well plate at a density of 1.5 x 10^5 cells/mL (500 µL/well) were transduced with one aliquot of concentrated lentiviruses described above. 48 after transduction, 1 µg/mL puromycin were added to the culture for antibiotic selection of transduced cells. For two weeks, cells were passaged when they become %80 confluent and fresh puromycin was added to the culture every two days.

2.2.16.4.T7 Endonuclease I assay

After two weeks of selection, cell populations were checked for the presence of mismatch DNA with T7E1 Assay. First, DNA from *IRAK4* CRISPR1 and *IRAK4* CRISPR2 cells were obtained using Phire Tissue Direct PCR Master Mix. Cell pellets of *IRAK4* CRISPR1 and *IRAK4* CRISPR2 were obtained after centrifugation at 13,000 rpm for 1 minute. Pellets were resuspended with 20 µL dilution buffer containing 0.5 µL DNA release reagent. Suspensions were mixed thoroughly by vortexing and incubated at RT for 2 minutes. Next, they were placed at 98°C previously heated hat-block for 2 minutes. Suspensions were centrifuged at 13,000 rpm for 2 minutes and supernatant was transferred into a new 1.5 mL centrifuge tube. Extracted DNA containing supernatants were stored at -20°C for further use.

PCR amplicons were obtained using Phire Tissue Direct PCR Master Mix. The expected size of the PCR amplicons was confirmed with agarose gel electrophoresis.

Table 2. 36 PCR reaction for *IRAK4* region targeted for CRISPR KO

Component	**Volume (µL)**
2X Phire Tissue Direct PCR Master Mix	10
IRAK4 CRISPR Out Fwd	2
IRAK4 CRISPR Out Rev	2
Extracted DNA sample	1
Molecular Biology grade water	up to 20
Total volume	**20**

Table 2. 37 PCR reaction conditions for *IRAK4* region targeted for CRISPR KO

Step	**Temperature (°C)**	**Duration (s)**	**Cycle**
Initial Denaturation	98	300	1
Denaturation	98	5	40
Annealing	60	5	
Extension	72	30	
Final extension	72	60	1
Final hold	4	-	Hold

Upon confirmation, all of the PCR amplicons were digested with T7E1. Digested products were checked by agarose gel electrophoresis.

Table 2. 38 T7E1 reaction

Component	**Volume (µL)**
PCR amplicon	5
10X NEbuffer 2	2
Molecular Biology grade water	up to 19.5
Total volume	**19.5**
T7E1	0.5

Table 2. 39 T7E1 reaction conditions

Step	Temperature (°C)	Duration (s)	Ramp rate (°C/s)
Denaturation	95	300	-
Annealing	95-85	-	-2
	85-25	-	-0.1
Final hold	4	Hold	-

2.2.16.5.Single-cell selection and competition-based PCR

After T7E1 confirmation, cells were seeded on 96-well plate at a density of 9 cell/mL (100 µL/well) for single cell selection. One month later, single-cell clones were screened with competition-based PCR method[161] using Phire Tissue Direct PCR kit with following primers: IRAK4 CRISPR Out Fwd, IRAK4 CRISPR Out Rev, IRAK4 CRISPR1 In Fwd, IRAK4 CRISPR1 In Rev, IRAK4 CRISPR2 In Fwd, IRAK4 CRISPR2 In Rev. Single-cell clones confirmed with competition-based PCR method were validated with an NFκB-dependent reporter assay for the functional activity using Secreted Alkaline Phosphatase Reporter Gene Assay kit according to the manufacturer's instructions.

2.2.16.5.1.Secreted alkaline phosphatase reporter assay

IRAK4 KO HEK293 single cell clones were seeded on 96-well plates at a density of 2.5 x 10^5 cells/mL (100 µL/well) and incubated overnight at 37°C, 5% CO2. After 16 hours of incubation, confluency of the cells reached 70% and cells were ready for transfection. Cells were co-transfected with pCI-neo-N-3xFLAG IRAK4 WT, pNiFty-SEAP (containing NFκB promoter upstream to alkaline phosphatase) and p.CMV6 IL18RAP WT plasmids by transient transfection with Lipofectamine 2000 transfection

reagent as described above. Cells were incubated for 24 hours at 37°C, 5% CO2. After 24 hours of incubation, cells were stimulated with recombinant human IL-18 at a final concentration of 10 ng/mL. 12 hours after stimulation, culture supernatants were collected into 1.5 mL centrifuge tubes and placed at -20°C for further use. Briefly, 10 μL of culture supernatants were transferred into white opaque 96-well plate and placed at 65°C for 30 minutes to inactivate endogenous alkaline phosphatase. Standard dilutions were prepared and 10 μL of diluted standards were transferred into assigned wells. SEAP substrate were added at 40 μL onto each well and incubated at RT for 10 minutes. Last, chemiluminescence was measured using Synergy HT Microplate Reader. Standard curves were plotted using absorbance values of alkaline phosphatase standards and alkaline phosphatase activity of cells were calculated accordingly.

CHAPTER 3

Results

The work presented in this thesis was originally published as “Tepe ZG, Yazıcı YY, Tank U, Köse LI, Özer M, Aytekin C. Belkaya S. Inherited IRAK-4 Deficiency in Acute Human Herpesvirus-6 Encephalitis. J Clin Immunol. 2023;43(1):192-205. doi:10.1007/S10875-022-01369-4” and reproduced with permission from Springer Nature (Appendix E).

3.1.Clinical presentation of the patient

The patient was male and born in Turkey in 2020, with a normal birth weight and no complications during pregnancy. The parents were second-degree cousins, and the patient had a 2 years older healthy sister. At 10 months of age, the patient developed a fever, lethargy, vomiting, and focal seizures. Physical examination showed normal growth parameters, and he was fully vaccinated according to the national immunization schedule. The imaging tests revealed abnormal findings in the brain, periventricular white matter hyperintensities, indicating meningoencephalitis. Lumbar puncture showed no leukocytes, elevated protein levels and decreased glucose ratio in the CSF. As no microorganism was detected in CSF upon gram staining, a viral encephalitis panel, including adenovirus, CMV, EBV, HSV-1, HSV-2, VZV, HHV-6, HHV-7, Enterovirus, Parechovirus, and PV-B19 was employed. Viral encephalitis panel confirmed the presence of HHV-6 DNA in the CSF. Meanwhile, the patient also developed an erythematous rash primarily in the trunk spreading to extremities. Since there was no previous history of a febrile disease with rash in the patient, the diagnosis

was considered as acute HHV-6 encephalitis upon presumably a primary infection (Figure 3.1). Subsequent immunological evaluations were normal and patient was discharged from hospital upon improvement of his symptoms. During the follow up, the patient experienced recurrent respiratory infections and admitted to the hospital due to urinary tract infections (by *Klebsiella pneumonia*) and bronchiolitis (by human bocavirus).

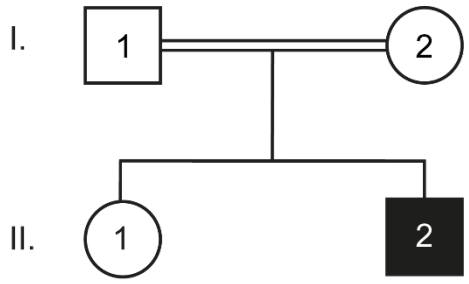

Figure 3. 1 Pedigree of the family affected with acute HHV-6 encephalitis. The patient is demonstrated in black, and the healthy family members are demonstrated in white. Adapted from Tepe ZG et al., 2023[185]

3.2.Analysis of WES data of the patient

We performed WES on patient's gDNA in order to test whether there are any candidate disease-causing monogenic variation, which may underlie susceptibility to acute HHV-6 encephalitis in this patient.

There were total of 147,225 annotated variants in total 22,483 different genes covered by WES of the patient (Table 3.1). In order to exclude possible low-quality annotated variants, following filtering criteria were employed. Depth coverage (DP) represents the number of reads for a single variant. Thus, we excluded variants with DP lower than 5. Moreover, map quality (MP) is calculated by comparing the quality score of best and other alignments for the variant site, which indicates whether the variant is misaligned or not. Genotype quality (GQ) is also a probabilistic calculation of the

correctness of a variant call. Therefore, we excluded variants with MP lower than 40 and GQ lower than 30 in order to remove the possible false-positive variants. After the quality filtering, the number of retained annotated variants were 111,507 (Table 3.1).

It is known that approximately 85% of disease causing mutations were protein-related[162,163]. Therefore, only nonsynonymous (missense, insertion, deletion, start-lost, stop-lost, stop-gain) and essential splicing variants were included, which accounted for 11,943 annotated variants in 6,029 genes in total (Table 3.1).

Table 3. 1 Genetic analysis of WES data of the patient

	Number of annotated variants (Number of mutated genes)
Total	147,225 (22,483)
DP > 5, MP > 40 and GQ > 30	111,507 (20,596)
Nonsynonymous (insertion, deletion, missense, start-lost, stop-lost and stop-gain) and essential splicing variants	11,943 (6,029)
MAF <1%	496 (448)
Homozygous	24 (24)

Since HHV-6 encephalitis is an extremely rare condition with only a couple of reported cases in the literature, common polymorphisms with MAF higher than 0.01 could not represent the epidemiology of HHV-6 encephalitis[75,97]. That's why, variants having MAF $\geq$ 0.01 were filtered out. In conclusion, 496 annotated nonsynonymous variants in 448 genes were retained (Table 3.1).

Patient was born to consanguineous parents and had an older sister. There was no known history of severe infection or immunodeficiency in his family. Since parents are

consanguineous and unaffected, we hypothesized that the genetic etiology of HHV-6 encephalitis in this family would display an Autosomal Recessive (AR) inheritance with complete penetrance. Therefore, priority was given to the homozygous variants among the aforementioned filtered variants annotated in the patient exome. A total of 24 annotated homozygous variants in 24 genes were identified in the patient (Table 3.1 and Table 3.2).

In order to assess the damaging potential of 24 rare homozygous nonsynonymous variants, *in silico* damage prediction tools were employed. Along with SIFT[158] and PolyPhen-2[159] tools, which can only predict missense variants, CADD scores[156], which can predict both missense and potential loss-of-function (pLOF) variants, were used. Calculated SIFT, PolyPhen-2 and CADD/MSC[157] scores were shown in Table 3.2.

Moreover, we checked if the 24 homozygous variants in the patient are also found at homozygous states in the gnomAD public database. The presence of a homozygous variant in the gnomAD public database may suggest that such mutation is likely benign[164]. For the majority of the nonsynonymous homozygous variants in the patient, there were no homozygotes found in gnomAD, except for 4 variants in *MRPS35, SMARCD1, PRR12* and *TSKS* (Table 3.2). Therefore, we filtered out those 4 variants. Additionally, we checked for the presence of any homozygous pLOF (start-lost, stop-lost, stop-gain, essential splicing, frameshift deletion and insertion) variations in the gnomAD for the mutated genes with homozygous variants in the patient. Prevalence of several homozygous pLOF mutations in a given gene in public databases may suggest the function of the gene could be potentially redundant, so that it may not be morbid in our patient[165]. Accordingly, we excluded 2 variants that are found in *PCDHGA6* and *TMPRSS9* (Table 3.2).

Regarding the predicted damaging impact of variants, 4 homozygous missense variants and 3 homozygous pLOF variants were found to be potentially damaging in total 7 genes: *CPA3, IRAK4, LTBP4, ZNF404, IGSF10, PCDHGA6 and KRTAP2-2* (Table 3.2). CADD scores of all these variants were above the predetermined mutation significance cutoff (MSC) values (in 95% confidence interval), implying the high damaging impact of such variants[157] (Table 3.2). Similarly, GDI scores of the genes with annotated variants were under 14, indicating a low level of nonsynonymous mutational load in the mutated genes[155] (Table 3.2).

Table 3. 2 Homozygous rare nonsynonymous variants found in the patient

GENE	GDI[a]	Variation		Zygosity	MAF	*In silico* Damage Prediction			gnomAD	gnomAD pLoF
		Type	Change			CADD/MSC	SIFT	PolyPhen-2	#Hom[b]	#Hom[c]
CPA3	4.26	Missense	ENST00000296046:p.Arg237His	HOM	1.56E-04	26.5/11.2	D	D	0	0
HPS3	3.26	Missense	ENST00000296051:p.Arg822Gln	HOM	7.98E-06	22.5/22.3	B	D	0	0
IGSF10	5.96	Stop Gain	ENST00000282466:p.Gln1828*	HOM	1.19E-05	38/25	NA	NA	0	0
PCDHGA6	3.90	Frameshift	ENST00000517434:p.Gln772fs	HOM	3.98E-06	24.7/12.7	NA	NA	0	1
SPRY4	2.31	Missense	ENST00000344120:p.Lys177Arg	HOM	1.61E-03	22.2/16.1	B	B	0	0
OR5M8	2.57	Missense	ENST00000327216:p.Ala105Thr	HOM	3.89E-05	0.003/20.2	B	B	0	0
MRPS35	4.95	Missense	ENST00000081029:p.Tyr27Cys	HOM	1.74E-04	7.69/16.5	B	B	1	1
IRAK4	5.20	Missense	ENST00000448290:p.Cys79Tyr	HOM	-	28/15.2	D	D	0	0
KMT2D	6.74	Missense	ENST00000301067:p.Gln3269Arg	HOM	-	23.4/17.3	B	D	0	0
SMARCD1	0.68	Missense	ENST00000394963:p.Val278Met	HOM	4.52E-04	23/22.2	B	B	1	0
ACAN	26.89	Missense	ENST00000439576:p.Gly1374Arg	HOM	6.07E-03	13.03/18	B	B	1	0
KRTAP2-2	6.42	Frameshift	ENST00000542910:p.Pro91fs	HOM	1.92E-05	33/ND	NA	NA	0	0
TMPRSS9	16.19	Missense	ENST00000332578:p.Arg852Cys	HOM	2.01E-04	26.1/11.2	B	D	0	2
SAFB	1.28	Missense	ENST00000588852:p.Ile126Val	HOM	7.95E-06	15.18/10	B	B	0	0
FUT3	10.86	Missense	ENST00000303225:p.Asp96Asn	HOM	1.99E-05	6.979/13.7	B	B	0	0
LTBP4	21.48	Missense	ENST00000308370:p.Gly650Asp	HOM	-	29.7/23	D	D	0	0
CCDC97	1.15	Missense	ENST00000269967:p.Ala65Thr	HOM	3.98E-06	22.6/12.1	B	D	0	0
DEDD2	0.92	Missense	ENST00000595337:p.Gly318Val	HOM	5.69E-04	17.93/12.7	D	B	0	0
ZNF404	14.45	Missense	ENST00000587539:p.His209Tyr	HOM	8.18E-05	24.4/15.7	D	D	0	0
ZNF226	4.21	Missense	ENST00000337433:p.Thr666Ala	HOM	7.98E-06	22.9/11.4	D	B	0	0
PRR12	3.89	Missense	ENST00000418929:p.Ala1427Val	HOM	1.80E-04	12.85/22.8	B	B	1	0
TSKS	9.20	Missense	ENST00000246801:p.Arg371Trp	HOM	1.34E-03	25.1/24.8	B	D	2	0
MYH14	7.88	Missense	ENST00000262269:p.Arg1531Gln	HOM	4.07E-06	24.6/20.1	B	D	0	0
KLK11	5.27	Missense	ENST00000594768:p.Arg140His	HOM	1.34E-04	23.3/11.3	B	B	0	0

a. Gene damaging index (GDI) represents mutation-load of genes, with a range from 0.0001 to 42.91 (from the least to the most).
b. Number of homozygote individuals in the gnomAD with the identical variant found in the patient. c. Number of homozygote individuals in the gnomAD carrying pLOF variants for the indicated genes.
D: Damaging B: Benign NA: Not available

In addition to the damaging prediction tools, expression patterns, known function and clinical significance of the genes with homozygous variants were examined (Table 3.3). Due to its broad expression in immune cells and known role in the immune system, Interleukin-1 receptor-associated kinase 4 (*IRAK4)* was thought to be the most plausible morbid gene candidate when compared with other 6 genes (Table 3.3).

IRAK-4 is an active kinase in Toll/IL-1 receptor (TIR) canonical signaling pathway, in which evolutionarily conserved microbial molecular patterns are sensed by TLRs[126,144]. TLR activation initiates dimerization of the receptor subunits, which in turn induces recruitment of cytosolic adaptor molecules containing TIR domains, such as MyD88[166]. By the recruitment of MyD88, IRAK-4 and IRAK-2 molecules form a complex with that adaptor molecule and transmit signaling through phosphorylating downstream TIR cascade proteins[126,144]. The classical TLR pathway results in the production of proinflammatory cytokines and chemokines that provide innate immunity in mice models and humans[167]. Mice lacking Irak-4 show had impaired IL-1R and TLR signaling and susceptibility to bacterial infections[166]. Similarly, IRAK-4 deficient patients mainly suffer from recurrent invasive pyogenic bacterial infections with Gram-positive bacteria, mostly caused by *S. pneumoniae*, *S. aureus* and *P. aeruginosa*[167–169]. Patients with inborn bi-allelic mutations in IRAK-4 demonstrated a defective TLR-mediated NF-kB signaling, leading to insufficient systemic and mucosal immune responses upon bacterial stimulation[169,170]. Upon stimulation with TLR or IL-1R ligands, leukocytes from IRAK-4 deficient patients had impaired production of inflammatory cytokines, such as IL-6 and TNF[171–174].

Apart from bacterial pathogen-associated molecular patterns (PAMPs), some TLRs recognize viral ones and mediate anti-viral innate immune responses[175,176]. In a mouse

model expressing a kinase-inactive Irak-4, influenza virus-induced type I interferon production was entirely abrogated due to impaired TLR7 and TLR9 signaling[177]. Similarly, Irak-4 deficient mice were incapable of producing IFN-γ upon LCMV infection[178]. Strikingly, most viral infections in IRAK-4-deficient patients are found to be tolerated as in normal individuals[179]. PBMCs and fibroblasts from IRAK-4-deficient patients have been shown to confer a normal IFN production after stimulation with most common viruses[179]. Similarly, patients with IRAK-4 deficiency had normal antibody responses to several viruses[171]. Six patients with IRAK-4 deficiency were found to be seropositive for HHV-6, however they showed mild symptoms with no indication of viral susceptibility[171]. In a recent study, IRAK-4 deficiency was described in a child with anti-NMDAR encephalitis and HHV-6 reactivation[143], implying the involvement of IRAK-4 in the pathogenesis of encephalitis and/or HHV-6 infection.

Table 3. 3 Characteristics of genes with homozygous rare nonsynonymous variations present in the patient

Gene description	Expression pattern	Known function	Clinical significance
Carboxypeptidase A3 (*CPA3)*	Biased expression in gallbladder and lung.	Degradation of endogenous proteins and the inactivation of venom-associated peptides.	Unknown
HPS3 Biogenesis Of Lysosomal Organelles Complex 2 Subunit 1 *(HPS3)*	Broad expression in liver, lymph node and other tissues.	Involved in the biogenesis of melanosomes, platelet dense granules, and lysosomes.	Biallelic mutations cause Hermansky-Pudlak syndrome 3.
Immunoglobulin Superfamily Member 10 *(IGSF10)*	Broad expresison in gall bladder, ovary and other tissues.	Regulates the migration of neurons expressing gonadotropin-releasing hormone.	Unknown
Protocadherin Gamma Subfamily A, 6 *(PCDHGA6)*	Biased expresison in brain.	Involved in the establishment of specific neuronal connections in the brain.	Unknown
Sprouty RTK Signaling Antagonist 4 *(SPRY4)*	Broad expression in lung, adrenal and other tissues.	Encodes an inhibitor of the receptor-transduced mitogen-activated protein kinase (MAPK) signaling pathway.	Mutations cause hypogonadotropic hypogonadism 17 with or without anosmia.
Olfactory Receptor Family 5 Subfamily M Member 8 *(OR5M8)*	Expression in Olfactory Mucosa.	Encoded protein is responsible for the recognition and G protein-mediated transduction of odorant signals.	Unknown
Mitochondrial Ribosomal Protein S35 *(MRPS35)*	Ubiquitous expression in kidney, colon and other tissues.	Involved in protein synthesis within the mitochondrion.	Unknown
Interleukin 1 Receptor Associated Kinase 4 *(IRAK4)*	Ubiquitous expression in lymph node, appendix and other tissues.	Encodes a kinase that activates NF-kappaB in both the Toll-like receptor and T-cell receptor signaling pathways.	Biallelic mutations cause recurrent severe systemic and invasive bacterial infections.
Lysine Methyltransferase 2D *(KMT2D)*	Ubiquitous expression in bone marrow, skin and other tissues.	Encodes a histone methyltransferase that regulates the beta-globin and estrogen.	Mutations cause Kabuki syndrome 1.
SWI/SNF related, matrix associated, actin dependent regulator of chromatin, subfamily d, member 1 *(SMARCD1)*	Ubiquitous expression in lymph node, testis and other tissues.	Thought to regulate transcription of certain genes by altering the chromatin structure around those genes.	Mutations cause Coffin-Siris syndrome 11.
Aggrecan *(ACAN)*	Broad expression in testis, urinary bladder and other tissues.	Encoded protein is an integral part of the extracellular matrix in cartilagenous tissue and it withstands compression in cartilage.	Biallelic mutations cause spondyloepimetaphyseal dysplasia, aggrecan type.
Keratin Associated Protein 2-2 *(KRTAP2-2)*	Distinct expression in the hair cortex.	May involve in keratinization	Unknown
Transmembrane Serine Protease 9 *(TMPRSS9)*	Broad expression in spleen, testis and other tissues.	Encodes a membrane-bound type II serine polyprotease.	Unknown

Table 3.3 Cont.

Scaffold Attachment Factor B *(SAFB)*	Ubiquitous expression in spleen, testis and other tissues.	Encodes a DNA-binding protein which has high specificity for scaffold or matrix attachment region DNA elements (S/MAR DNA).	Unknown
Fucosyltransferase 3 *(FUT3)*	Biased expression in colon, esophagus and other tissues.	Catalyzes the addition of fucose to precursor polysaccharides.	Mutations cause Lewis antigen-negative phenotypes.
Latent Transforming Growth Factor Beta Binding Protein 4 *(LTBP4)*	Broad expression in prostate, endometrium and other tissues.	Encoded protein binds transforming growth factor beta as it is secreted and targeted to the extracellular matrix.	Biallelic mutations cause cutis laxa, autosomal recessive, type IC.
Coiled-Coil Domain Containing 97 *(CCDC97)*	Ubiquitous expression in testis, ovary and other tissues.	Unknown	Unknown
Death Effector Domain Containing 2 *(DEDD2)*	Enhanced expression in bone marrow, broad expression in spleen and other tissues.	Functions in the extrinsic apoptosis pathway and regulate nuclear breakdown	Unknown
Zinc Finger Protein 404 *(ZNF404)*	Ubiquitous expression in brain, testis, and other tissues.	Predicted to be involved in transcriptional regulation.	Unknown
Zinc Finger Protein 226 *(ZNF226)*	Ubiquitous expression in prostate, thyroid, and other tissues.	Predicted to be involved in transcriptional regulation.	Unknown
Proline Rich 12 *(PRR12)*	Ubiquitous expression in spleen, fat and other tissues.	Thought to be involved in nervous system development.	Mutations cause neuro-ocular syndrome.
Testis Specific Serine Kinase Substrate *(TSKS)*	Restricted expression toward testis.	Involved in testicular physiology, spermatogenesis or spermiogenesis.	Unknown
Myosin Heavy Chain 14 *(MYH14)*	Broad expression in colon, duodenum and other tissues.	Encodes a conventional non-muscle myosin.	Mutations cause deafness, autosomal dominant 4A.
Kallikrein Related Peptidase 11 *(KLK11)*	Biased expression in esophagus, skin, and other tissues.	Encodes one of the fifteen kallikrein subfamily members as a subgroup of serine proteases	Unknown

The *IRAK4* variation (NM_016123.4:c.G236A: NP_057207.2:p.C79Y) found in the patient was located on the chromosome 12 (chr12:44165097:G>A) and presented by the substitution of guanine (G) to adenine (A) (Figure 3.2). This variant was not reported in any public databases including 1000 Genomes[180], the Single Nucleotide Polymorphism Database (dbSNP)[181], gnomAD, Bravo[182] and the Greater Middle East (GME) Variome Project[183]. Collectively, we selected *IRAK4* as the most plausible disease-causing gene in this patient to study.

The familial segregation of the mutant *IRAK4* allele was confirmed by Sanger sequencing. Both parents and sibling were found to be heterozygote for the *IRAK4* mutant allele, whereas patient was homozygote (Figure 3.2). Segregation of this allele with the disease in the family was consistent with the AR mode of inheritance with complete penetrance.

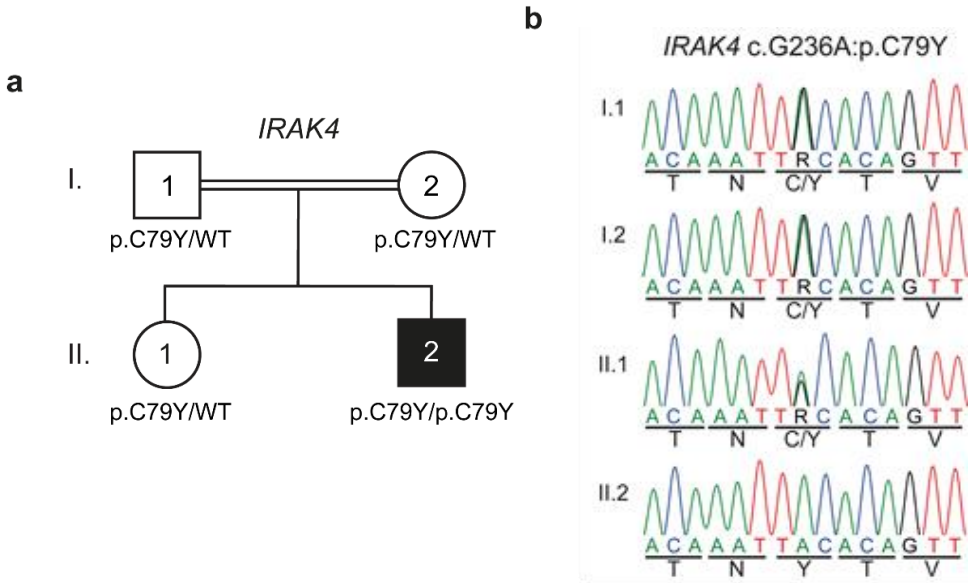

Figure 3. 2 A novel homozygous missense mutation was identified in *IRAK4*. a. Sanger sequencing confirmed the homozygosity of the patient and familial segregation of the *IRAK4* mutation. b. Pedigree of the family affected with acute HHV-6 encephalitis. Patient is demonstrated in black, and the healthy family members are demonstrated in white. *IRAK4* exome status are indicated for each family member on the pedigree. Adapted from Tepe ZG et al., 2023[185]

3.3.*In silico* prediction of the damaging impact of IRAK-4 p.C79Y

This variation on *IRAK4*, c. G236A: p.C79Y substitutes guanine in 236th position of the *IRAK4* coding sequence to adenine, which results in the substitution of cysteine in 79th position (p.C79) to Tyrosine (p.C79Y) on the protein.

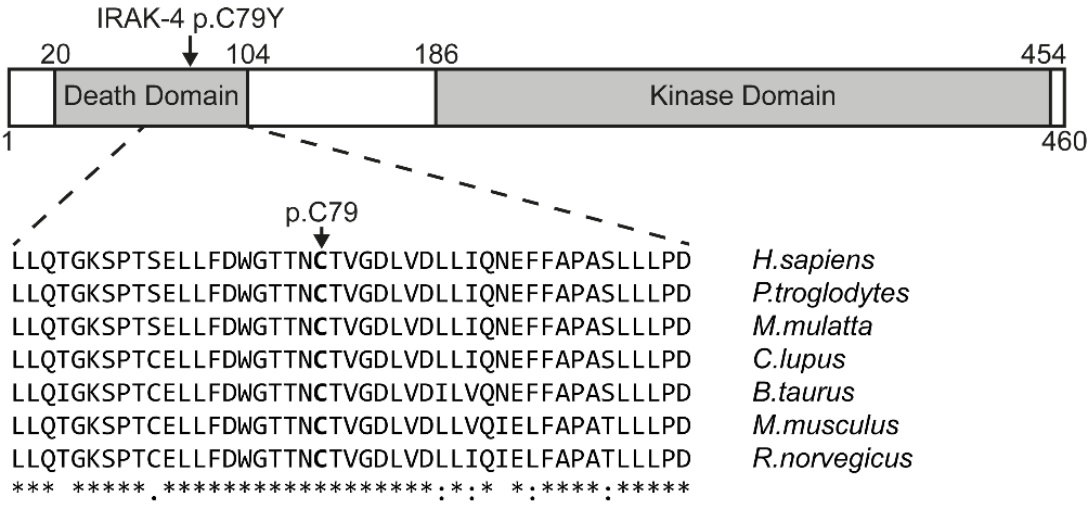

Figure 3. 3 The p.C79Y affects a conserved residue in the Death domain of IRAK-4. Schematic representation of IRAK-4 (460 amino acids) and its domains are shown on top. Conservation of the C79 residue of IRAK-4 across various species is shown below. Source is NCBI HomoloGene. C79 residue is highlighted in bold. Adapted from Tepe ZG et al., 2023[185]

IRAK4 mRNA contains 11 exons in total, encoding a protein of 460 amino acids, with two domains: The Death domain (DD) and the Kinase domain (KD). The C-terminal region of IRAK-4 is called KD, which is responsible for the enzymatic activity of the protein[144,184]. Indeed, KD phosphorylates the downstream components in the signaling cascade, leading to signal transmission[144,184]. The N-terminal region of IRAK-4 is called DD, which is responsible for the intermolecular interactions with other proteins, such as MyD88 and IRAK-1[144]. Interaction with other proteins facilitates the formation of downstream signaling complexes[144]. The DD includes 85 amino acids between the

20^{th} and 104^{th} amino acids[144]. In this context, cysteine to tyrosine substitution at p.C79 was located in the middle of the DD (Figure 3.3). IRAK-4 DD was involved in the interaction with MyD88 and subsequent formation of Myddosomes during TIR signaling[144,185]. It is plausible that IRAK-4 p.C79Y could potentially interfere with the recruitment of IRAK-4 to MyD88 adaptor molecule upon activation of TIRs.

Moreover, p.C79 was highly conserved across different species (Figure 3.3). Not only cysteine itself, but also the 16 amino acid residues flanking p.C79 seemed to be conserved across various species (Figure 3.3). It is known that disease-causing mutations are more likely to be located at evolutionary conserved residues[158]. Therefore, orthologue conservation of p.C79 fortifies the damaging potential of p.C79Y.

We also checked the previously reported disease-causing variations in *IRAK4* in ClinVar database and the literature. We found 31 disease-causing mutations either presented as homozygous or compound heterozygous (Figure 3.4). The CADD score of p.C79Y was calculated as 28 (Figure 3.4). When we compared the CADD score of p.C79Y with the scores of previously reported disease-causing mutations, almost all variations (except c.1188+520A>G) were found to be above predetermined MSC value (in 95% confidence interval) of 15.15 for *IRAK4* (Figure 3.4). Accordingly, the score of p.C79Y was comparable to 29.5, the median CADD score of the previously reported disease-causing mutations in *IRAK4*.

a

Variation	Zygosity	CADD	References
NM_016123.4:c.1A>G:NP_057207.2:p.M1V	COMP HET	23.6	Ku et al., 2007
NM_016123.4:c.29_30delAT:NP_057207.2:p.Y10Cfs*9	COMP HET	29.1	Nishimura et al., 2021
NM_016123.4:c.34C>T:NP_057207.2:p.R12C	COMP HET	28.9	Hoarau et al., 2007
NM_016123.4:c.35G>C:NP_057207.2:p.R12P	COMP HET	28.5	Nishimura et al., 2021
NM_016123.4:c.123dup:NP_057207.2:p.P42Tfs*3	HOM	29.1	Takada et al., 2016
NM_016123.4:c.144C>G:NP_057207.2:p.Y48*	COMP HET	37	Ku et al., 2007
NM_016123.4:c.161G>A:NP_057207.2:p.R54K	HOM	34	Gokturk et al., 2018
NM_016123.4:c.228_230del:NP_057207.2:p.T77del	COMP HET	22.1	Andres et al., 2013
NM_016123.4:c.255_260dup:NP_057207.2:p.D86_L87dup	COMP HET	21	Grazioli et al., 2016
NM_016123.4:c.524del:NP_057207.2:p.N175Mfs*31	HOM	25.7	Enders et al., 2004
NM_016123.4:c.547C>T:NP_057207.2:p.R183*	COMP HET	35	Picard et al., 2010
NM_016123.4:c.574del:NP_057207.2:p.p.M192Wfs*14	HOM	23.3	Enders et al., 2004
NM_016123.4:c.593del:NP_057207.2:p.G198Efs*8	COMP HET	32	Bouma et al., 2009
NM_016123.4:c.623_624delCA:NP_057207.2:p.T208Nfs*12	COMP HET	23	Medvedev et al., 2003
NM_016123.4:c.631del:NP_057207.2:p.A211Qfs*2	COMP HET	24	Ku et al., 2007
NM_016123.4:c.821del:NP_057207.2:p.L274Pfs*14	HOM	32	Picard et al., 2003
NM_016123.4:c.823del:NP_057207.2:p.S275Lfs*13	COMP HET	29.9	Karananou et al., 2020
NM_016123.4:c.831+5G>T	COMP HET	22.3	Hoarau et al., 2007
NM_016123.4:c.877C>T:NP_057207.2:p.Q293*	HOM	40	Picard et al., 2010
NM_016123.4:c.893G>A:NP_057207.2:p.G298D	COMP HET	28.6	Bouma et al., 2009
NM_016123.4:c.897_900del:NP_057207.2:p.N300Ffs*44	COMP HET	33	Picard et al., 2010
NM_016123.4: c.1079T>A:NP_057207.2:p.L360*	HOM	39	Maglione et al., 2014
NM_016123.4:c.1126-1G>T	COMP HET	35	Maglione et al., 2014
NM_016123.4:c.1146del:NP_057207.2:p.G383Dfs*15	COMP HET	32	Grazioli et al., 2016
NM_016123.4:c.1188+520A>G	COMP HET	5.529	Ku et al., 2007
NM_016123.4:c.1189-1G>T	COMP HET	34	Ku et al., 2007
NM_016123.4:c.1204G>T:NP_057207.2:p.E402*	HOM	44	Picard et al., 2010; Cardenes et al., 2006
NM_016123.4:c.1240dup:NP_057207.2:p.I414Nfs*2	COMP HET	26.5	Ku et al., 2007
NM_016123.4:c.1290C>G:NP_057207.2:p.Y430*	COMP HET	37	Maglione et al., 2014
NM_016123.4:c.942-1481_1125+547del	COMP HET	NA	Ku et al., 2007
NM_016123.4:c.-9-1087_63del	HOM	NA	Ku et al., 2007

b

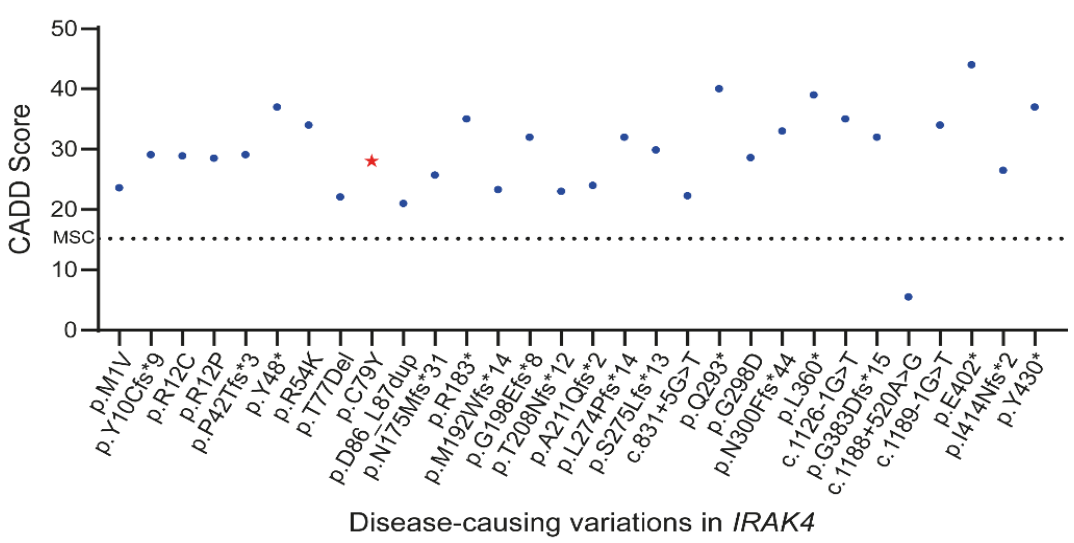

Figure 3. 4 Disease-causing variations in *IRAK4* and their predicted CADD scores. a. Table showing previously reported disease-causing variations in *IRAK4*. Homozygous mutations are shown as HOM and compound heterozygous variations are shown as COMP HET. b. Graph showing predicted CADD scores of previously reported disease-causing variations in *IRAK4* (blue circles) and p.C79Y found in the patient (red star). Adapted from Tepe ZG et al., 2023[185]

Additionally, when we visualized the WT and mutant IRAK-4 DD structures with the help of Yılmaz Yücehan Yazıcı, we observed a novel pi-stacking between p.Y79 and p.W74 due to the p.C79Y substitution in the IRAK-4 DD (Data not shown)[186]. Change in intermolecular interactions suggested a slight structural alteration that may disturb the recruitment of mutant IRAK-4 by MyD88. Given that MyD88-IRAK-4 complex formation is required for the downstream TIR signaling, we hypothesized that p.C79Y could impair the function of IRAK-4.

3.4.Assessment of IRAK-4 mRNA and protein levels in patient's leukocytes

We checked for IRAK-4 expression at both mRNA and protein levels in PBMCs from the patient, his sibling, parents and three unrelated healthy donors.

We performed flow cytometric analysis of IRAK-4 expression in PBMCs from the patient, his sibling, parents and three unrelated healthy controls upon intracellular staining of IRAK-4. We demonstrated that IRAK-4 expression was almost abolished in $CD3^+CD4^+$ T cell, $CD3^+CD8^+$ T cell and $CD19^+$ B cell populations of the patient, compared to that of his family members and unrelated healthy donors (Figure 3.5). Although $CD14^+$ monocytes were affected in a lesser extent, there was 70% reduction in the IRAK-4 expression in patient's monocytes (Figure 3.5). However, we found similar *IRAK4* mRNA expression levels by RT-qPCR in the patient when compared to healthy controls (Figure 3.6).

These findings showed that IRAK-4 expression was severely diminished in patient's leukocytes (Figure 3.5).

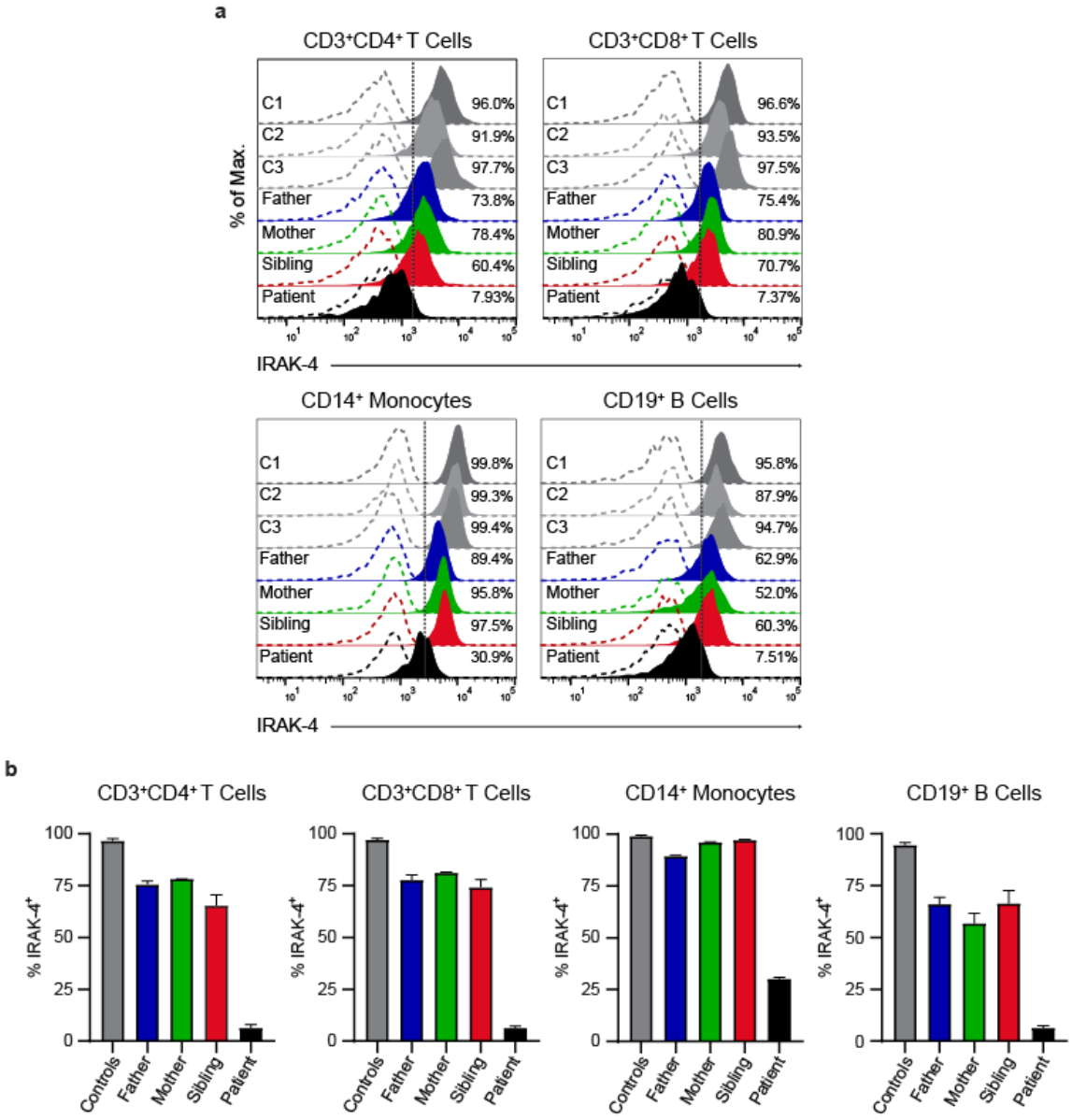

Figure 3. 5 Impaired IRAK-4 expression in patient's leukocytes. a. Representative histograms showing intracellular IRAK-4 expression in PBMCs from three unrelated healthy controls (represented as C1, C2 and C3), the patient and his family (father, mother, and sibling). PBMCs were defined through forward and side scatter. Percentage of IRAK-4$^+$ cells was determined on the respected PBMC subsets by gating on surface expression of CD3$^+$ and CD4$^+$, CD3$^+$ and CD8$^+$, CD14$^+$, or CD19$^+$. Dashed lines represent isotype control staining for IRAK-4. b. Graphs showing the percentages of IRAK-4 expressing CD3$^+$CD4$^+$ T cells, CD3$^+$CD8$^+$ T cells, CD14$^+$ monocytes, and CD19$^+$ B cells from controls, the patient and his family. Controls are shown as the average of three healthy controls (C1, C2, and C3). Bars present the mean ± SEM of two independent experiments using PBMCs isolated form peripheral blood at different times. Adapted from Tepe ZG et al., 2023[185]

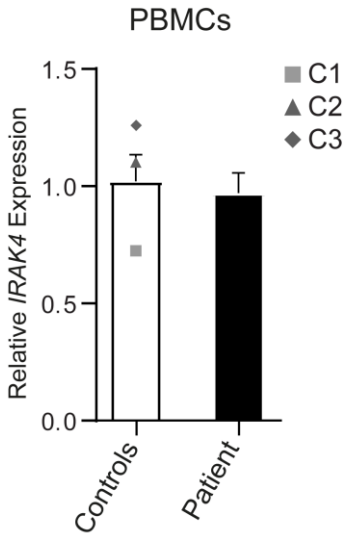

Figure 3. 6 The p.C79Y did not affect *IRAK4* mRNA expression. Bar graphs showing expression of *IRAK4* levels normalized to *HPRT1* expression by RT-qPCR on PBMCs from the patient and three unrelated healthy controls (represented as C1, C2 and C3). Relative *IRAK4* expression was calculated by normalizing individual ΔΔCq values to the mean of that of control cells, which was set to 1. Bars present the mean ± SEM of two independent experiments performed in duplicates. Adapted from Tepe ZG et al., 2023[185]

3.5.Impact of p.C79Y on IRAK-4 expression

We generated constructs with full length *IRAK4* ORF encoding WT or mutant IRAK-4 with an in-frame N-terminal 3X FLAG tag or without tag in order to reveal the impact of p.C79Y on IRAK-4 expression *in vitro*. We also generated an IRAK-4 construct with c.C34T:p.R12C, a previously reported disease-causing mutation[187].

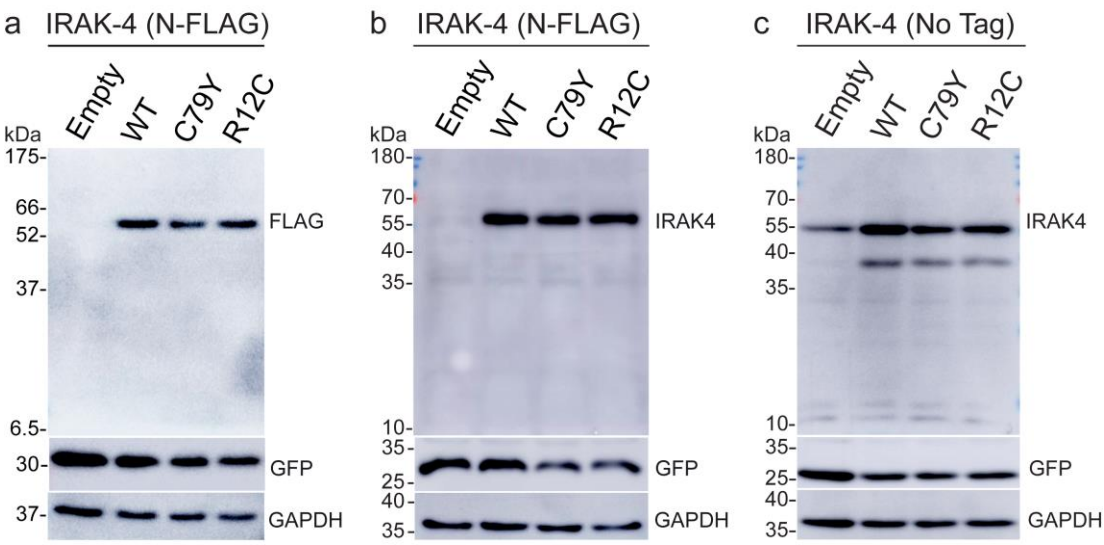

Figure 3. 7 Impact of p.C79Y on IRAK-4 expression *in vitro*. Representative immunoblot images showing expression levels of WT and mutant IRAK-4 with FLAG-tagged (left and middle panels) or without a tag (right panel) in whole cell lysates from transiently transfected HEK293 cells. 30 µg proteins were loaded on each lane. Adapted from Tepe ZG et al., 2023[185]

We transiently transfected HEK293 cells with either empty vector or plasmids encoding WT or mutant IRAK-4 with N-terminal FLAG tag, along with a GFP-expressing plasmid as a transfection efficiency control. At 48 hours post-transfection, we lysed the cells and checked for IRAK-4 expression by immunoblotting. We found similar expression levels of FLAG-tagged WT and mutant IRAK-4 with p.C79Y or p.R12C in transiently over-expressed HEK293 cells (Figure 3.7). Moreover, we transiently transfected HEK293 cells with constructs encoding WT and mutant IRAK-4 without a tag, yet there were similar expression levels of WT and mutant IRAK-4 (Figure 3.7). Of note, the expression of IRAK-4 with p.R12C variant was comparable to the WT IRAK-4, consistent with previous findings[143].

3.6.Impact of p.C79Y on IRAK-4 stability

We sought to test whether p.C79Y could affect the stability of IRAK-4. We transiently transfected HEK293 cells with either empty vector or plasmids encoding WT or mutant IRAK-4 with N-terminal FLAG tag, along with a GFP-expressing plasmid as a transfection efficiency control. At 24 hours post-transfection, we treated the cells with cycloheximide (50ug/mL) or 0.5% DMSO as vehicle control for 12 hours, followed by cell lysis for immunoblotting. Cycloheximide (CHX) is a protein synthesis inhibitor and frequently used for the assessment of protein stability *in vitro*[188]. We found that WT IRAK-4 levels decreased approximately 30%, whereas around 73% and 84% reductions were seen in the levels of mutant IRAK-4 with p.C79Y and p.R12C, respectively, upon CHX treatment (Figure 3.8). Consistent with our results, p.R12C was previously shown to reduce the stability of IRAK-4[189]. Moreover, decrease in GFP levels (~30%) were comparable in all transfected cells treated with CHX, suggesting that differences in IRAK-4 levels were due to the damaging impact of the variations. (Figure 3.8). Overall, we showed that the reduction in IRAK-4 mutants was at least 2 times that of the WT, whereas reduction in GFP levels were similar in all transfectants (Figure 3.8). Collectively, we demonstrated that p.C79Y decreased IRAK-4 stability (Figure 3.8).

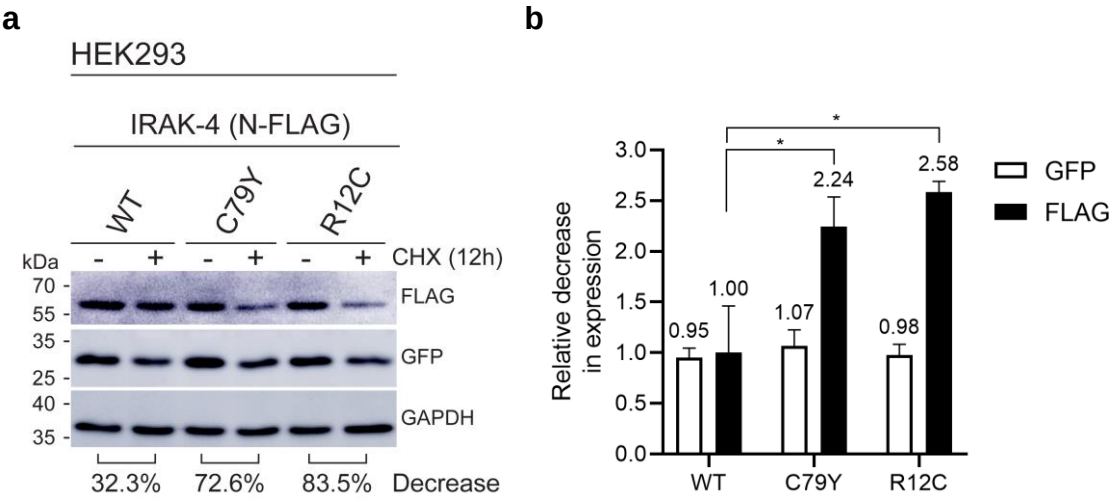

Figure 3. 8 The p.C79Y decreases IRAK-4 protein stability. a. Representative immunoblot image shows the expression levels of WT and mutant IRAK-4 with FLAG-tag in transiently transfected HEK293 cells following treatment with DMSO (vehicle control) or cycloheximide (CHX) for 12 h. Total 30 μg protein per lane was loaded. The ImageJ software was used to calculate band intensities. Percent reduction in IRAK-4 expression levels in the WT and mutant IRAK-4 transfected cells were determined by normalizing the FLAG to GAPDH ratio of CHX treatment to that of DMSO treatment, which was set as 100 for each genotype. Average percent decreases from two independent experiments were shown. b. The relative decrease in IRAK-4 expression was calculated by normalizing against the mean percent decrease levels in WT IRAK-4 of two independent experiments., which was set as 1. The relative decrease in GFP levels were calculated by normalizing against the average of percent decrease levels in GFP of each experiment, which was set as 1. The values shown are the mean ± SEM of two independent experiments (*$P < 0.05$; two-way ANOVA). Adapted from Tepe ZG et al., 2023[185]

3.7.Assessment of innate immune responses in patient's leukocytes

It was previously demonstrated that IRAK-4 is involved in the induction of pro-inflammatory cytokines, such as IL-6 and TNF, in response to TLR stimulation via pyogenic bacteria[170–173]. In a recent study, impaired intracellular TNF production in $CD14^+$ monocytes of an IRAK-4-deficient patient upon induction with various TLR ligands was shown by flow cytometry[143]. Therefore, we sought to assess intracellular TNF production from CD14+ monocytes in PBMCs of the patient and two healthy controls by flow cytometry following stimulation with Pam3CSK4 (TLR 1/2 agonist),

Flagellin (TLR5 agonist) and LPS (TLR4 agonist) for 6 hours. We found aberrant deterioration of intracellular TNF production in patient's $CD14^+$ monocytes when compared to the healthy controls, particularly upon stimulation with Pam3CSK4 and Flagellin (Figure 3.9). In response to LPS, reduction in TNF production in patient's $CD14^+$ monocytes were to a lesser extent (Figure 3.9). Overall, these findings revealed impaired innate immune responses in patient's monocytes, which had severely diminished IRAK-4 expression.

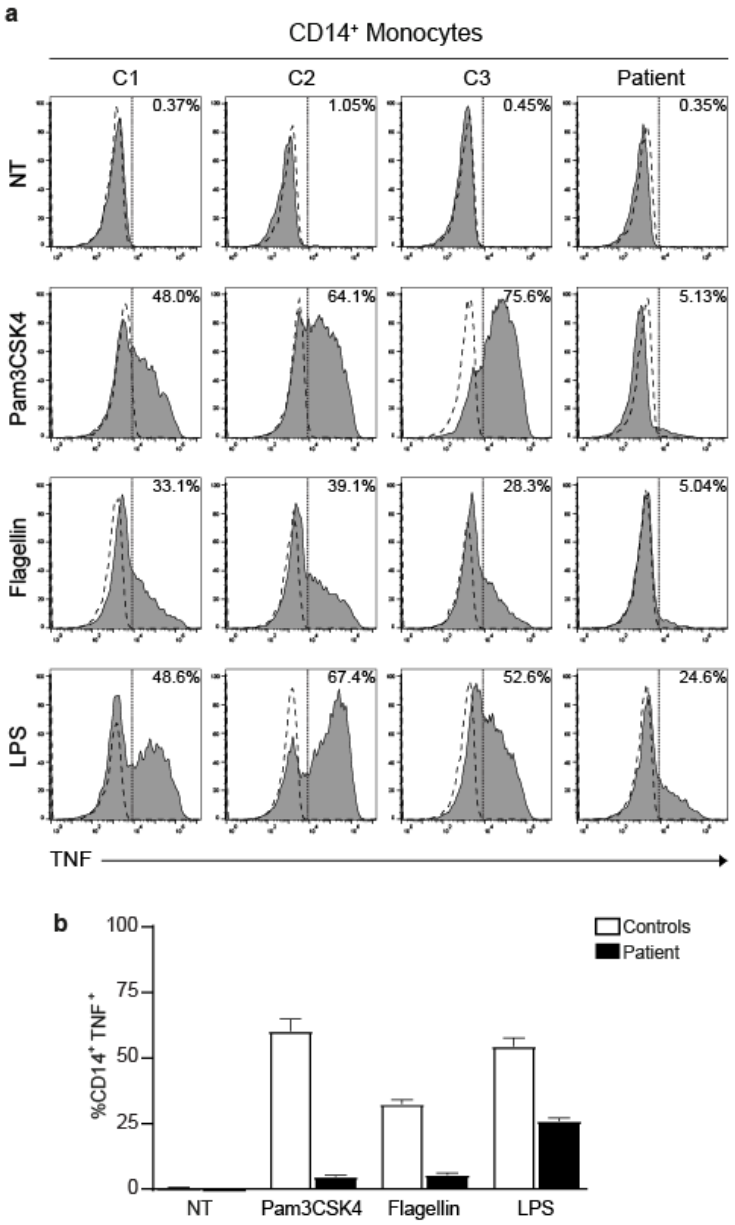

Figure 3. 9 Impaired innate immune responses in patient's monocytes a. Representative histograms showing intracellular TNF production in $CD14^+$ monocytes from PBMCs of the patient and three healthy controls (C1, C2, and C3) upon stimulation with Pam3CSK4 (TLR1/TLR2), Flagellin (TLR5), and LPS (TLR4). PBMCs were defined through forward and side scatter. Percentages of TNF^+ cells were determined on the respected PBMC subsets by gating on $CD14^+$ cells. Dashed lines indicate isotype control staining. NT: no treatment (Medium only). b. Bar graph shows the percentages of TNF^+ in $CD14^+$ monocytes in PBMCs of the patient and three healthy controls (C1, C2, and C3) upon treatment with indicated stimuli. Bars present the mean ± SEM of two independent experiments using PBMCs isolated form peripheral blood at different times. Adapted from Tepe ZG et al., 2023[185]

3.8.Impact of p.C79Y on IRAK-4 function

In order to determine the impact of mutations on IRAK-4 function *in vitro*, we sought to generate *IRAK4* knock-out (KO) HEK293 cell lines by CRISPR-Cas9 gene editing technology, as previously suggested[143]. First, we performed T7E1 assay to check the *IRAK4* knock-out efficiency in HEK293 cells transduced with two different gRNAs targeting *IRAK4* (Figure 3.10). We demonstrated that multiple bands were present in the agarose gel images after T7E1 treatment, indicating presence of double-strand breaks in *IRAK4* KO cells (Figure 3.10). However, it was clear from the T7E1 assay that *IRAK4* KO cell lines were comprised of mixed populations of HEK293 cells bearing both edited and non-edited genomes (Figure 3.10). Therefore, we decided to perform single-cell selection to ensure the homozygosity of HEK293 KO cell lines. After obtaining pure single cell clones by dilution method, we screened single-cell clones to select the most efficient *IRAK4* KO HEK293 single-cell clones.

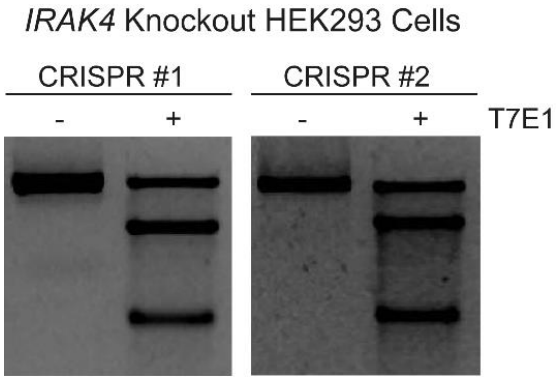

Figure 3. 10 T7E1 Assay of *IRAK4* KO HEK293 cells**.** Agarose gel images showing T7E1 assay on *IRAK4* KO HEK293 cells. Cell lines CRISPR #1 and CRISPR #2 were generated by IRAK4 gRNA1 and IRAK4 gRNA2 primer sets, respectively. Adapted from Tepe ZG et al., 2023[185]

Next, we screened 10 *IRAK4* KO HEK293 single-cell clones by NFκB-dependent Secreted Alkaline Phosphates (SEAP) reporter assay. We found two KO cell lines (KO#1 and KO#2), which did not show any alkaline phosphatase activity driven by NFκB promoter upon IL-18 treatment when transfected with the empty vector. Both lines were able to restore high alkaline phosphatase activity upon transient over-expression of WT IRAK-4 (Figure 3.11). Therefore, we selected KO #1 and KO#2 single-cell clones for further analyses.

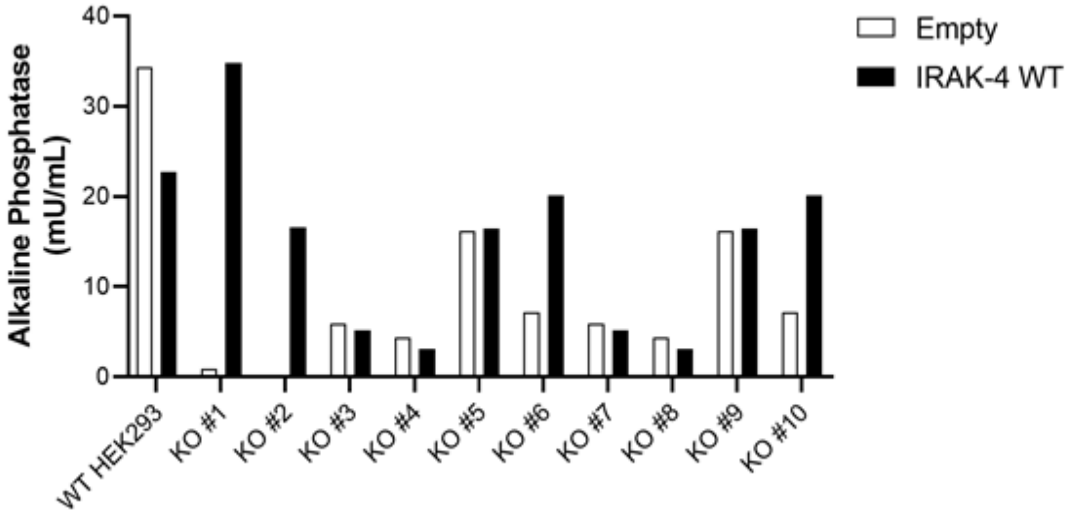

Figure 3. 11 Screening of *IRAK4* KO HEK293 single-cell clones using secreted alkaline phosphatase reporter assay. IL-18 induced reporter activity of WT IRAK-4 was used to screen *IRAK4* KO single-cell clones. Ten *IRAK4* KO HEK293 single-cell clones and WT HEK293 cells were transfected with plasmids expressing NFκB-dependent alkaline phosphatase, IL18RAP and either empty vector (shown in white) or WT IRAK-4 (shown in black). At 24 hours post-transfection, cells were stimulated with IL-18 for 12 hours and culture supernatants were collected to measure alkaline phosphatase activity. Alkaline phosphatase activity was calculated from standard curves plotted using alkaline phosphatase standards. Bars represent alkaline phosphatase levels.[185]

We validated the removal of targeted *IRAK4* exon region in both KO#1 and KO#2 HEK293 single cell clones with competition-based PCR (Figure 3.12). When compared with WT HEK293, it was evident that PCR products amplified with reverse "in" primers in KO#1 and KO#2 HEK293 single cell clones were higher in size, indicating the inefficient binding of reverse "in" primers (Figure 3.12). Those inefficient binding of "in" primers were resulting from the excision of CRISPR-targeted exome, thus longer PCR products were expected in KO cells. As a result, we confirmed that *IRAK4* was efficiently knocked out in both KO#1 and KO#2 HEK293 single cell clones.

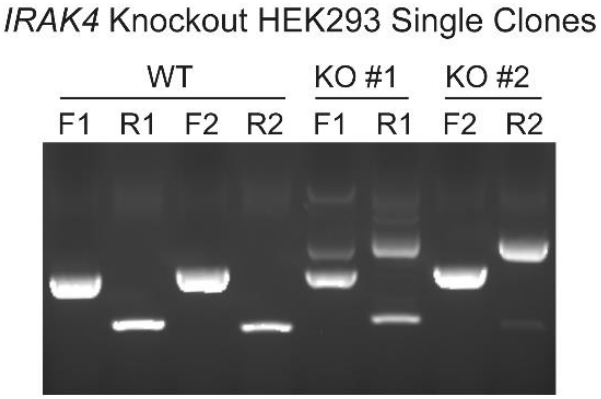

Figure 3. 12 Competition-based PCR assay. Agarose image showing competition-based PCR assay on *IRAK4* KO single clones of HEK293 cells (KO #1 and KO #2) generated by IRAK4 gDNA1 and IRAK4 gDNA2 primer sets respectively. Adapted from Tepe ZG et al., 2023[185]

Moreover, we checked for IRAK-4 expression in KO#1 and KO#2 HEK293 single cell clones. We showed that IRAK-4 expression was abolished in both KO#1 and KO#2 HEK293 single-cell clones by both flow cytometry and immunoblotting (Figure 3.13). Collectively, we generated two different *IRAK4* KO HEK293 cell lines to be utilized in order to test the damaging impact of p.C79Y on IRAK-4 function *in vitro*.

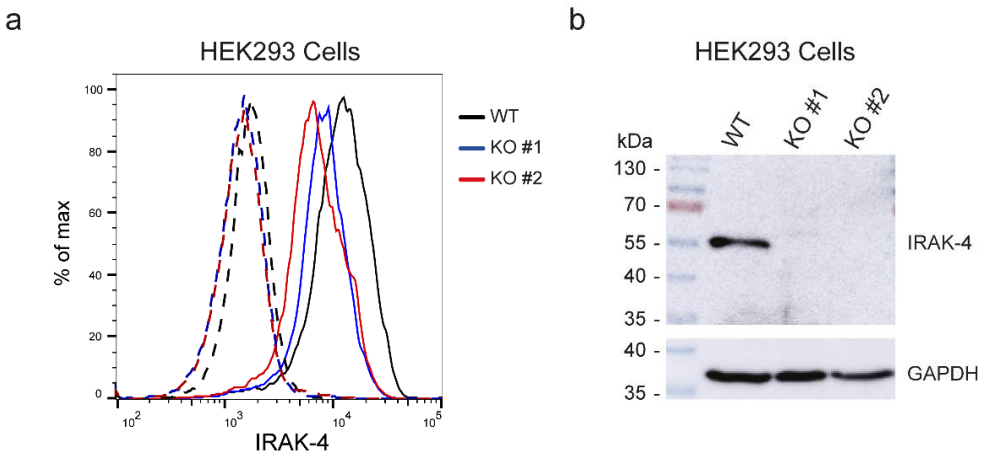

Figure 3. 13 Validation of IRAK-4 deficiency in *IRAK4* KO HEK293 single-cell clones a. Histogram showing intracellular IRAK-4 expression in WT and *IRAK4* KO single clones of HEK293 cells (KO #1 and KO #2) by flow cytometry. Dashed lines show unstained controls. b. Representative immunoblot image showing IRAK-4 expression in whole cell lysates (75 µg protein/lane) from WT, KO #1 and KO #2 HEK293 cells. Immunoblotting was performed with the IRAK-4 antibody, followed by GAPDH antibodies after stripping of the membrane, respectively. Expected molecular weights: IRAK-4; ~55 kDa, GAPDH: ~36 kDa. Adapted from Tepe ZG et al., 2023[185]

Finally, we transiently transfected KO#1 and KO#2 HEK293 single-cell clones with plasmids expressing NF-kB-dependent Firefly luciferase, IL18RAP, Renilla luciferase as internal control for normalization, and either empty vector, WT, or mutant (p.C79Y and p.R12C) *IRAK4* constructs. At 24 hours post-transfection, cells were treated with IL-18 for 12 hours. We found that expression of IRAK-4 with p.C79Y had reduced (up to 60%) relative luciferase activity, whereas p.R12C had almost abolished luciferase activity, as expected[143], compared to the WT in *IRAK4* KO HEK293 cells treated with IL-18. (Figure 3.14). Collectively, these results indicated that the p.C79Y was hypomorphic, impairing the IRAK-4 function.

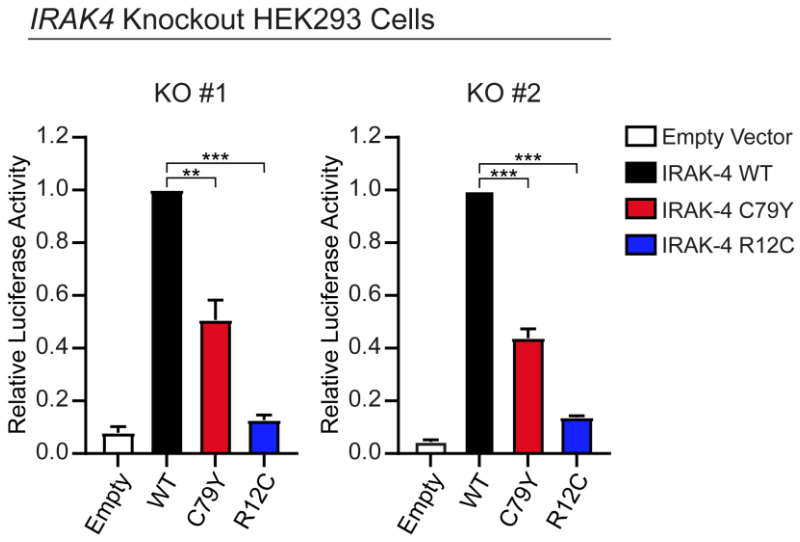

Figure 3. 14 The p.C79Y impairs IRAK-4 function *in vitro*. *IRAK4* KO HEK293 single cell clones, KO #1 and KO #2, were transiently transfected with plasmids expressing NFκB-dependent Firefly luciferase, Renilla luciferase, IL18RAP, and either empty vector, WT, or mutant (p.C79Y and p.R12C) IRAK-4. At 24 h post-transfection, cells were stimulated with human recombinant IL-18 for 12 h, followed by measurement of luciferase activity. Relative luciferase activity was calculated as normalization of Firefly luciferase to Renilla luciferase activity. The values shown are the mean ± SEM of two independent experiments performed in duplicates (*$P < 0.05$; **$P < 0.01$; ***$P < 0.001$; two-tailed unpaired Student's t test). Adapted from Tepe ZG et al., 2023[185]

3.9.Assessment of anti-viral immune responses in patient's leukocytes

It was previously shown that IRAK-4 deficient patients' cells have impaired type I IFN production, such as IFN-α/β and IFN-λ, in response to TLR7, TLR8 and TLR9 stimulation[190,191]. On the other hand, no susceptibility to a severe viral disease was previously reported in patients with IRAK-4 deficiency[192]. Given that the patient investigated in this study was diagnosed with acute HHV-6 encephalitis, we therefore sought to assess anti-viral immune responses in patient's leukocytes upon stimulation with various ligands, such as R848 for TLR7 and TLR8, poly(I:C) for TLR3, CpG for TLR9, 2'3'-cGAMP for STING and poly(dA:dT) for cytosolic DNA sensors, such as

DAI, DDX41, cGAS, LRRFIP1 and AIM2[193,194]. We utilized a multiplex fluorescence-encoded bead-based immunoassay, using cell culture supernatants, which allows simultaneous quantification of 13 human cytokines: IL-1β, IL-6, IL-8, IL-10, IL-12p70, IFN-α2, IFN-β, IFN-λ1, IFN-λ2/3, IFN-γ, TNF, IP-10 and GM-CSF, involved in anti-viral innate immunity. IL-1β activates adaptive immunity, induces antiviral effector molecules, regulates inflammatory processes by promoting inflammation and modulates innate immune responses by activating natural killer (NK) cells and maturation of dendritic cells[195–197]. IL-6 induces the production and secretion of acute phase proteins in response to viral infection, promotes inflammation, enhances cytotoxic activity of NK cells, and stimulates B cell and T cell differentiation[198–200]. IL-8, also known as CXCL8, is a chemokine involved in the attraction and activation of neutrophils in response to viral pathogens[200–202]. IL-10 possesses anti-inflammatory activity, by which it prevents antigen presenting cells to produce pro-inflammatory cytokines and modulates T cell activation by downregulating co-stimulatory molecules on dendritic cells[203,204]. IL-12 promotes the differentiation and activation of T_H1 cells, activates APCs, and enhances NK cell and cytotoxic T cell responses[198,205]. Type I IFNs, IFN-α2 and IFN-β, blocks viral replication by upregulating IFN-stimulated genes, activates natural killer cells and antigen presenting cells, and amplifies immune responses against viruses by inducing pro-inflammatory cytokines[196,198,206]. Similarly, type III IFNs, IFN-λ1 and IFN-λ2/3, inhibits viral replication, protects epithelial barriers and stimulates antigen presentation[207,208]. IFN-γ activates macrophages, enhances antigen presentation, promotes cytotoxic T cell responses, regulates T helper cell differentiation and boosts NK cell activity[198,209]. TNF induces inflammation and apoptosis in infected cells, activates macrophages, stimulates antigen presentation,

modulates T cell responses, and regulates adaptive immune responses[198,200,203]. IP-10, also known as CXCL10, is a chemokine involved in the recruitment of activated T cells and induction of NK cell-mediated cytolysis[198,200]. GM-CSF promotes myeloid cell differentiation, modulating granulocyte function and activates macrophages and dendritic cells[210,211].

Upon TLR7 and TLR8 stimulation by R848 treatment, we found that production of all cytokines, except IL-8, was significantly reduced in the patient's leukocytes when compared with that of healthy controls. The reduction was more than 10-fold for IL-1β, IFN-γ, TNF, IP-10 and GM-CSF in patient's leukocytes. Additionally, IL-12p70 and IFN-β production was reduced nearly 10-fold in patient's leukocytes. IL-8 production in the patient was comparable to healthy controls upon R848 treatment (Figure 3.15, 3.16 and 3.17).

Upon TLR3 stimulation by poly(I:C) treatment, we observed that the expression of several cytokines, such as IL-6, IL-12p70, IFN-λ1, TNF, IP-10 and GM-CSF, was reduced up to 3-fold in patient's leukocytes. Production of IL-1β and IL-8 was reduced around 5-fold in patient's leukocytes when compared with healthy controls. Additionally, dramatic reduction in the production of IFN-β, IFN-λ2/3 and IFN-γ was observed in patient's leukocytes, 10-fold, 40-fold and 20-fold, respectively. No significant changes in the expression of IL-10 and IFN-α2 were seen in patient's leukocytes compared to healthy controls (Figure 3.15, 3.16 and 3.17).

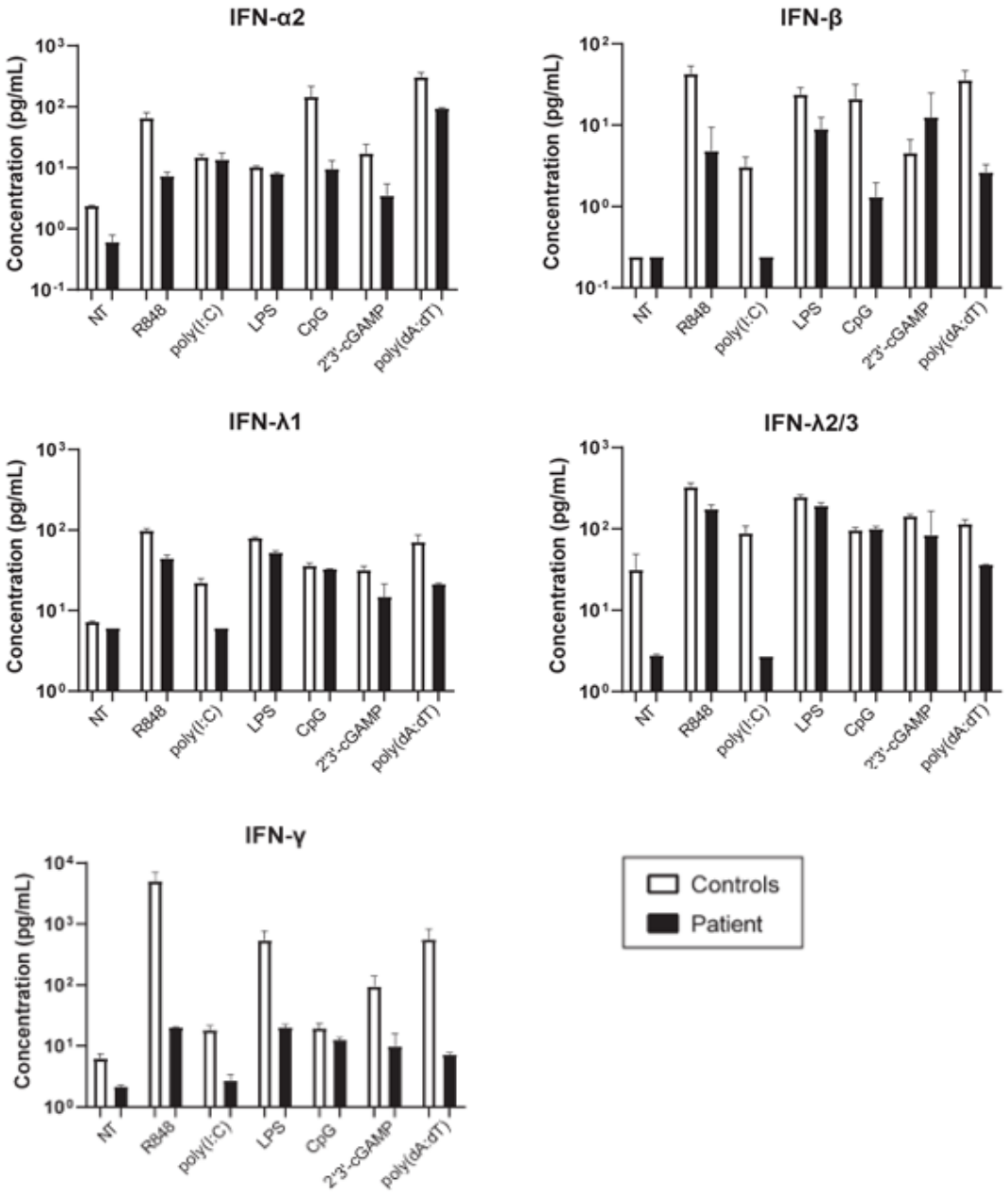

Figure 3. 15 Assessment of IFN-α2, IFN-β, IFN-λ1, IFN-λ2/3 and IFN-γ responses in patient's leukocytes. Bead-based immunoassay cytokine profiling was performed to measure cytokine levels using supernatants of PBMCs from the patient (P) and two healthy controls (C1 and C2) upon 24 h treatment with various stimuli indicated. The control average was calculated as the mean of two healthy controls (C1 and C2). Bars are on a base-10 logarithmic scale representing the mean ± SEM of two independent experiments using PBMCs isolated from peripheral blood at different times. Adapted from Tepe ZG et al., 2023[185]

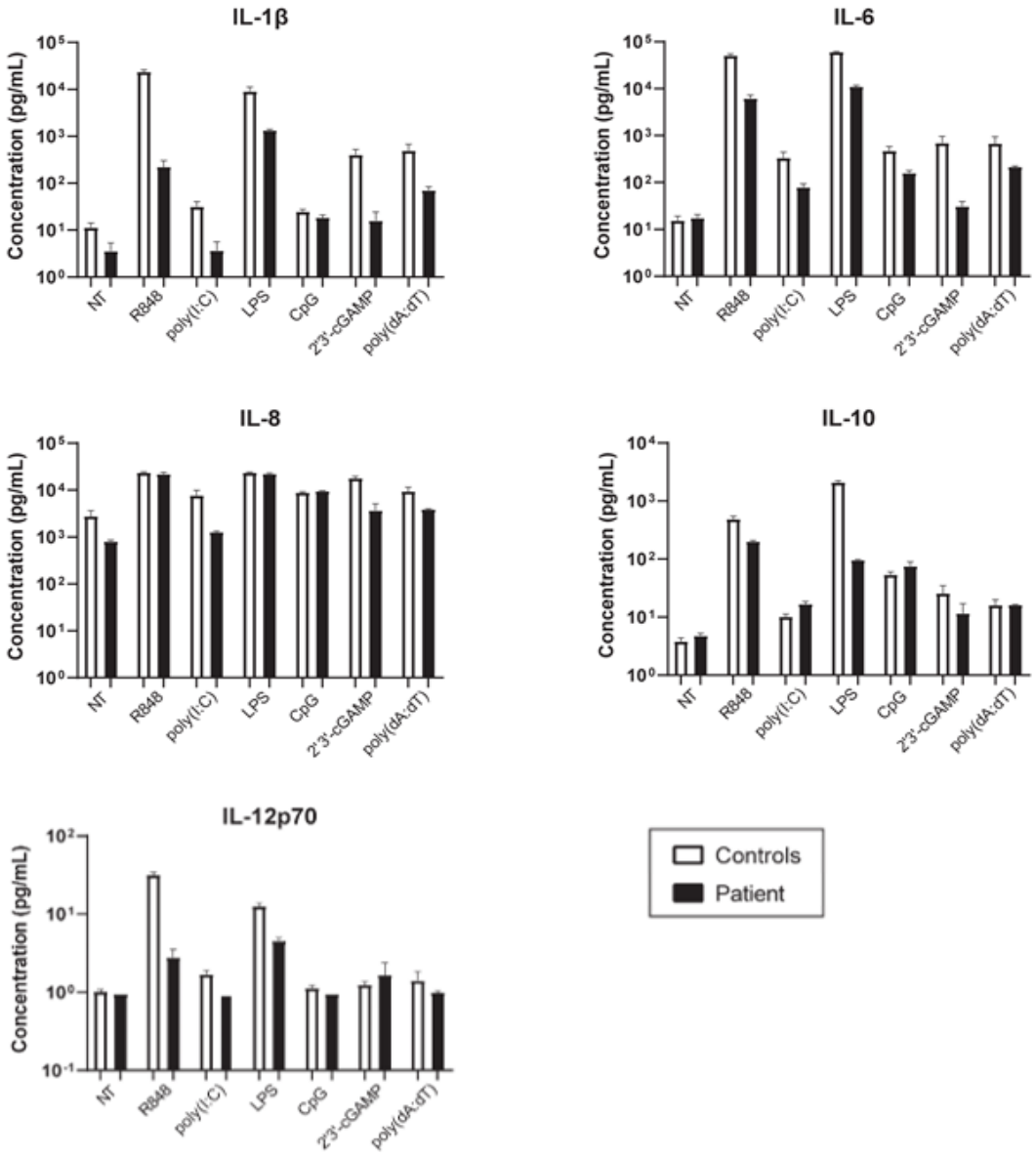

Figure 3. 16 Assessment of IL-1β, IL-6, IL-8, IL-10 and IL-12p70 responses in patient's leukocytes. Bead-based immunoassay cytokine profiling was performed to measure cytokine levels using supernatants of PBMCs from the patient (P) and two healthy controls (C1 and C2) upon 24 h treatment with various stimuli indicated. The control average was calculated as the mean of two healthy controls (C1 and C2). Bars are on a base-10 logarithmic scale representing the mean ± SEM of two independent experiments using PBMCs isolated from peripheral blood at different times. Adapted from Tepe ZG et al., 2023[185]

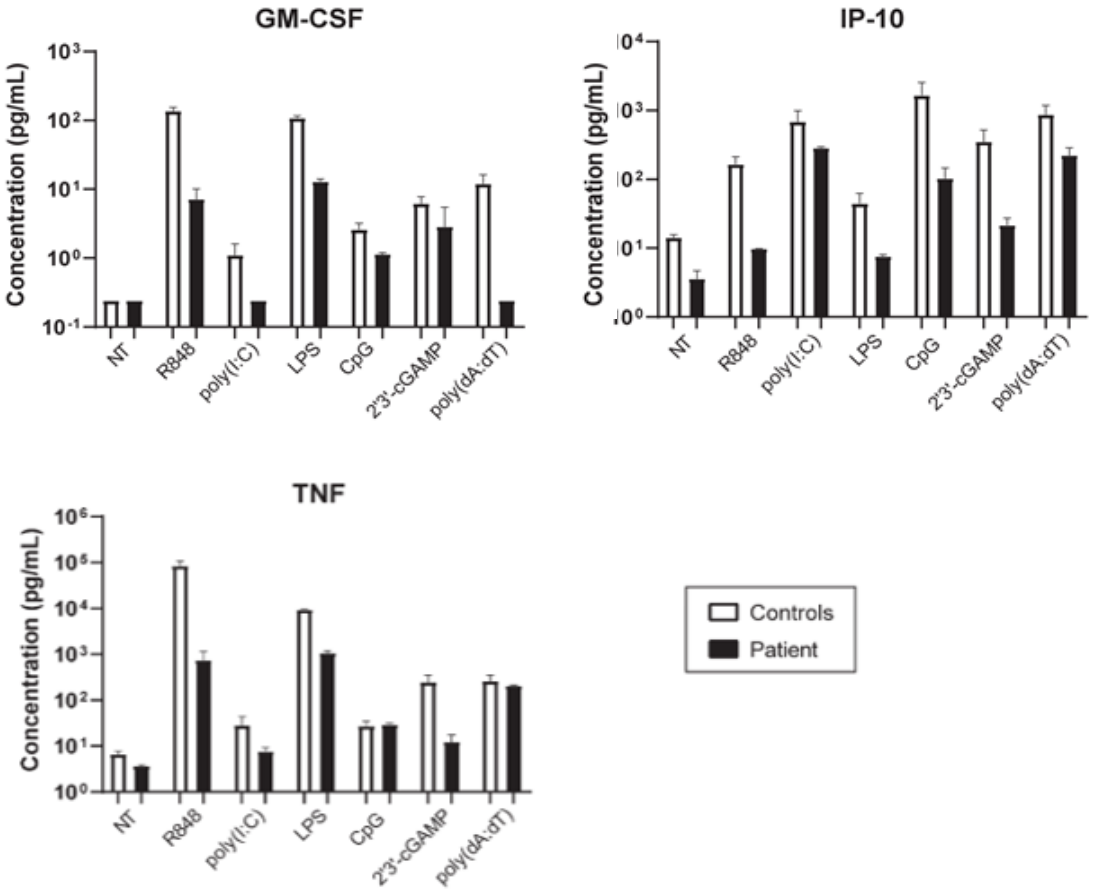

Figure 3. 17 Assessment of GM-CSF, IP-10 and TNF responses in patient's leukocytes. Bead-based immunoassay cytokine profiling was performed to measure cytokine levels using supernatants of PBMCs from the patient (P) and two healthy controls (C1 and C2) upon 24 h treatment with various stimuli indicated. The control average was calculated as the mean of two healthy controls (C1 and C2). Bars are on a base-10 logarithmic scale representing the mean ± SEM of two independent experiments using PBMCs isolated from peripheral blood at different times. Adapted from Tepe ZG et al., 2023[185]

Upon TLR9 stimulation by CpG treatment, expression of IL-6, IFN-α2, IFN-β and IP-10 were reduced in the patient's leukocytes. Levels of several cytokines, such as IL-1β, IL-8, IL-10, IL-12p70 and TNF, in patient's leukocytes were comparable to healthy controls upon CpG induction (Figure 3.15, 3.16 and 3.17).

Upon cytosolic DNA sensor STING activation by 2'3'-cGAMP, we showed that production of almost all cytokines tested, such as IL-1β, IL-6, IL-8, IL-10, IFN-α2,

IFN-λ1, IFN-λ2/3, IFN-γ, TNF, IP-10 and GM-CSF, were decreased in patient's leukocytes compared to healthy controls, whereas no significant changes were observed for the production of IL-12p70 and IFN-β (Figure 3.15, 3.16 and 3.17).

Upon activation of cytosolic nucleic acid sensors by poly(dA:dT), we found the impaired induction of almost all cytokines tested in patient's leukocytes when compared with healthy controls. Only the production of IL-10 and TNF in patient's leukocytes were similar to that of control leukocytes in response to poly(dA:dT) treatment (Figure 3.15, 3.16 and 3.17).

We also stimulated patient's leukocytes with a bacterial ligand, LPS, which induces TLR4 activation, as a control. Upon TLR4 stimulation by LPS treatment, we found that the production of several cytokines, such as IL-1β, IL-6, IL-10, IFN-γ, TNF, IP-10 and GM-CSF, was diminished in patient's leukocytes when compared with healthy controls. Moreover, impaired induction of the following cytokines: IL-12p70, IFN-β, IFN-λ1 and IFN-λ2/3, was also observed in patient's leukocytes but only up to 2- fold compared to healthy controls (Figure 3.15, 3.16 and 3.17).

Finally, we sought to further validate reduced anti-viral immune responses, such as IFN-α2 and IL-6, in patient's leukocytes by utilizing ELISA. We therefore stimulated PBMCS from the patient, his 2 years older sibling and parents, and three unrelated healthy donors with R848, Poly(I:C), CpG, 2'3'-cGAMP and poly(dA: dT) and PMA/Ionomycin for 24 hours (Figure 3.18). Upon R848, CpG treatment, poly (dA:dT) treatment, IFN-α2 production was not detected in patient's cells compared to that of healthy donors and his family members (Figure 3.18). IFN-α2 response to 2'3'-cGAMP was variable, and no IFN-α2 responses were detected from patient's, his sibling's and two unrelated controls' cells by ELISA. (Figure 3.18). Similarly, there

was no IFN-α2 response detected by ELISA from patient's and his mother's cells upon poly(I:C) treatment (Figure 3.18). We also found that patient's leukocytes had apparently decreased IL-6 responses to R848, poly(I:C), CpG, and poly(dA:dT), when compared to healthy donors and his family members. On the other hand, 2′3′-cGAMP was less potent compared to other stimuli, leading to variably low or undetectable IL-6 responses, like IFN-α2, by ELISA among the patient and healthy individuals. Finally, we found similar levels of IL-6 production in patient's and healthy controls' cells upon PMA/Ionomycin stimulation, indicating that decreased IL-6 responses from patient's leukocytes were due to IRAK-4 deficiency rather than defective IL-6 machinery (Figure 3.18). As expected, no IFN-α2 production was detected from PBMCs upon PMA/Ionomycin stimulation (Figure 3.18).

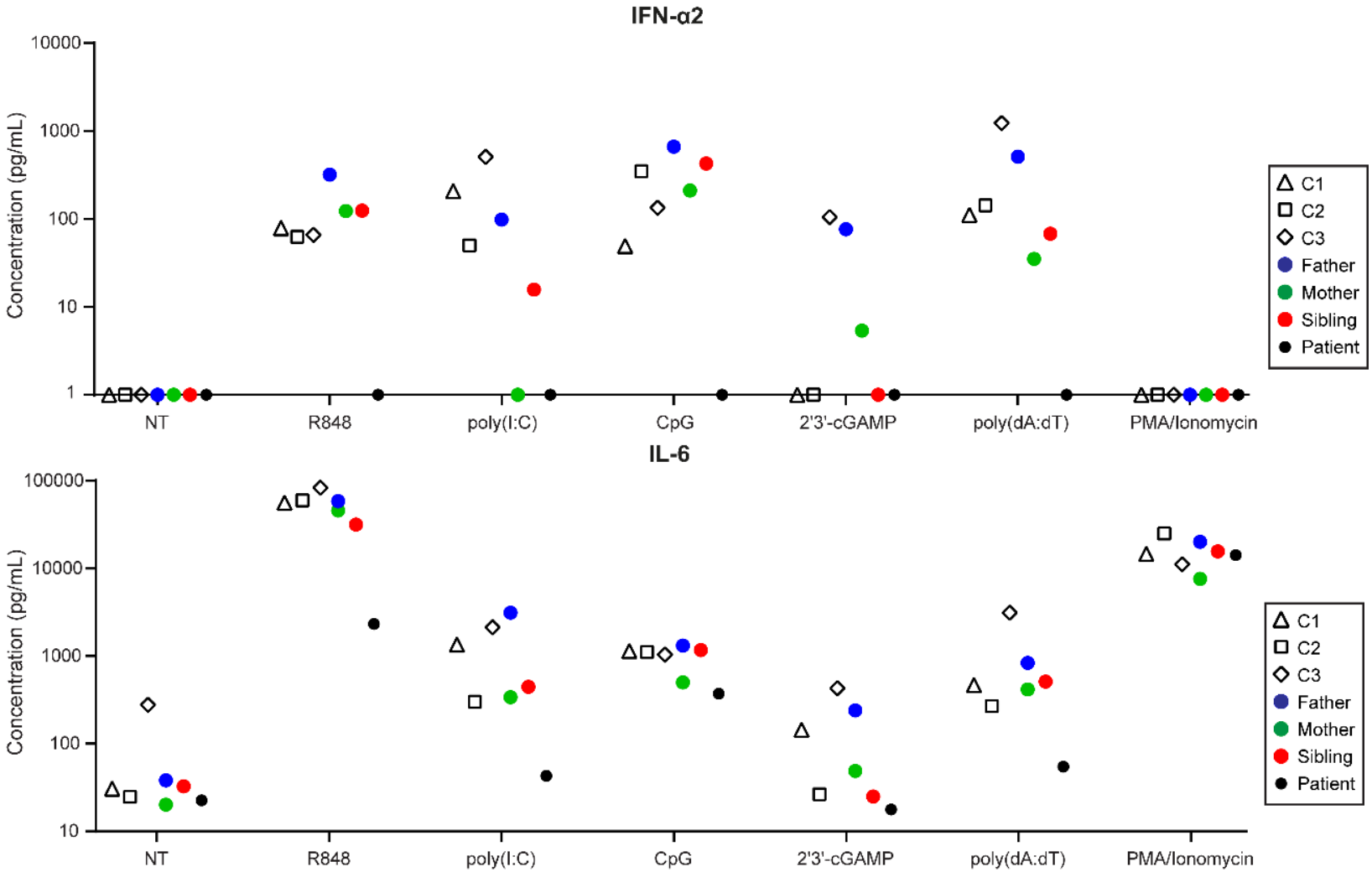

Figure 3. 18 Validation of reduced IFNa2 and IL-6 responses in patient's leukocytes by ELISA. ELISA was performed using supernatants of PBMCs from the patient, his family members (Sibling, Mother and Father) and three healthy controls (C1, C2, C3) upon 24 h treatment with various stimuli indicated. Adapted from Tepe ZG et al., 2023[185]

CHAPTER 4

Discussion

In this study, we have revealed a possible causal connection between inherited IRAK-4 deficiency and HHV-6 encephalitis in a 10-months old male infant. Human Herpesvirus-6 (HHV-6) is a ubiquitous virus belonging to the Herpesviridae family[70]. Primary HHV-6 infection usually occurs during childhood, causing roseola infantum, a self-limiting febrile illness[79]. In immunocompetent individuals, HHV-6 infection is generally mild and resolve spontaneously[49]. However, in individuals with impaired immune responses, HHV-6 can lead to severe complications, including encephalitis[79,98]. However, encephalitis is a very rare complication of primary HHV-6 infection in otherwise healthy children[212]. Various inborn errors of immunity were reported to cause viral encephalitis in otherwise healthy children[121]. The patient in this study was diagnosed with acute HHV-6 encephalitis upon presumably a primary infection at the age of 10 months. His past medical history included only recurrent upper respiratory tract infections. His immunological evaluation was normal, with no family history of primary immunodeficiency or other immunological disorders. Therefore, we hypothesized that a monogenic defect could underlie the susceptibility to HHV-6 encephalitis in this patient[213]. We performed WES analysis on the patient's gDNA and identified a homozygous *IRAK4* p.C79Y variant in the patient. Inherited IRAK-4 deficiency is a rare primary immunodeficiency disorder characterized by impaired innate immune responses[214]. *IRAK4* encodes a kinase involved in the TLR and IL-1R signaling pathways,

which plays a crucial role in the pathogen recognition signaling and subsequent immune activation[144]. Bi-allelic damaging mutations in the *IRAK4* lead to defective innate immune responses, resulting in predisposition to recurrent severe bacterial infections[215]. Up to the now, 31 disease-causing mutations in IRAK-4 were identified in patients and still, none of them has been associated with a severe viral susceptibility[143,216]. One recent publication reported a case with anti-NMDAR encephalitis upon HHV-6 reactivation in a patient with IRAK-4 deficiency[143]. Nonetheless, limited evidence in the literature implies the involvement of IRAK-4 in viral immune response[147,217]. According to the *in silico* damage prediction tools, we found that IRAK-4 p.C79Y was potentially damaging like most of the previously reported 31 disease-causing mutations, all of which impaired IRAK-4 function *in vitro*[143]. Thus, we investigated whether the p.C79Y could affect IRAK-4 expression and/or function. The patient's leukocytes showed impaired IRAK-4 expression in various leukocyte subsets. In line with this, in transiently over-expressed HEK293 cells, the p.C79Y variation had dramatically reduced IRAK-4 stability compared to WT, which was evident following treatment with cycloheximide, a protein synthesis inhibitor. Additionally, the p.C79Y significantly reduced the NF-kB activation based on the *in vitro* luciferase reporter assay performed in *IRAK4* KO HEK293 cells. Collectively, we showed that the p.C79Y variation was severely hypomorphic, affecting both the expression and function of IRAK-4.

Furthermore, we revealed that the patient had impaired anti-bacterial and anti-viral immune responses against various stimuli inducing different TLRs and cytosolic nucleic acid sensors, likely due to impaired IRAK-4 expression and function as a result of the hypomorphic effect of the p.C79Y variant. Known IRAK-4-deficient patients presented with susceptibility only to pyogenic invasive bacteria, with normal immune responses to

viral infections[192]. Interestingly, the patient studied in this thesis was diagnosed with HHV-6 encephalitis, a very rare complication of acute HHV-6 infection, with no medical history of susceptibility to any invasive bacterial infection. Previously, no patients with IRAK-4 deficiency reported for severe viral diseases[96,117,137,147,148]. Our findings represent the first evidence linking inherited IRAK-4 immunodeficiency to severe viral diseases It was reported that PCR testing against HHV-6 was performed in 6 different IRAK-4 deficient patients, and all of them tested positive[171]. It was unclear whether the patients had an acute infection or ciHHV-6[171]. However, no unusual symptoms were identified in those patients prior to bacterial infections reported[171]. Moreover, a previously reported case of a patient with IRAK-4 deficiency had demonstrated an association between HHV-6 reactivation and anti-NMDAR encephalitis in an otherwise healthy child[143]. Of note, *IRAK4* is highly expressed in neuronal cells of mice and humans, particularly in the microglia, which was demonstrated in several studies[218–220]. It was possible that IRAK-4 deficiency impairs cell-intrinsic immunity in the brain, rather than leukocyte mediated innate and adaptive immunity. That could explain why the patient in this study experienced severe complications restricted to the brain upon acute HHV-6 infection. It is noteworthy that the patient in this study showed susceptibility to HHV-6 infection only in the brain, whereas no other major symptoms were associated with other viral infections in the patient. Following the genetic diagnosis of IRAK-4 deficiency in the patient, he was given prophylactic treatment including antibiotic prophylaxis, vaccination, and IVIG replacement therapy. During this period, the patient had once SARS-CoV-2 infection, but only with mild symptoms[186]. We do not know the precise mechanisms, by which inherited IRAK-4 deficiency could underlie development of HHV-6 encephalitis in this patient. Collectively, this study expanded the clinical spectrum of human IRAK-4 deficiency by

providing compelling evidence for the involvement of IRAK-4 in HHV-6 pathogenesis in the brain.

Although the exact molecular and cellular mechanisms of IRAK-4 in the development of HHV-6 encephalitis remain to be dissected, possible mechanisms could imply the involvement of IRAK-4 in brain-intrinsic anti-viral immunity. It was demonstrated in both mice and human studies that TLR3 signaling plays a central role upon neurotropic viral infection, whereas TLR2, TLR4, TLR7, TLR8 and TLR9 were found to be crucial for the initiation of immune responses against viral pathogens in the CNS[221]. IRAK-4 is involved in all TLR pathways, except TLR3[144]. Therefore, IRAK-4 deficiency might disrupt the initiation of anti-viral responses upon TLR2, TLR4, TLR7, TLR8 and TLR9 activation in the brain. TLR9 is highly expressed in microglia, which are the primary immune cells of the CNS[222,223]. In a mouse model of HHV-6A-induced brain infection, it was shown that TLR9 signaling is associated with the development of virus-induced neuroinflammation[224]. It was also previously demonstrated in human $CD4^+$ T cells that TLR9 signaling is required for sensing HHV-6 infection, which in turn induces expression of the receptor[225,226]. TLR9 pathway involves MyD88 and IRAK-4 molecules to transmit signaling upon activation[184]. Therefore, IRAK-4 deficiency might prevent the sensing of HHV-6 by TLR9 in neuronal cells, that may promote the development of encephalitis upon HHV-6 infection. Accordingly, the patient in this study showed impaired immune responses against the ligands of TLR7, TLR8 and TLR9, which may potentially underlie the development of HHV-6 encephalitis. Moreover, IFNα/β-mediated immunity is found to be crucial for the protection against viral encephalitis[124]. We found that the patient had reduced IFN production when compared to healthy controls upon stimulation with various TLR and, in particular, cytosolic nucleic acid sensor ligands. Defective TLR3-dependent

type I IFN production was found to underlie HSE in otherwise healthy children[124]. Upon poly(I:C) treatment, which is a synthetic ligand for TLR3, production of IFN-β, IFN-λ1, IFN-λ2/3 (measured by bead-based immunoassay) and IFN-α2 (measured by cytokine ELISA) were reduced in patient's leukocytes compared to healthy controls and his family members. However, previous studies demonstrated that IRAK-4 deficient patients' leukocytes showed similar production of IFN-α/β and IFN-λ compared to control cells upon TLR3 stimulation[146]. Although the reduction in type I IFN response upon poly(I:C) in the patient in this study might be TLR3 independent, it still may underlie the development of HHV-6 encephalitis. Interestingly, patient's leukocytes had also reduced immune responses to poly(dA:dT), which typically triggers cytosolic nucleic acid sensors that are expected to function independently of IRAK-4. Nevertheless, we did not perform in-depth experiments to reveal whether this deficiency in the patient's cells resulted from impaired signaling of cytosolic nucleic acid sensing pathways or simply indirect consequences of poly(dA:dT). Previous studies stated that impaired IFN production specifically in the CNS could underlie susceptibility to viral encephalitis[124]. In this study, we did not perform any experiments on patient-derived neuronal cells. Therefore, it is difficult to predict with our data whether altered IFN responses were present in the CNS or relevant to the development of HHV-6 encephalitis. Additionally, MyD88 signaling was previously shown to be important for both innate and adaptive immunity during CNS infections[227,228]. It was shown that in MyD88 deficient mice, production of IFN-α/β and further induction of interferon-stimulating genes were impaired during the course of mouse hepatitis virus (MHV) infection[227]. Given that IFN-α/β is essential for preventing viral spread in the CNS[206,229,230], MyD88 signaling was suggested to be involved in the control of viral dissemination[227]. As IRAK-4 recruitment is required for the formation of

the Myddosome complex downstream of TLR activation, IRAK-4 deficiency might disrupt MyD88 signaling and early anti-viral immune responses. Thus, the induction of IFNs in the early phase of infection would be impaired, leading the uncontrolled viral replication[231]. These findings implied that IRAK-4 may involve in the CNS-specific cell-intrinsic immunity as it functions downstream of MyD88.

Additionally, it was demonstrated that $CD4^+$ T cell recruitment to the brain was impaired upon MHV infection in MyD88 deficient mice, leading to encephalomyelitis[227]. Moreover, in another study, they showed that $CD8^+$ T cell recruitment to the brain was impaired upon vesicular stomatitis virus infection in MyD88/TRIF double KO mice, resulting in the development of encephalitis[228]. Collectively, it was clear that MyD88 is crucial for the protection against encephalitis upon viral infection in mice[227,228]. Therefore, IRAK-4 might be also associated with the development of encephalitis through MyD88-dependent signaling in brain.

The mutation found in the patient is located in the DD of IRAK-4, which could potentially impact on its interaction with other molecules. Only 5 of the previously reported IRAK-4 mutations were located in the DD, including one frameshift, one stop-gain, one missense, one deletion and one duplication mutations. Impact of these mutations on the molecular interactions of IRAK-4 is unknown and further mechanistic studies are required. IRAK-4 DD interacts with MyD88 during Myddosome complex formation[185]. However, it needs to be further investigated whether DD is involved in the interaction with other molecules. It was previously shown that IRAK-4 interacts with TRAF6 upstream to NFκB singaling pathway, however the exact structural involvement is unknown[144,232,233]. Previous studies demonstrated that binding of TRAF6-HSV virion tegument protein is required for the activation of NFκB signaling, for the recognition of virus following the viral entry[234]. C79

might also be involved in the interaction between IRAK-4 and TRAF6. This variation might disrupt TRAF6 interaction of IRAK-4, leading to impaired NFκB activation in response to herpesviruses. Similarly, IRF7 was shown to interact with Myddosome complex proteins including IRAK-4[233]. IRF7 is a transcriptional factor, involving in the regulation of IFN production, which is crucial for anti-viral immunity[235,236]. Similar to TRAF6, it is plausible that p.C79Y might impair the interaction of IRAK-4 with IRF7, leading to impaired induction of IFNs in response to viruses.

Additionally, IRAK-4 might interact with other proteins in CNS through its DD. Since the role of IRAK-4 in CNS is not well-understood, little information is available on its interactome in CNS. In particular, the p.C79Y could potentially impair the interactions of IRAK-4 in the brain, suggesting the need for further studies to elucidate the impact of p.C79Y on the interaction of IRAK-4 DD with other molecules.

The identification of inherited IRAK-4 deficiency in patients with acute HHV-6 encephalitis has important clinical implications and might expand potential management strategies. Early recognition of this immunodeficiency can guide appropriate management strategies to improve patient outcomes. Prophylactic antibiotic treatments are already commonly employed in patients with IRAK-4 deficiency to prevent recurrent bacterial infections and reduce the overall disease burden[192]. After identification of IRAK-4 deficiency in the patient in this study, prophylactic antibiotic treatment was prescribed immediately. After that, no severe bacterial infection was reported in the patient. In some cases, additional immunoglobulin replacement therapy was also prescribed to individuals to address the underlying immunodeficiency and provide passive immunity against bacterial and viral pathogens[237]. The patient in this case also had intravenous immunoglobulin replacement therapy, which improved his symptoms. In addition to the

treatment strategies used in the clinics, targeted antiviral therapies could be used for IRAK-4 deficient patients. While antiviral therapies specifically targeting HHV-6 are currently limited, advancements in anti-viral research may lead to the development of targeted therapies for patients with IRAK-4 deficiency and HHV-6 encephalitis[238]. Future studies focusing on understanding the specific mechanisms of HHV-6 replication and the host-virus interactions in the context of IRAK-4 deficiency could provide valuable insights for the development of novel therapeutic strategies.

There have been some limitations of this study. First of all, this study was based on only one patient. Generalization of single-patient genetic studies to broader populations might be challenging[164]. The impact of genetic variations on disease prognosis shows inter-individual differences possibly through both genetic, epigenetic and environmental factors[164]. Multiple gene contributions to clinical phenotype are also possible, where single-patient studies generally exclude such contributions[164]. Yet, several studies provided that most genetic cases of life-threating infectious diseases during childhood result from monogenic inborn error of immunity, whereas such diseases in elderly are more influenced by polygenic, somatic and epigenetic factors[213]. Moreover, environmental factors and the medical history of the patient could have implications on the prognosis of disease[164]. Drawing definitive conclusions and identifying direct connections between inherited variations and clinical phenotype could be challenging and further in-depth mechanistic studies may be required to establish the association between the genetic variant and the clinical phenotype.

CHAPTER 5

Conclusion and Future Perspectives

In conclusion, this study showed that inherited IRAK-4 deficiency can be presented with susceptibility to a severe viral disease, notably HHV-6 encephalitis. The association between inherited IRAK-4 deficiency and acute HHV-6 encephalitis represents a relatively emerging field of research. Further studies are needed to elucidate the underlying mechanisms and determine the exact role of IRAK-4 in HHV-6 pathogenesis in brain. Indeed, the cell-specific roles of IRAK-4 in the brain are unknown and warrant further investigation. The existing studies have provided valuable insights into the involvement of IRAK-4 in neuroinflammatory responses and its potential implications in neurological disorders[239,240]. However, a comprehensive understanding of IRAK-4's specific functions within different regions of the brain and its contribution to various cellular processes are still lacking. Future studies may focus on elucidating the precise mechanisms, by which IRAK-4 deficiency affects brain physiology and pathology during acute HHV-6 infection. Additionally, cell-intrinsic roles of IRAK-4 in neuronal regulation of immunity should be investigated. Advanced techniques, such as cell-specific gene editing, transcriptomics and proteomics can be employed to unravel the molecular pathways and signaling networks involving IRAK-4 in specific brain cell types utilizing infection models of human primary cell lines or patient's induced pluripotent stem cells. These will provide better understanding of the clinical relevance of IRAK-4 deficiency with viral encephalitis. Additionally, identification and characterization of novel

interaction partners of IRAK-4 will provide a more comprehensive understanding of its role in neuronal tissues. Therefore, investigating the potential therapeutic implication of modulating IRAK-4 activity in the brain is an exciting avenue for future research.

In summary, further exploration of the tissue-specific roles of IRAK-4 in the brain will undoubtedly enhance our knowledge of brain inflammation, notably upon HHV-6 infections. Better understanding the mechanisms underlying this association is crucial for improving disease outcomes and developing targeted therapeutic strategies.

REFERENCES

1. Bloch KC, Glaser CA, Tunkel AR. *Encephalitis and Myelitis*. Fourth Edi. Elsevier Ltd; 2017. doi:10.1016/B978-0-7020-6285-8.00020-4

2. Roos KL. ENCEPHALITIS. *Neurol Clin*. 1999;17(4):813-833. doi:10.1016/S0733-8619(05)70168-7

3. Venkatesan A, Michael BD, Probasco JC, Geocadin RG, Solomon T. Acute encephalitis in immunocompetent adults. *Lancet*. 2019;393(10172):702-716. doi:10.1016/S0140-6736(18)32526-1/ATTACHMENT/1DDC3C1C-917C-41FB-8ADD-E483E71EDD2F/MMC1.PDF

4. Johnson FT. Acute Encephalitis. 1996. https://academic.oup.com/cid/article/23/2/219/366873. Accessed April 11, 2023.

5. Frohman EM, Wingerchuk DM. Transverse Myelitis. *https://doi.org/101056/NEJMcp1001112*. 2010;363(6):564-572. doi:10.1056/NEJMCP1001112

6. Sotoudeh H, Razaei A, Saadatpour Z, et al. Brainstem Encephalitis. The Role of Imaging in Diagnosis. *Curr Probl Diagn Radiol*. 2021;50(6):946-960. doi:10.1067/J.CPRADIOL.2020.09.004

7. Foli-Andersen PJ, Munkholm A, Rønde G, et al. Acute flaccid rhombencephalomyelitis with radiculitis in a child with an enterovirus A71 infection seen for the first time in Denmark: a case report. *J Med Case Rep*. 2022;16(1):1-5. doi:10.1186/S13256-021-03246-X/FIGURES/1

8. Swanson D. Meningitis. *Pediatr Rev*. 2015;36(12):514-526. doi:10.1542/PIR.36-12-514

9. Hart YM, Andermann F, Fish DR, et al. Chronic encephalitis and epilepsy in adults and adolescents: a variant of Rasmussen's syndrome? *Neurology*. 1997;48(2):418-424. doi:10.1212/WNL.48.2.418

10. Kherallah B, Manrique L, Vennavaram S, Samaha E. Acute Fulminant Encephalitis in the Setting of Acute COVID-19 Infection (P12-3.008). *Neurology*. 2023;100(17 Supplement 2):4658. doi:10.1212/WNL.0000000000204136

11. Alam AM, Easton A, Nicholson TR, et al. Encephalitis: diagnosis, management and recent advances in the field of encephalitides. *Postgrad Med J*. 2022;0:1-10. doi:10.1136/POSTGRADMEDJ-2022-141812

12. Bohmwald K, Andrade CA, Gálvez NMS, Mora VP, Muñoz JT, Kalergis AM. The Causes and Long-Term Consequences of Viral Encephalitis. *Front Cell Neurosci*. 2021;15:481. doi:10.3389/FNCEL.2021.755875/BIBTEX

13. Jain S, Ray A, Soneja M, et al. Cavitating lung lesions with encephalopathy in a patient with long standing Sjogren's syndrome: An elusive cause. *J Assoc Physicians India*. 2016;64(OCTOBER):79-83.

14. Gundamraj V, Hasbun R. Viral meningitis and encephalitis: an update. *Curr Opin Infect Dis*. 2023;36(3):177-185. doi:10.1097/QCO.0000000000000922

15. Orozco E, Valencia-Sanchez C, Britton J, et al. Autoimmune Encephalitis Criteria in Clinical Practice. *Neurol Clin Pract*. 2023;13(3):e200151. doi:10.1212/CPJ.0000000000200151

16. Thompson C, Kneen R, Riordan A, Kelly D, Pollard AJ. Encephalitis in children. *Arch Dis Child*. 2012;97(2):150-161. doi:10.1136/ARCHDISCHILD-2011-300100

17. Oh SJ. PARANEOPLASTIC VASCULITIS OF THE PERIPHERAL NERVOUS SYSTEM. *Neurol Clin*. 1997;15(4):849-863. doi:10.1016/S0733-8619(05)70351-0

18. Grinker RR, Stone TT. ACUTE TOXIC ENCEPHALITIS IN CHILDHOOD: A CLINICOPATHOLOGIC STUDY OF THIRTEEN CASES. *Arch Neurol Psychiatry*. 1928;20(2):244-274. doi:10.1001/ARCHNEURPSYC.1928.02210140012002

19. Politsky JM. Encephalitis, encephalopathy, and epilepsy. *Enceph Diagnosis Treat*. January 2007:19-45. doi:10.3109/9781420013979-5/ENCEPHALITIS-ENCEPHALOPATHY-EPILEPSY-JEFFREY-POLITSKY

20. Dalmau J, Rosenfeld MR. Autoimmune encephalitis update. *Neuro Oncol*. 2014;16(6):771-778. doi:10.1093/NEUONC/NOU030

21. Leypoldt F, Wandinger KP, Bien CG, Dalmau J. Autoimmune Encephalitis. *Eur Neurol Rev*. 2013;8(1):31. doi:10.17925/ENR.2013.08.01.31

22. Goodfellow JA, Mackay GA. Autoimmune encephalitis. *J R Coll Physicians Edinb*. 2019;49(4):287-294. doi:10.4997/JRCPE.2019.407

23. Venkatesan A. Epidemiology and outcomes of acute encephalitis. *Curr Opin Neurol*. 2015;28(3):277-282. doi:10.1097/WCO.0000000000000199

24. Sonneville R, Klein I, de Broucker T, Wolff M. Post-infectious encephalitis in adults: Diagnosis and management. *J Infect*. 2009;58(5):321. doi:10.1016/J.JINF.2009.02.011

25. Ferrari S, Toniolo A, Monaco S, et al. *Viral Encephalitis: Etiology, Clinical Features, Diagnosis and Management*. Vol 3.; 2009.

26. Glaser CA, Honarmand S, Anderson LJ, et al. Beyond viruses: clinical profiles and etiologies associated with encephalitis. *Clin Infect Dis*. 2006;43(12):1565-1577. doi:10.1086/509330

27. Ben Abid F, Abukhattab M, Ghazouani H, et al. Epidemiology and clinical outcomes of viral central nervous system infections. *Int J Infect Dis*. 2018;73:85-90. doi:10.1016/J.IJID.2018.06.008

28. Lewis P, Glaser CA. Encephalitis. *Pediatr Rev*. 2005;26:353-363. doi:10.1542/pir.26-10-353

29. Matthews E, Beckham JD, Piquet AL, Tyler KL, Chauhan L, Pastula DM. Herpesvirus-Associated Encephalitis: an Update. *Curr Trop Med Reports*. 2022;9(3):92-

100. doi:10.1007/S40475-022-00255-8/METRICS

30. Soung A, Klein RS. Viral Encephalitis and Neurologic Diseases: Focus on Astrocytes Neurotrophic Viruses Cause Acute and Chronic Neuropathology. doi:10.1016/j.molmed.2018.09.001

31. Taskinen E, Koskiniemi ML, Vaheri A. Herpes simplex virus encephalitis: Prolonged intrathecal IgG synthesis and cellular activity in the cerebrospinal fluid with transient impairment of blood-brain barrier. *J Neurol Sci*. 1984;63(3):331-338. doi:10.1016/0022-510X(84)90156-4

32. Cain MD, Salimi H, Gong Y, et al. Virus entry and replication in the brain precedes blood-brain barrier disruption during intranasal alphavirus infection. *J Neuroimmunol*. 2017;308:118-130. doi:10.1016/J.JNEUROIM.2017.04.008

33. Miner JJ, Diamond MS. Mechanisms of restriction of viral neuroinvasion at the blood–brain barrier. *Curr Opin Immunol*. 2016;38:18-23. doi:10.1016/J.COI.2015.10.008

34. Al-Obaidi JMM, Bahadoran A, Wang SM, Manikam R, Raju CS, Sekaran SD. Disruption of the blood brain barrier is vital property of neurotropic viral infection of the central nervous system. *Acta Virol*. 2018;62(1):16-27. doi:10.4149/AV_2018_102

35. Roy A, Hooper DC. Immune evasion by rabies viruses through the maintenance of blood-brain barrier integrity. *J Neurovirol*. 2008;14(5):401-411. doi:10.1080/13550280802235924

36. Engels M, Ackermann M. Pathogenesis of ruminant herpesvirus infections. *Vet Microbiol*. 1996;53(1-2):3-15. doi:10.1016/S0378-1135(96)01230-8

37. Laval K, Poelaert KCK, Van Cleemput J, et al. The Pathogenesis and Immune Evasive Mechanisms of Equine Herpesvirus Type 1. *Front Microbiol*. 2021;12:662686. doi:10.3389/FMICB.2021.662686/BIBTEX

38. Said S, Kang M. Viral Encephalitis. *StatPearls*. August 2022. https://www.ncbi.nlm.nih.gov/books/NBK470162/. Accessed April 29, 2023.

39. Pönkä A, Pettersson T. The incidence and aetiology of central nervous system infections in Helsinki in 1980. *Acta Neurol Scand*. 1982;66(5):529-535. doi:10.1111/J.1600-0404.1982.TB03139.X

40. Nicolosi A, Hauser WA, Beghi E, Kurland LT. Epidemiology of central nervous system infections in Olmsted County, Minnesota, 1950-1981. *J Infect Dis*. 1986;154(3):399-408. doi:10.1093/INFDIS/154.3.399

41. Kohl S, James AR. Herpes simplex virus encephalitis during childhood: Importance of brain biopsy diagnosis. *J Pediatr*. 1985;107(2):212-215. doi:10.1016/S0022-3476(85)80127-X

42. Kohl S. Herpes simplex virus encephalitis in children. *Pediatr Clin North Am*. 1988;35(3):465-483. doi:10.1016/s0031-3955(16)36466-5

43. Whitley RJ. Herpes Simplex Virus Infections of the Central Nervous System.

Continuum (Minneap Minn). 2015;21(6 Neuroinfectious Disease):1704-1713. doi:10.1212/CON.0000000000000243

44. Ward KN. The natural history and laboratory diagnosis of human herpesviruses-6 and -7 infections in the immunocompetent. *J Clin Virol*. 2005;32(3):183-193. doi:10.1016/J.JCV.2004.11.008

45. Baldwin KJ, Cummings CL. Herpesvirus Infections of the Nervous System. *Contin Lifelong Learn Neurol*. 2018;24(5, Neuroinfectious Disease):1349-1369. doi:10.1212/CON.0000000000000661

46. Guo Y, Audry M, Ciancanelli M, et al. Herpes simplex virus encephalitis in a patient with complete TLR3 deficiency: TLR3 is otherwise redundant in protective immunity. *J Exp Med*. 2011;208(10):2083-2098. doi:10.1084/JEM.20101568

47. Guo Y, Audry M, Ciancanelli M, et al. Herpes simplex virus encephalitis in a patient with complete TLR3 deficiency: TLR3 is otherwise redundant in protective immunity. *J Exp Med*. 2011;208(10):2083-2098. doi:10.1084/JEM.20101568

48. Mori Y, Yamanishi K. HHV-6A, 6B, and 7: pathogenesis, host response, and clinical disease. *Hum Herpesviruses Biol Ther Immunoprophyl*. 2007;9780521827140:833-842. doi:10.1017/CBO9780511545313.047

49. Ongrádi J, Ablashi D V., Yoshikawa T, Stercz B, Ogata M. Roseolovirus-associated encephalitis in immunocompetent and immunocompromised individuals. *J Neurovirol*. 2017;23(1). doi:10.1007/S13365-016-0473-0

50. Tesini BL, Epstein LG, Caserta MT. Clinical impact of primary infection with roseoloviruses. *Curr Opin Virol*. 2014;9:91-96. doi:10.1016/J.COVIRO.2014.09.013

51. Griffiths PD, Clark DA, Emery VC. Betaherpesviruses in transplant recipients. *J Antimicrob Chemother*. 2000;45(TOPIC T3):29-34. doi:10.1093/jac/45.suppl_4.29

52. Chapenko S, Krumina A, Logina I, et al. Association of Active Human Herpesvirus-6, -7 and Parvovirus B19 Infection with Clinical Outcomes in Patients with Myalgic Encephalomyelitis/Chronic Fatigue Syndrome. *Adv Virol*. 2012;2012. doi:10.1155/2012/205085

53. Lee SJ, Kim JM, Keum HR, et al. Seasonal Trends in the Prevalence and Incidence of Viral Encephalitis in Korea (2015–2019). *J Clin Med*. 2023;12(5):2003. doi:10.3390/JCM12052003/S1

54. Granerod J, Crowcroft NS. The epidemiology of acute encephalitis. *https://doi.org/101080/09602010600989620*. 2007;17(4-5):406-428. doi:10.1080/09602010600989620

55. Stahl JP, Mailles A, Dacheux L, Morand P. Epidemiology of viral encephalitis in 2011. *Med Mal Infect*. 2011;41(9):453-464. doi:10.1016/J.MEDMAL.2011.05.015

56. Cascella M, Rajnik M, Cuomo A, Dulebohn SC, Di Napoli R. *Features, Evaluation and Treatment Coronavirus (COVID-19)*. StatPearls Publishing; 2020. http://www.ncbi.nlm.nih.gov/pubmed/32150360. Accessed April 8, 2020.

57. Jmor F, Emsley HCA, Fischer M, Solomon T, Lewthwaite P. The incidence of acute encephalitis syndrome in Western industrialised and tropical countries. *Virol J*. 2008;5. doi:10.1186/1743-422X-5-134

58. Laskus T, Radkowski M, Adair DM, Wilkinson J, Scheck AC, Rakela J. Emerging evidence of hepatitis C virus neuroinvasion. *AIDS*. 2005;19(SUPPL. 3). doi:10.1097/01.AIDS.0000192083.41561.00

59. Baloul L, Lafon M. Apoptosis and rabies virus neuroinvasion. *Biochimie*. 2003;85(8):777-788. doi:10.1016/S0300-9084(03)00137-8

60. Bergstrom T, Lycke E. Neuroinvasion by herpes simplex virus. An in vitro model for characterization of neurovirulent strains. *J Gen Virol*. 1990;71 (Pt 2)(2):405-510. doi:10.1099/0022-1317-71-2-405

61. Chauhan L, Matthews E, Piquet AL, et al. Nervous System Manifestations of Arboviral Infections. *Curr Trop Med Reports*. 2022;9(4):107. doi:10.1007/S40475-022-00262-9

62. Zaki Salahuddin S, Ablashi D V., Markham PD, et al. Isolation of a new virus, HBLV, in patients with lymphoproliferative disorders. *Science*. 1986;234(4776):596-601. doi:10.1126/SCIENCE.2876520

63. Clark DA. Human herpesvirus 6 and human herpesvirus 7: Emerging pathogens in transplant patients. *Int J Hematol*. 2002;76:246-252. doi:10.1007/BF03165124

64. Berger JR. Learning More About HHV-6 Encephalitis. *Neurol - Neuroimmunol Neuroinflammation*. 2021;8(2):e948. doi:10.1212/NXI.0000000000000948

65. Ablashi D V., Josephs SF, Buchbinder A, et al. Human B-lymphotropic virus (human herpesvirus-6). *J Virol Methods*. 1988;21(1-4):29-48. doi:10.1016/0166-0934(88)90050-X

66. Yao K, Crawford JR, Komaroff AL, Ablashi D V., Jacobson S. Review Part 2: Human Herpesvirus-6 in Central Nervous System Diseases. *J Med Virol*. 2010;82(10):1669. doi:10.1002/JMV.21861

67. Handley G, Hasbun R, Okhuysen P. Human herpesvirus 6 and central nervous system disease in oncology patients: A retrospective case series and literature review. *J Clin Virol*. 2021;136. doi:10.1016/J.JCV.2021.104740

68. Louten J. Herpesviruses. *Essent Hum Virol*. January 2016:235-256. doi:10.1016/B978-0-12-800947-5.00013-2

69. De Bolle L, Naesens L, De Clercq E. Update on Human Herpesvirus 6 Biology, Clinical Features, and Therapy. *Clin Microbiol Rev*. 2005;18(1):217. doi:10.1128/CMR.18.1.217-245.2005

70. Strausbaugh LJ, Caserta MT, Mock DJ, Dewhurst S. Human herpesvirus 6. *Clin Infect Dis*. 2001;33(6):829-833. doi:10.1086/322691/2/33-6-829-TBL002.GIF

71. Santoro F, Kennedy PE, Locatelli G, Malnati MS, Berger EA, Lusso P. CD46 is a cellular receptor for human herpesvirus 6. *Cell*. 1999;99(7):817-827.

doi:10.1016/S0092-8674(00)81678-5

72. Endo A, Watanabe K, Ohye T, et al. Molecular and virological evidence of viral activation from chromosomally integrated human herpesvirus 6A in a patient with X-linked severe combined immunodeficiency. *Clin Infect Dis*. 2014;59(4):545-548. doi:10.1093/CID/CIU323

73. Hall CB, Caserta MT, Schnabel KC, et al. Persistence of human herpesvirus 6 according to site and variant: possible greater neurotropism of variant A. *Clin Infect Dis*. 1998;26(1):132-137. doi:10.1086/516280

74. Ward KN. Child and adult forms of human herpesvirus 6 encephalitis: Looking back, looking forward. *Curr Opin Neurol*. 2014;27(3):349-355. doi:10.1097/WCO.0000000000000085

75. Agut H, Bonnafous P, Gautheret-Dejean A. Laboratory and Clinical Aspects of Human Herpesvirus 6 Infections. *Clin Microbiol Rev*. 2015;28(2):313. doi:10.1128/CMR.00122-14

76. Mekheal E, Tagliaferri AR, Vasquez K s, et al. A Rare Case of HHV-6 Encephalitis in an Immunocompetent Host: Case Report and Literature Review. *Cureus*. 2022;14(3). doi:10.7759/CUREUS.23007

77. Lusso P, De Maria A, Malnati M, et al. Induction of CD4 and susceptibility to HIV-1 infection in human CD8+ T lymphocytes by human herpesvirus 6. *Nature*. 1991;349(6309):533-535. doi:10.1038/349533A0

78. Lusso P, Garzino-Demo A, Crowley RW, Malnati MS. Infection of gamma/delta T lymphocytes by human herpesvirus 6: transcriptional induction of CD4 and susceptibility to HIV infection. *J Exp Med*. 1995;181(4):1303-1310. doi:10.1084/JEM.181.4.1303

79. Hall CB, Long CE, Schnabel KC, et al. Human Herpesvirus-6 Infection in Children -- A Prospective Study of Complications and Reactivation. *https://doi.org/101056/NEJM199408183310703*. 1994;331(7):432-438. doi:10.1056/NEJM199408183310703

80. Takahashi K, Segal E, Kondo T, et al. Interferon and natural killer cell activity in patients with exanthem subitum. *Pediatr Infect Dis J*. 1992;11(5):369-373. doi:10.1097/00006454-199205000-00006

81. Mossman KL. Activation and inhibition of virus and interferon: the herpesvirus story. *Viral Immunol*. 2002;15(1):3-15. doi:10.1089/088282402317340198

82. Kikuta H, Nakane A, Lu H, Taguchi Y, Minagawa T, Matsumoto S. Interferon induction by human herpesvirus 6 in human mononuclear cells. *J Infect Dis*. 1990;162(1):35-38. doi:10.1093/INFDIS/162.1.35

83. Mayne M, Cheadle C, Soldan SS, et al. Gene Expression Profile of Herpesvirus-Infected T Cells Obtained Using Immunomicroarrays: Induction of Proinflammatory Mechanisms. *J Virol*. 2001;75(23):11641-11650. doi:10.1128/JVI.75.23.11641-11650.2001/ASSET/D633DB69-E54E-4C0C-AD94-

F1740467AF54/ASSETS/GRAPHIC/JV2311022004.JPEG

84. Gosselin J, Flamand L, D'Addario M, Hiscott J, Menezes J. Infection of peripheral blood mononuclear cells by herpes simplex and Epstein-Barr viruses. Differential induction of interleukin 6 and tumor necrosis factor-alpha. *J Clin Invest*. 1992;89(6):1849-1856. doi:10.1172/JCI115789

85. Flamand L, Gosselin,' Mario D'addario J, Hiscott J, Ablashi D V, Gallo RC, Menezesl J. Human herpesvirus 6 induces interleukin-1 beta and tumor necrosis factor alpha, but not interleukin-6, in peripheral blood mononuclear cell cultures. *J Virol*. 1991;65(9):5105-5110. doi:10.1128/JVI.65.9.5105-5110.1991

86. Basta S, Bennink JR. A survival game of hide and seek: cytomegaloviruses and MHC class I antigen presentation pathways. *Viral Immunol*. 2003;16(3):231-242. doi:10.1089/088282403322396064

87. Hall CB, Long CE, Schnabel KC, et al. Human Herpesvirus-6 Infection in Children -- A Prospective Study of Complications and Reactivation. *N Engl J Med*. 1994;331(7):432-438. doi:10.1056/NEJM199408183310703

88. Arena A, Liberto MC, Iannello D, Capozza AB, Focà A. Altered cytokine production after human herpes virus type 6 infection. *New Microbiol*. 1999;22(4):293-300. https://europepmc.org/article/med/10555198. Accessed June 18, 2023.

89. Li C, Goodrich JM, Yang X. Interferon-gamma (IFN-γ) regulates production of IL-10 and IL-12 in human herpesvirus-6 (HHV-6)-infected monocyte/macrophage lineage. *Clin Exp Immunol*. 2003;109(3):421-425. doi:10.1046/J.1365-2249.1997.4661362.X

90. Kakimoto M, Hasegawa A, Fujita S, Yasukawa M. Phenotypic and Functional Alterations of Dendritic Cells Induced by Human Herpesvirus 6 Infection. *J Virol*. 2002;76(20):10338-10345. doi:10.1128/JVI.76.20.10338-10345.2002/ASSET/039DE495-6110-4365-A69A-30FBF9191BA5/ASSETS/GRAPHIC/JV2020325007.JPEG

91. Flamand L, Gosselin J, Stefanescu I, Ablashi D, Menezes J. Immunosuppressive effect of human herpesvirus 6 on T-cell functions: suppression of interleukin-2 synthesis and cell proliferation [published erratum appears in Blood 1995 Jul 1;86(1):418]. *Blood*. 1995;85(5):1263-1271. doi:10.1182/BLOOD.V85.5.1263.BLOODJOURNAL8551263

92. Flamand L, Stefanescu I, Menezes J. Human herpesvirus-6 enhances natural killer cell cytotoxicity via IL-15. *J Clin Invest*. 1996;97(6):1373-1381. doi:10.1172/JCI118557

93. Atedzoe BN, Ahmad A, Menezes J. Enhancement of natural killer cell cytotoxicity by the human herpesvirus-7 via IL-15 induction. *J Immunol*. 1997;159(10):4966-4972. doi:10.4049/JIMMUNOL.159.10.4966

94. Flamand L. Pathogenesis from the reactivation of chromosomally integrated human herpesvirus type 6: facts rather than fiction. *Clin Infect Dis*. 2014;59(4):549-551. doi:10.1093/CID/CIU326

95. Komaroff AL, Rizzo R, Ecker JL. Human Herpesviruses 6A and 6B in

Reproductive Diseases. *Front Immunol*. 2021;12. doi:10.3389/FIMMU.2021.648945

96. Chan PKS, Ng H-K, Hui M, Cheng AF. Prevalence and Distribution of Human Herpesvirus 6 Variants A and B in Adult Human Brain. *J Med Virol*. 2001;64:42. doi:10.1002/jmv.1015

97. Tesini BL, Epstein LG, Caserta MT. Clinical impact of primary infection with roseoloviruses. *Curr Opin Virol*. 2014;9:91-96. doi:10.1016/J.COVIRO.2014.09.013

98. Zerr DM, Meier AS, Selke SS, et al. A Population-Based Study of Primary Human Herpesvirus 6 Infection. *N Engl J Med*. 2005;352(8):768-776. doi:10.1056/NEJMOA042207

99. Torigoe S, Koide W, Yamada M, Miyashiro E, Tanaka-Taya K, Yamanishi K. Human herpesvirus 7 infection associated with central nervous system manifestations. *J Pediatr*. 1996;129(2):301-305. doi:10.1016/S0022-3476(96)70259-7

100. Sevilla-Acosta F, Araya-Amador J, Ulate-Campos A. Human Herpesvirus 6 Associated Encephalitis with Fulminant Brain Edema in a Previously Healthy Child. *Cureus*. 2020;12(5). doi:10.7759/CUREUS.8018

101. Şener Okur D, Pota Ü, Güngör O, Zeliha Öner Pamukkale Tıp Dergisi S, Makalesi A, Zeliha Öner S. Evaluation of pediatric patients with Human Herpes Virus-6 and/or Human Herpes Virus-7 detected in cerebrospinal fluid: a single center experience Beyin omurilik sıvısında Human Herpes Virus-6 ve/veya Human Herpes Virus-7 saptanan çocuk hastaların değerlendirilmesi-tek merkez deneyimi. doi:10.31362/patd.1104844

102. Asano Y, Yoshikawa T, Kajita Y, et al. Fatal encephalitis/encephalopathy in primary human herpesvirus-6 infection. *Arch Dis Child*. 1992;67(12):1484. doi:10.1136/ADC.67.12.1484

103. Asano Y, Yoshikawa T, Suga S, Yazaki T, Kondo K, Yamanishi K. Fatal fulminant hepatitis in an infant with human herpesvirus-6 infection. *Lancet (London, England)*. 1990;335(8693):862-863. doi:10.1016/0140-6736(90)90983-C

104. Tajiri H, Nose O, Baba K, Okada S. Human herpesvirus-6 infection with liver injury in neonatal hepatitis. *Lancet (London, England)*. 1990;335(8693):863. doi:10.1016/0140-6736(90)90984-D

105. Yoshikawa T, Asano Y, Kobayashi I, Nakashima T, Yazaki T. Exacerbation of idiopathic thrombocytopenic purpura by primary human herpesvirus 6 infection. *Pediatr Infect Dis J*. 1993;12(5):409-410. doi:10.1097/00006454-199305000-00014

106. Cone RW, Huang MLW, Corey L, Zeh J, Ashley R, Bowden R. Human herpesvirus 6 infections after bone marrow transplantation: clinical and virologic manifestations. *J Infect Dis*. 1999;179(2):311-318. doi:10.1086/314581

107. Drobyski WR, Knox KK, Majewski D, Carrigan DR. Brief report: fatal encephalitis due to variant B human herpesvirus-6 infection in a bone marrow-transplant recipient. *N Engl J Med*. 1994;330(19):1356-1360. doi:10.1056/NEJM199405123301905

108. Tsujimura H, Iseki T, Date Y, et al. Human herpesvirus-6 encephalitis after bone marrow transplantation: magnetic resonance imaging could identify the involved sites of encephalitis. *Eur J Haematol*. 1998;61(4):284-285. doi:10.1111/J.1600-0609.1998.TB01718.X

109. Rodrigues GDA, Nagendra S, Lee CK, De Magalhães-Silverman M. Human herpes virus 6 fatal encephalitis in a bone marrow recipient. *Scand J Infect Dis*. 1999;31(3):313-315. doi:10.1080/00365549950163644

110. Cone RW, Hackman RC, Huang M-LW, et al. Human herpesvirus 6 in lung tissue from patients with pneumonitis after bone marrow transplantation. *N Engl J Med*. 1993;329(3):156-161. doi:10.1056/NEJM199307153290302

111. Singh N, Carrigan DR, Gayowski T, Singh J, Marino IR. Variant B human herpesvirus-6 associated febrile dermatosis with thrombocytopenia and encephalopathy in a liver transplant recipient. *Transplantation*. 1995;60(11):1355-1357. https://europepmc.org/article/med/8525536. Accessed June 16, 2023.

112. Singh N, Bentlejewski C, Carrigan DR, Gayowski T, Zeevi A, Knox KK. Persistent lack of human herpesvirus-6 specific T-helper cell response in liver transplant recipients. *Transpl Infect Dis*. 2002;4(2):59-63. doi:10.1034/J.1399-3062.2002.T01-1-02001.X

113. Singh N, Husain S, Carrigan DR, et al. Impact of human herpesvirus-6 on the frequency and severity of recurrent hepatitis C virus hepatitis in liver transplant recipients. *Clin Transplant*. 2002;16(2):92-96. doi:10.1034/J.1399-0012.2002.1O096.X

114. Zhang SY, Clark NE, Freije CA, et al. Inborn Errors of RNA Lariat Metabolism in Humans with Brainstem Viral Infection. *Cell*. 2018;172(5):952-965.e18. doi:10.1016/j.cell.2018.02.019

115. Casrouge A, Zhang SY, Eidenschenk C, et al. Herpes simplex virus encephalitis in human UNC-93B deficiency. *Science (80-)*. 2006;314(5797):308-312. doi:10.1126/science.1128346

116. Zhang SY, Casanova JL. Inborn errors underlying herpes simplex encephalitis: From TLR3 to IRF3. *J Exp Med*. 2015;212(9):1340-1343. doi:10.1084/JEM.2129INSIGHT4

117. Audry M, Ciancanelli M, Yang K, et al. NEMO is a key component of NF-κB- and IRF-3-dependent TLR3-mediated immunity to herpes simplex virus. *J Allergy Clin Immunol*. 2011;128(3). doi:10.1016/J.JACI.2011.04.059

118. De Tiège X, Rozenberg F, Héron B. The spectrum of herpes simplex encephalitis in children. *Eur J Paediatr Neurol*. 2008;12(2):72-81. doi:10.1016/J.EJPN.2007.07.007

119. Andersen LL, Mørk N, Reinert LS, et al. Functional IRF3 deficiency in a patient with herpes simplex encephalitis. *J Exp Med*. 2015;212(9):1371-1379. doi:10.1084/JEM.20142274

120. Dupuis S, Jouanguy E, Al-Hajjar S, et al. Impaired response to interferon-alpha/beta and lethal viral disease in human STAT1 deficiency. *Nat Genet*.

2003;33(3):388-391. doi:10.1038/NG1097

121. Jouanguy E, Béziat V, Mogensen TH, Casanova JL, Tangye SG, Zhang SY. Human inborn errors of immunity to herpes viruses. *Curr Opin Immunol*. 2020;62:106. doi:10.1016/J.COI.2020.01.004

122. Lim HK, Seppänen M, Hautala T, et al. TLR3 deficiency in herpes simplex encephalitis: High allelic heterogeneity and recurrence risk. *Neurology*. 2014;83(21):1888-1897. doi:10.1212/WNL.0000000000000999

123. Mørk N, Kofod-Olsen E, Sørensen KB, et al. Mutations in the TLR3 signaling pathway and beyond in adult patients with herpes simplex encephalitis. *Genes Immun*. 2015;16(8):552-566. doi:10.1038/GENE.2015.46

124. Zhang SY. Herpes simplex virus encephalitis of childhood: inborn errors of central nervous system cell-intrinsic immunity. *Hum Genet*. 2020;139(6-7):911-918. doi:10.1007/S00439-020-02127-5/FIGURES/1

125. Sancho-Shimizu V, Pérez De Diego R, Lorenzo L, et al. Herpes simplex encephalitis in children with autosomal recessive and dominant TRIF deficiency. *J Clin Invest*. 2011;121(12):4889-4902. doi:10.1172/JCI59259

126. Duan T, Du Y, Xing C, Wang HY, Wang RF. Toll-Like Receptor Signaling and Its Role in Cell-Mediated Immunity. *Front Immunol*. 2022;13:812774. doi:10.3389/FIMMU.2022.812774/BIBTEX

127. Casrouge A, Zhang SY, Eidenschenk C, et al. Herpes simplex virus encephalitis in human UNC-93B deficiency. *Science*. 2006;314(5797):308-312. doi:10.1126/SCIENCE.1128346

128. Guo Y, Audry M, Ciancanelli M, et al. Herpes simplex virus encephalitis in a patient with complete TLR3 deficiency: TLR3 is otherwise redundant in protective immunity. *J Exp Med*. 2011;208(10):2083-2098. doi:10.1084/JEM.20101568

129. Lafaille FG, Pessach IM, Zhang SY, et al. Impaired intrinsic immunity to HSV-1 in human iPSC-derived TLR3-deficient CNS cells. *Nature*. 2012;491(7426):769-773. doi:10.1038/NATURE11583

130. Gnann JW, Whitley RJ. Herpes Simplex Encephalitis: an Update. *Curr Infect Dis Rep*. 2017;19(3). doi:10.1007/S11908-017-0568-7

131. Lafaille FG, Harschnitz O, Lee YS, et al. Human SNORA31 variations impair cortical neuron-intrinsic immunity to HSV-1 and underlie herpes simplex encephalitis. *Nat Med*. 2019;25(12):1873-1884. doi:10.1038/S41591-019-0672-3

132. Kiss AM, Jády BE, Bertrand E, Kiss T. Human box H/ACA pseudouridylation guide RNA machinery. *Mol Cell Biol*. 2004;24(13):5797-5807. doi:10.1128/MCB.24.13.5797-5807.2004

133. Chapman KB, Boeke JD. Isolation and characterization of the gene encoding yeast debranching enzyme. *Cell*. 1991;65(3):483-492. doi:10.1016/0092-8674(91)90466-C

134. Jacquier A, Rosbash M. RNA splicing and intron turnover are greatly diminished

by a mutant yeast branch point. *Proc Natl Acad Sci U S A*. 1986;83(16):5835-5839. doi:10.1073/PNAS.83.16.5835

135. Naesens L, Muppala S, Acharya D, et al. GTF3A mutations predispose to herpes simplex encephalitis by disrupting biogenesis of the host-derived RIG-I ligand RNA5SP141. *Sci Immunol*. 2022;7(77). doi:10.1126/SCIIMMUNOL.ABQ4531

136. Shastry BS. Transcription factor IIIA (TFIIIA) in the second decade. *J Cell Sci*. 1996;109 (Pt 3)(3):535-539. doi:10.1242/JCS.109.3.535

137. Braun DK, Dominguez G, Pellett PE. Human herpesvirus 6. *Clin Microbiol Rev*. 1997;10(3):521-567. doi:10.1128/CMR.10.3.521

138. Levy JA, Ferro F, Greenspan D, Lennette ET. Frequent isolation of HHV-6 from saliva and high seroprevalence of the virus in the population. *Lancet (London, England)*. 1990;335(8697):1047-1050. doi:10.1016/0140-6736(90)92628-U

139. Okuno T, Takahashi K, Balachandra K, et al. Seroepidemiology of human herpesvirus 6 infection in normal children and adults. *J Clin Microbiol*. 1989;27(4):651-653. doi:10.1128/JCM.27.4.651-653.1989

140. Clark DA, Griffiths PD. Human herpesvirus 6: relevance of infection in the immunocompromised host. *Br J Haematol*. 2003;120(3):384-395. doi:10.1046/J.1365-2141.2003.04048.X

141. Singh N, Paterson DL. Encephalitis caused by human herpesvirus-6 in transplant recipients: relevance of a novel neurotropic virus. *Transplantation*. 2000;69(12):2474-2479. doi:10.1097/00007890-200006270-00002

142. Robertson N, Engelhardt KR, Morgan N V., et al. Astute Clinician Report: A Novel 10 bp Frameshift Deletion in Exon 2 of ICOS Causes a Combined Immunodeficiency Associated with an Enteritis and Hepatitis. *J Clin Immunol*. 2015;35(7):598-603. doi:10.1007/S10875-015-0193-X

143. Nishimura S, Kobayashi Y, Ohnishi H, et al. IRAK4 Deficiency Presenting with Anti-NMDAR Encephalitis and HHV6 Reactivation. *J Clin Immunol*. 2021;41(1):125. doi:10.1007/S10875-020-00885-5

144. Li S, Strelow A, Fontana EJ, Wesche H. IRAK-4: A novel member of the IRAK family with the properties of an IRAK-kinase. *Proc Natl Acad Sci U S A*. 2002;99(8):5567-5572. doi:10.1073/PNAS.082100399/ASSET/658509E4-88CF-4230-B99A-6A6B507AD926/ASSETS/GRAPHIC/PQ0821003005.JPEG

145. García-García A, Pérez de Diego R, Flores C, et al. Humans with inherited MyD88 and IRAK-4 deficiencies are predisposed to hypoxemic COVID-19 pneumonia. *J Exp Med*. 2023;220(5). doi:10.1084/JEM.20220170

146. Yang K, Puel A, Zhang S, et al. Human TLR-7-, -8-, and -9-mediated induction of IFN-alpha/beta and -lambda Is IRAK-4 dependent and redundant for protective immunity to viruses. *Immunity*. 2005;23(5):465-478. doi:10.1016/J.IMMUNI.2005.09.016

147. Ku CL, Von Bernuth H, Picard C, et al. Selective predisposition to bacterial infections in IRAK-4-deficient children: IRAK-4-dependent TLRs are otherwise redundant in protective immunity. *J Exp Med*. 2007;204(10):2407-2422. doi:10.1084/jem.20070628

148. Casanova J-L. From second thoughts on the germ theory to a full-blown host theory. *Proc Natl Acad Sci*. 2023;120(26):e2301186120. doi:10.1073/PNAS.2301186120

149. Casanova JL, Abel L. From rare disorders of immunity to common determinants of infection: Following the mechanistic thread. *Cell*. 2022;185(17):3086-3103. doi:10.1016/J.CELL.2022.07.004

150. Bousfiha A, Moundir A, Tangye SG, et al. The 2022 Update of IUIS Phenotypical Classification for Human Inborn Errors of Immunity. *J Clin Immunol*. 2022;42(7):1508-1520. doi:10.1007/S10875-022-01352-Z/FIGURES/10

151. Casanova JL, Abel L. Lethal Infectious Diseases as Inborn Errors of Immunity: Toward a Synthesis of the Germ and Genetic Theories. *https://doi.org/101146/annurev-pathol-031920-101429*. 2021;16:23-50. doi:10.1146/ANNUREV-PATHOL-031920-101429

152. Lim HK, Seppänen M, Hautala T, et al. TLR3 deficiency in herpes simplex encephalitis: high allelic heterogeneity and recurrence risk. *Neurology*. 2014;83(21):1888-1897. doi:10.1212/wnl.0000000000000999

153. Jordi M, Marty J, Mordasini V, et al. IRAK4 is essential for TLR9-induced suppression of Epstein-Barr virus BZLF1 transcription in Akata Burkitt's lymphoma cells. *PLoS One*. 2017;12(10). doi:10.1371/JOURNAL.PONE.0186614

154. Belkaya S, Michailidis E, Korol CB, et al. Inherited IL-18BP deficiency in human fulminant viral hepatitis. 2019. doi:10.1084/jem.20190669

155. Itan Y, Shang L, Boisson B, et al. The human gene damage index as a gene-level approach to prioritizing exome variants. *Proc Natl Acad Sci U S A*. 2015;112(44):13615-13620. doi:10.1073/PNAS.1518646112/SUPPL_FILE/PNAS.1518646112.SD01.XLSX

156. Kircher M, Witten DM, Jain P, O'roak BJ, Cooper GM, Shendure J. A general framework for estimating the relative pathogenicity of human genetic variants. *Nat Genet 2014 463*. 2014;46(3):310-315. doi:10.1038/ng.2892

157. Itan Y, Shang L, Boisson B, et al. The mutation significance cutoff: gene-level thresholds for variant predictions. *Nat Methods 2016 132*. 2016;13(2):109-110. doi:10.1038/nmeth.3739

158. Ng PC, Henikoff S. SIFT: predicting amino acid changes that affect protein function. *Nucleic Acids Res*. 2003;31(13):3812-3814. doi:10.1093/NAR/GKG509

159. Adzhubei IA, Schmidt S, Peshkin L, et al. A method and server for predicting damaging missense mutations. *Nat Methods*. 2010;7(4):248-249. doi:10.1038/NMETH0410-248

160. Belkaya S, Michailidis E, Korol CB, et al. Inherited IL-18BP deficiency in human fulminant viral hepatitis. *J Exp Med*. 2019;216(8):1777-1790. doi:10.1084/JEM.20190669

161. Harayama T, Riezman H. Detection of genome-edited mutant clones by a simple competition-based PCR method. *PLoS One*. 2017;12(6):e0179165. doi:10.1371/JOURNAL.PONE.0179165

162. Choi M, Scholl UI, Ji W, et al. Genetic diagnosis by whole exome capture and massively parallel DNA sequencing. *Proc Natl Acad Sci U S A*. 2009;106(45):19096-19101. doi:10.1073/PNAS.0910672106/SUPPL_FILE/0910672106SI.PDF

163. Barbitoff YA, Polev DE, Glotov AS, et al. Systematic dissection of biases in whole-exome and whole-genome sequencing reveals major determinants of coding sequence coverage. *Sci Reports 2020 101*. 2020;10(1):1-13. doi:10.1038/s41598-020-59026-y

164. Casanova JL, Conley ME, Seligman SJ, Abel L, Notarangelo LD. Guidelines for genetic studies in single patients: lessons from primary immunodeficiencies. *J Exp Med*. 2014;211(11):2137-2149. doi:10.1084/JEM.20140520

165. Gudmundsson S, Singer-Berk M, Watts NA, et al. Variant interpretation using population databases: Lessons from gnomAD. *Hum Mutat*. 2022;43(8):1012. doi:10.1002/HUMU.24309

166. Akira S, Uematsu S, Takeuchi O. Pathogen recognition and innate immunity. *Cell*. 2006;124(4). doi:10.1016/j.cell.2006.02.015

167. Picard C, Puel A, Bonnet M, et al. Pyogenic bacterial infections in humans with IRAK-4 deficiency. *Science (80-)*. 2003;299(5615). doi:10.1126/science.1081902

168. Picard C, Casanova JL, Puel A. Infectious diseases in patients with IRAK-4, MyD88, NEMO, or IκBα deficiency. *Clin Microbiol Rev*. 2011;24(3). doi:10.1128/CMR.00001-11

169. Ku CL, Yang K, Bustamante J, et al. Inherited disorders of human Toll-like receptor signaling: Immunological implications. *Immunol Rev*. 2005;203. doi:10.1111/j.0105-2896.2005.00235.x

170. Puel A, Picard C, Ku CL, Smahi A, Casanova JL. Inherited disorders of NF-κB-mediated immunity in man. *Curr Opin Immunol*. 2004;16(1). doi:10.1016/j.coi.2003.11.013

171. Picard C, Von Bernuth H, Ghandil P, et al. Clinical features and outcome of patients with IRAK-4 and MyD88 deficiency. *Medicine (Baltimore)*. 2010;89(6):403-425. doi:10.1097/MD.0B013E3181FD8EC3

172. Zhang SY, Jouanguy E, Ugolini S, et al. TLR3 deficiency in patients with herpes simplex encephalitis. *Science*. 2007;317(5844):1522-1527. doi:10.1126/SCIENCE.1139522

173. Von Bernuth H, Ku CL, Rodriguez-Gallego C, et al. A fast procedure for the

detection of defects in Toll-like receptor signaling. *Pediatrics*. 2006;118(6):2498-2503. doi:10.1542/PEDS.2006-1845

174. Von Bernuth H, Picard C, Jin Z, et al. Pyogenic bacterial infections in humans with MyD88 deficiency. *Science*. 2008;321(5889):691-696. doi:10.1126/SCIENCE.1158298

175. Hemmi H, Kaisho T, Takeuchi O, et al. Small-antiviral compounds activate immune cells via the TLR7 MyD88-dependent signaling pathway. *Nat Immunol*. 2002;3(2). doi:10.1038/ni758

176. Meylan E, Tschopp J. Toll-Like Receptors and RNA Helicases: Two Parallel Ways to Trigger Antiviral Responses. *Mol Cell*. 2006;22(5). doi:10.1016/j.molcel.2006.05.012

177. Tae WK, Staschke K, Bulek K, et al. A critical role for IRAK4 kinase activity in Toll-like receptor-mediated innate immunity. *J Exp Med*. 2007;204(5). doi:10.1084/jem.20061825

178. Suzuki N, Suzuki S, Duncan GS, et al. Severe impairment of interleukin-1 and toll-like receptor signalling in mice lacking IRAK-4. *Nature*. 2002;416(6882). doi:10.1038/nature736

179. Zhang SY, Jouanguy E, Sancho-Shimizu V, et al. Human Toll-like receptor-dependent induction of interferons in protective immunity to viruses. *Immunol Rev*. 2007;220(1). doi:10.1111/j.1600-065X.2007.00564.x

180. Altshuler DL, Durbin RM, Abecasis GR, et al. A map of human genome variation from population-scale sequencing. *Nature*. 2010;467(7319):1061-1073. doi:10.1038/NATURE09534

181. Sherry ST, Ward MH, Kholodov M, et al. dbSNP: the NCBI database of genetic variation. *Nucleic Acids Res*. 2001;29(1):308-311. doi:10.1093/NAR/29.1.308

182. Taliun D, Harris DN, Kessler MD, et al. Sequencing of 53,831 diverse genomes from the NHLBI TOPMed Program. *Nature*. 2021;590(7845):290-299. doi:10.1038/S41586-021-03205-Y

183. Scott EM, Halees A, Itan Y, et al. Characterization of Greater Middle Eastern genetic variation for enhanced disease gene discovery. *Nat Genet*. 2016;48(9):1071-1079. doi:10.1038/NG.3592

184. Kawagoe T, Sato S, Jung A, et al. Essential role of IRAK-4 protein and its kinase activity in Toll-like receptor–mediated immune responses but not in TCR signaling. *J Exp Med*. 2007;204(5):1013-1024. doi:10.1084/JEM.20061523

185. Dossang ACG, Motshwene PG, Yang Y, et al. The N-terminal loop of IRAK-4 death domain regulates ordered assembly of the Myddosome signalling scaffold. *Sci Reports 2016 61*. 2016;6(1):1-12. doi:10.1038/srep37267

186. Tepe ZG, Yazıcı YY, Tank U, et al. Inherited IRAK-4 Deficiency in Acute Human Herpesvirus-6 Encephalitis. *J Clin Immunol*. 2023;43(1):192-205. doi:10.1007/S10875-

022-01369-4

187. De S, Karim F, Kiessu E, et al. Mechanism of dysfunction of human variants of the IRAK4 kinase and a role for its kinase activity in interleukin-1 receptor signaling. *J Biol Chem*. 2018;293(39):15208. doi:10.1074/JBC.RA118.003831

188. Kao S-H, Wang W-L, Chen C-Y, et al. Analysis of Protein Stability by the Cycloheximide Chase Assay. *Bio-protocol*. 2015;5(1). doi:10.21769/BIOPROTOC.1374

189. Yamamoto T, Tsutsumi N, Tochio H, et al. Functional assessment of the mutational effects of human IRAK4 and MyD88 genes. *Mol Immunol*. 2014;58(1):66-76. doi:10.1016/J.MOLIMM.2013.11.008

190. Ku CL, Von Bernuth H, Picard C, et al. Selective predisposition to bacterial infections in IRAK-4–deficient children: IRAK-4–dependent TLRs are otherwise redundant in protective immunity. *J Exp Med*. 2007;204(10):2407-2422. doi:10.1084/JEM.20070628

191. Yang K, Puel A, Zhang S, et al. Human TLR-7-, -8-, and -9-mediated induction of IFN-α/β and -λ Is IRAK-4 dependent and redundant for protective immunity to viruses. *Immunity*. 2005;23(5):465-478. doi:10.1016/j.immuni.2005.09.016

192. Picard C, Casanova JL, Puel A. Infectious diseases in patients with IRAK-4, MyD88, NEMO, or IκBα deficiency. *Clin Microbiol Rev*. 2011;24(3):490-497. doi:10.1128/CMR.00001-11

193. Unterholzner L. The interferon response to intracellular DNA: why so many receptors? *Immunobiology*. 2013;218(11):1312-1321. doi:10.1016/J.IMBIO.2013.07.007

194. Jones JW, Kayagaki N, Broz P, et al. Absent in melanoma 2 is required for innate immune recognition of Francisella tularensis. *Proc Natl Acad Sci U S A*. 2010;107(21):9771-9776. doi:10.1073/PNAS.1003738107/SUPPL_FILE/PNAS.201003738SI.PDF

195. Briend E, Piper S, Rider D, et al. IL-1 Family Members Have Differential Effects On The Innate Pro-Inflammatory And Anti-Viral Responses Of Epithelial Cells To Rhinovirus Infection. *Am Thorac Soc Int Conf Meet Abstr*. May 2011:A2757-A2757. doi:10.1164/AJRCCM-CONFERENCE.2011.183.1_MEETINGABSTRACTS.A2757

196. O'neill LAJ, Bowie AG. Sensing and Signaling in Antiviral Innate Immunity. *Curr Biol*. 20:328-333. doi:10.1016/j.cub.2010.01.044

197. Aarreberg LD, Wilkins C, Ramos HJ, et al. Interleukin-1β Signaling in Dendritic Cells Induces Antiviral Interferon Responses. *MBio*. 2018;9(2). doi:10.1128/MBIO.00342-18

198. Ramshaw IA, Ramsay A, Karupiah G, et al. Cytokines and immunity to viral infections. *Immunol Rev*. 1997;159(1):119-135. doi:10.1111/J.1600-065X.1997.TB01011.X

199. Karnowski A, Chevrier S, Belz GT, et al. B and T cells collaborate in antiviral responses via IL-6, IL-21, and transcriptional activator and coactivator, Oct2 and OBF-

1. *J Exp Med*. 2012;209(11):2049-2064. doi:10.1084/JEM.20111504

200. Sládková T, Kostolanský F. The role of cytokines in the immune response to Influenza A virus infection. *Acta Virol*. 2006;50:151-162. https://www.researchgate.net/publication/6666557. Accessed July 11, 2023.

201. Gehring AJ, Koh S, Chia A, et al. Licensing Virus-Specific T Cells to Secrete the Neutrophil Attracting Chemokine CXCL-8 during Hepatitis B Virus Infection. *PLoS One*. 2011;6(8):e23330. doi:10.1371/JOURNAL.PONE.0023330

202. Gibbons D, Fleming P, Virasami A, et al. Interleukin-8 (CXCL8) production is a signatory T cell effector function of human newborn infants. *Nat Med 2014 2010*. 2014;20(10):1206-1210. doi:10.1038/nm.3670

203. Renauld JC. Class II cytokine receptors and their ligands: Key antiviral and inflammatory modulators. *Nat Rev Immunol 2003 38*. 2003;3(8):667-676. doi:10.1038/nri1153

204. Richter K, Perriard G, Behrendt R, et al. Macrophage and T Cell Produced IL-10 Promotes Viral Chronicity. *PLOS Pathog*. 2013;9(11):e1003735. doi:10.1371/JOURNAL.PPAT.1003735

205. Guo Y, Cao W, Zhu Y. Immunoregulatory Functions of the IL-12 Family of Cytokines in Antiviral Systems. *Viruses 2019, Vol 11, Page 772*. 2019;11(9):772. doi:10.3390/V11090772

206. Danastas K, Miranda-Saksena M, Cunningham AL. Herpes Simplex Virus Type 1 Interactions with the Interferon System. *Int J Mol Sci*. 2020;21(14):1-31. doi:10.3390/IJMS21145150

207. Andreakos E, Zanoni I, Galani IE. Lambda interferons come to light: dual function cytokines mediating antiviral immunity and damage control. *Curr Opin Immunol*. 2019;56:67-75. doi:10.1016/J.COI.2018.10.007

208. Ank N, West H, Paludan SR. IFN-λ: Novel Antiviral Cytokines. *https://home.liebertpub.com/jir*. 2006;26(6):373-379. doi:10.1089/JIR.2006.26.373

209. Kang S, Brown HM, Hwang S. Direct Antiviral Mechanisms of Interferon-Gamma. *Immune Netw*. 2018;18(5). doi:10.4110/IN.2018.18.E33

210. Kedzierska K, Rainbird MA, Lopez AF, Crowe SM. Effect of GM-CSF on HIV-1 replication in monocytes/macrophages in vivo and in vitro: a review. *Vet Immunol Immunopathol*. 1998;63(1-2):111-121. doi:10.1016/S0165-2427(98)00087-7

211. Rösler B, Herold S. Lung epithelial GM-CSF improves host defense function and epithelial repair in influenza virus pneumonia—a new therapeutic strategy? *Mol Cell Pediatr 2016 31*. 2016;3(1):1-6. doi:10.1186/S40348-016-0055-5

212. Sevilla-Acosta F, Araya-Amador J, Ulate-Campos A. Human Herpesvirus 6 Associated Encephalitis with Fulminant Brain Edema in a Previously Healthy Child. *Cureus*. 2020;12(5). doi:10.7759/CUREUS.8018

213. Casanova JL, Abel L. The Genetic Theory of Infectious Diseases: A Brief History

and Selected Illustrations. *https://doi.org/101146/annurev-genom-091212-153448*. 2013;14:215-243. doi:10.1146/ANNUREV-GENOM-091212-153448

214. Ku CL, Yang K, Bustamante J, et al. Inherited disorders of human Toll-like receptor signaling: immunological implications. *Immunol Rev*. 2005;203(1):10-20. doi:10.1111/J.0105-2896.2005.00235.X

215. Von Bernuth H, Picard C, Jin Z, et al. Pyogenic bacterial infections in humans with IRAK4 deficiency. *Science (80-).* 2008;321(5889):691-696. doi:10.1126/science.1158298

216. Gonzales JA, Nortey J, Reddy A, Doan T, Acharya NR. Intraocular Inflammation Associated with IRAK4 Deficiency. *https://doi.org/101080/09273948202222059523*. 2022. doi:10.1080/09273948.2022.2059523

217. Casanova JL, Abel L. The human model: a genetic dissection of immunity to infection in natural conditions. *Nat Rev Immunol 2004 41*. 2004;4(1):55-66. doi:10.1038/nri1264

218. Harris RA, McCarthy GM, Bridges CR, Blednov YA. CNS cell-type localization and LPS response of TLR signaling pathways. *F1000Research*. 2017;6. doi:10.12688/F1000RESEARCH.12036.1

219. Zhang Y, Chen K, Sloan SA, et al. An RNA-sequencing transcriptome and splicing database of glia, neurons, and vascular cells of the cerebral cortex. *J Neurosci*. 2014;34(36):11929-11947. doi:10.1523/JNEUROSCI.1860-14.2014

220. Zhang Y, Sloan SA, Clarke LE, et al. Purification and Characterization of Progenitor and Mature Human Astrocytes Reveals Transcriptional and Functional Differences with Mouse. *Neuron*. 2016;89(1):37-53. doi:10.1016/J.NEURON.2015.11.013

221. Gern OL, Mulenge F, Pavlou A, et al. Toll-like Receptors in Viral Encephalitis. *Viruses*. 2021;13(10). doi:10.3390/V13102065

222. Fiebich BL, Batista CRA, Saliba SW, Yousif NM, de Oliveira ACP. Role of microglia TLRs in neurodegeneration. *Front Cell Neurosci*. 2018;12:402689. doi:10.3389/FNCEL.2018.00329/BIBTEX

223. Tiwari RK, Singh S, Gupta CL, Bajpai P. Microglial TLR9: Plausible Novel Target for Therapeutic Regime Against Glioblastoma Multiforme. *Cell Mol Neurobiol*. 2021;41(7):1391-1393. doi:10.1007/S10571-020-00925-Z/METRICS

224. Reynaud JM, Jégou J-F, Welsch JC, Horvat B. Human Herpesvirus 6A Infection in CD46 Transgenic Mice: Viral Persistence in the Brain and Increased Production of Proinflammatory Chemokines via Toll-Like Receptor 9. *J Virol*. 2014;88(10):5421-5436. doi:10.1128/JVI.03763-13

225. West JA, Gregory SM, Damania B. Toll-like receptor sensing of human herpesvirus infection. *Front Cell Infect Microbiol*. 2012;2:122. doi:10.3389/FCIMB.2012.00122

226. Chi J, Wang F, Li L, et al. The role of MAPK in CD4(+) T cells toll-like receptor 9-mediated signaling following HHV-6 infection. *Virology*. 2012;422(1):92-98. doi:10.1016/J.VIROL.2011.09.026

227. Butchi N, Kapil P, Puntambekar S, Stohlman SA, Hinton DR, Bergmann CC. Myd88 Initiates Early Innate Immune Responses and Promotes CD4 T Cells during Coronavirus Encephalomyelitis. *J Virol*. 2015;89(18):9299. doi:10.1128/JVI.01199-15

228. Ghita L, Spanier J, Chhatbar C, et al. MyD88 signaling by neurons induces chemokines that recruit protective leukocytes to the virus-infected CNS. *Sci Immunol*. 2021;6(60):9165. doi:10.1126/SCIIMMUNOL.ABC9165/SUPPL_FILE/SCIIMMUNOL.ABC9165_TABLES_S1_TO_S3.ZIP

229. Ireland DDC, Stohlman SA, Hinton DR, Atkinson R, Bergmann CC. Type I Interferons Are Essential in Controlling Neurotropic Coronavirus Infection Irrespective of Functional CD8 T Cells. *J Virol*. 2008;82(1):300. doi:10.1128/JVI.01794-07

230. Tian H, Yu K, He L, et al. RNF213 modulates γ-herpesvirus infection and reactivation via targeting the viral Replication and Transcription Activator. *Proc Natl Acad Sci*. 2023;120(12):e2218825120. doi:10.1073/PNAS.2218825120/SUPPL_FILE/PNAS.2218825120.SAPP.PDF

231. Li X. IRAK4 in TLR/IL-1R signaling: Possible clinical applications. *Eur J Immunol*. 2008;38(3):614-618. doi:10.1002/EJI.200838161

232. Jiang Z, Johnson HJ, Nie H, Qin J, Bird TA, Li X. Pellino 1 is required for interleukin-1 (IL-1)-mediated signaling through its interaction with the IL-1 receptor-associated kinase 4 (IRAK4)-IRAK-tumor necrosis factor receptor-associated factor 6 (TRAF6) complex. *J Biol Chem*. 2003;278(13):10952-10956. doi:10.1074/JBC.M212112200

233. Honda K, Yanai H, Mizutani T, et al. Role of a transductional-transcriptional processor complex involving MyD88 and IRF-7 in Toll-like receptor signaling. *Proc Natl Acad Sci U S A*. 2004;101(43):15416-15421. doi:10.1073/PNAS.0406933101/ASSET/1126FF4E-98E5-4A79-BE79-4377088E5F7C/ASSETS/GRAPHIC/ZPQ0440463320005.JPEG

234. Liu X, Fitzgerald K, Kurt-Jones E, Finberg R, Knipe DM. Herpesvirus tegument protein activates NF-κB signaling through the TRAF6 adaptor protein. *Proc Natl Acad Sci U S A*. 2008;105(32):11335. doi:10.1073/PNAS.0801617105

235. Daffis S, Samuel MA, Suthar MS, Keller BC, Michael Gale J, Diamond MS. Interferon Regulatory Factor IRF-7 Induces the Antiviral Alpha Interferon Response and Protects against Lethal West Nile Virus Infection. *J Virol*. 2008;82(17):8465. doi:10.1128/JVI.00918-08

236. Chiang H Sen, Liu HM. The molecular basis of viral inhibition of IRF- and STAT-dependent immune responses. *Front Immunol*. 2019;10(JAN):422992. doi:10.3389/FIMMU.2018.03086/BIBTEX

237. Maglione PJ, Simchoni N, Black S, et al. IRAK-4 and MyD88 deficiencies impair IgM responses against T-independent bacterial antigens. *Blood*. 2014;124(24):3561. doi:10.1182/BLOOD-2014-07-587824

238. Akhyani N, Fotheringham J, Yao K, Rashti F, Jacobson S. Efficacy of antiviral compounds in human herpesvirus-6-infected glial cells. *J Neurovirol*. 2006;12(4):284-293. doi:10.1080/13550280600880772

239. Yuan B, Shen H, Lin L, Su T, Zhong L, Yang Z. MicroRNA367 negatively regulates the inflammatory response of microglia by targeting IRAK4 in intracerebral hemorrhage. *J Neuroinflammation*. 2015;12(1):1-9. doi:10.1186/S12974-015-0424-3/FIGURES/6

240. Hoozemans JJM, Haastert ES van, S, et al. Increased IRAK-4 Kinase Activity in Alzheimerand#8217;s Disease; IRAK-1/4 Inhibitor I Prevents Pro-inflammatory Cytokine Secretion but not the Uptake of Amyloid Beta by Primary Human Glia. *J Clin Cell Immunol*. 2014;5(4):1-10. doi:10.4172/2155-9899.1000243

APPENDIX

A. Expanded view of Sanger sequencing of the gDNA region encompassing the *IRAK4* mutation in the family affected with HHV-6 encephalitis

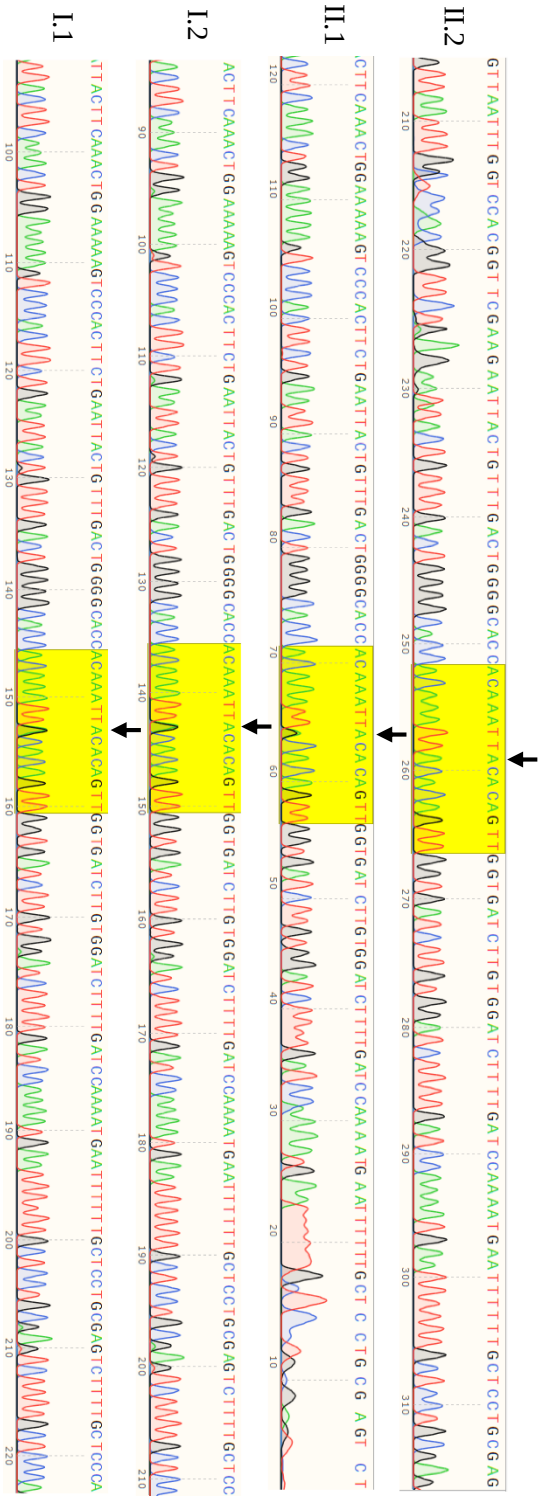

Appendix Figure 1. Expanded view of Sanger sequencing of the gDNA region encompassing the IRAK mutation from patient (II.2), his sibling (II.1), his mother (I.2) and his father (I.1). Region used for the illustration of Figure 3.2 was highlighted in yellow. The mutation site was shown with black arrow.

B. Plasmid Maps

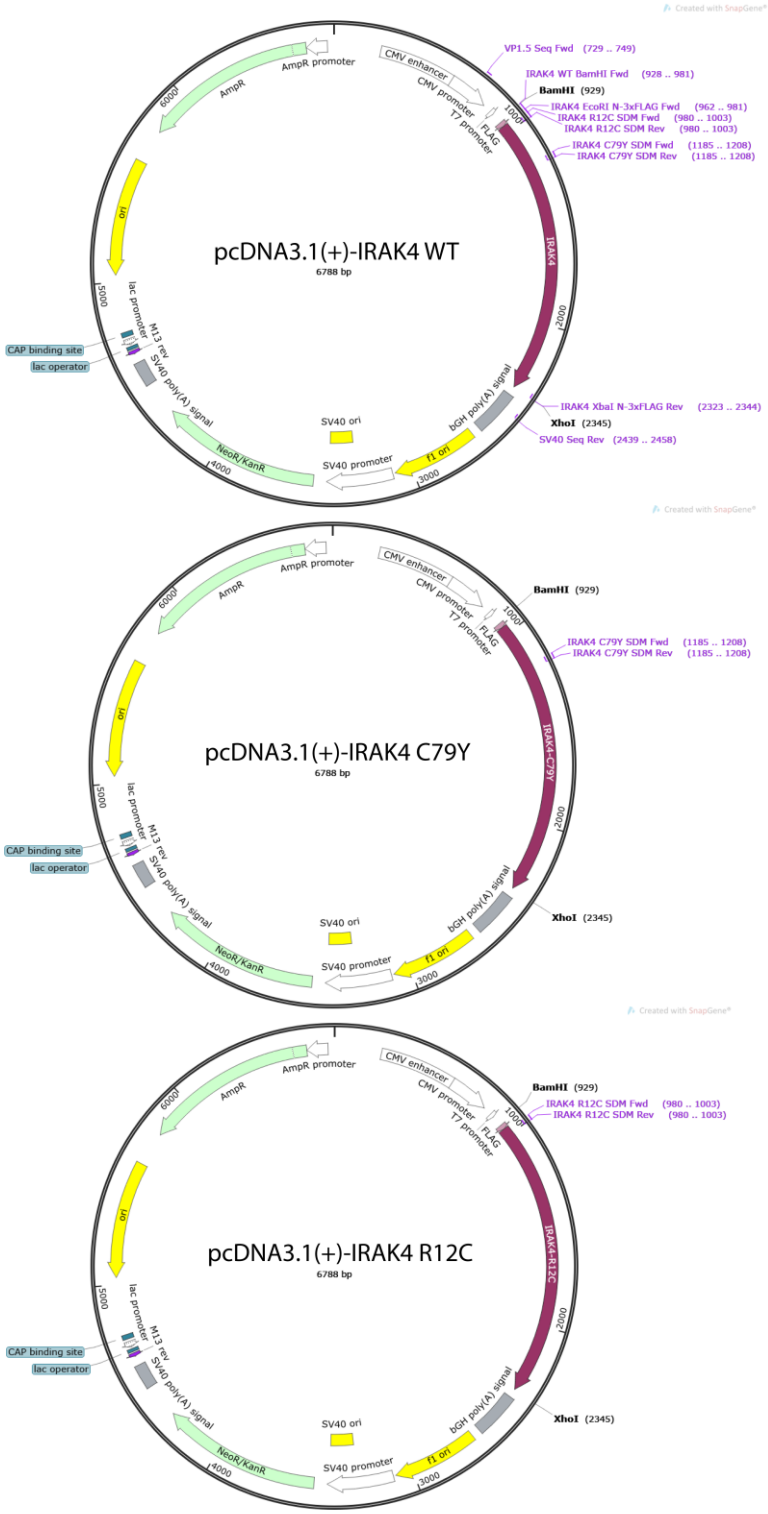

Appendix Figure 2.Constructed IRAK-4 plasmid maps using pcDNA3.1 mammalian expression vector

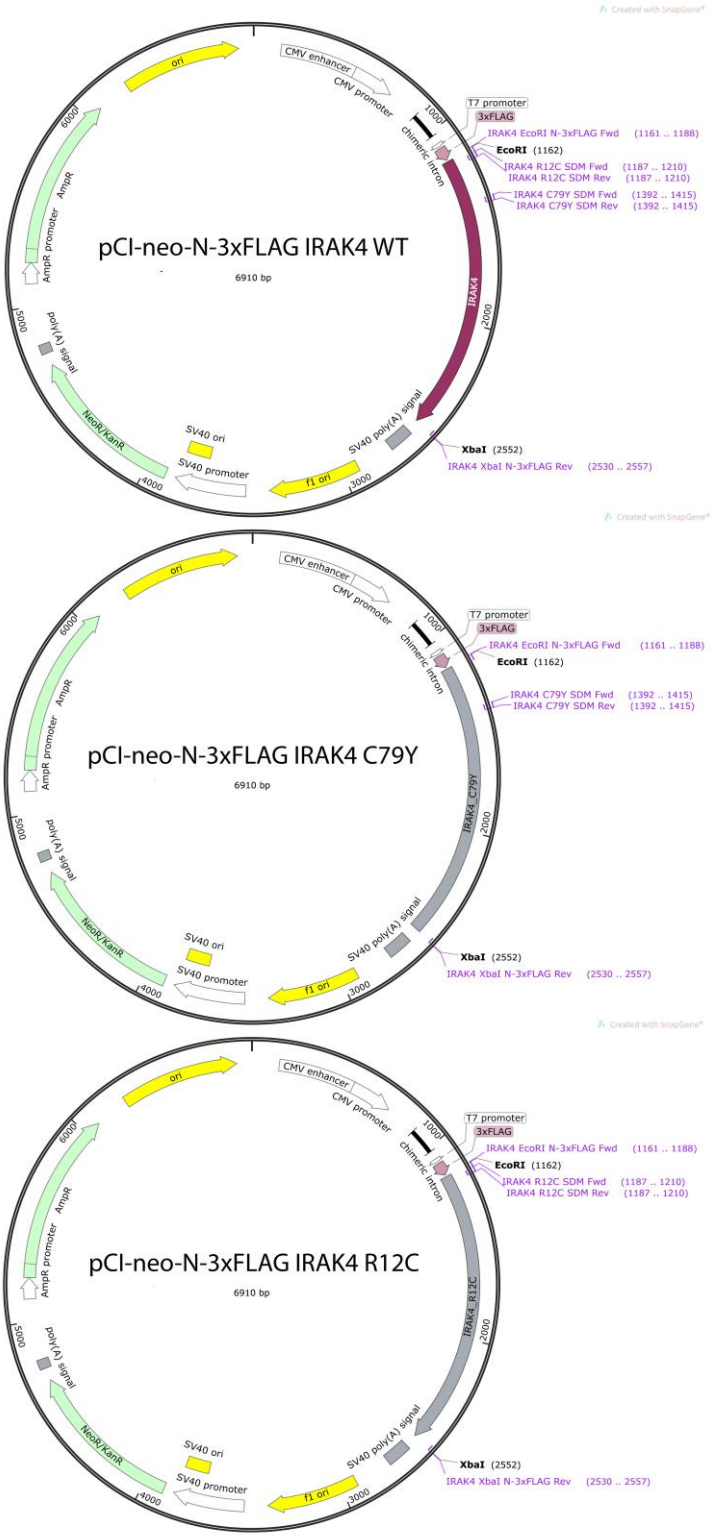

Appendix Figure 3. Constructed IRAK-4 plasmid maps using pCI-neo-N-3xFLAG mammalian expression vector

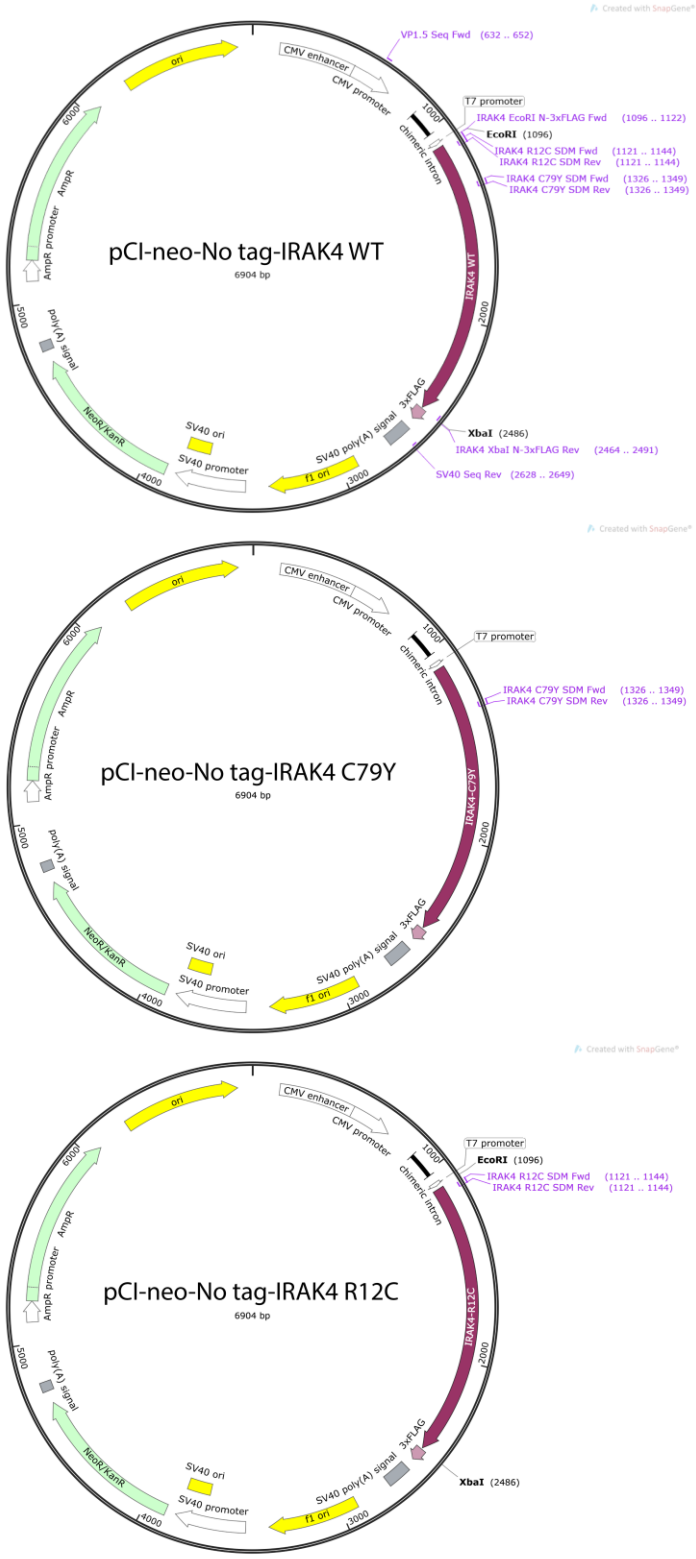

Appendix Figure 4. Constructed IRAK-4 plasmid maps using pCI-neo mammalian expression vector

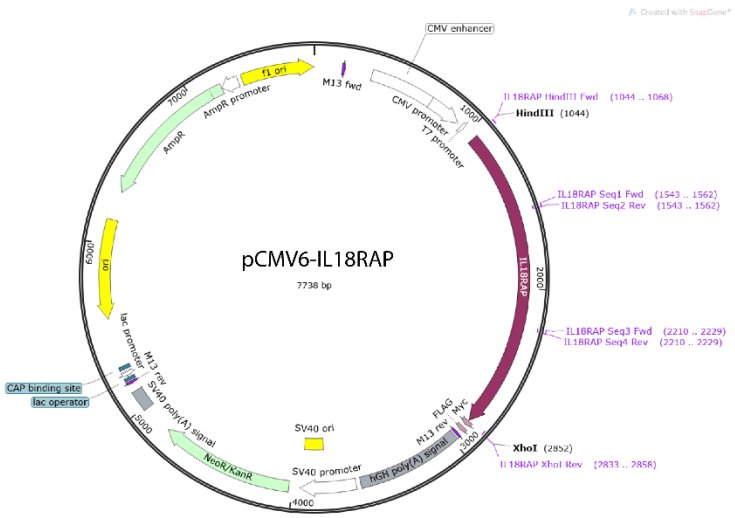

Appendix Figure 5. Constructed IL18RAP plasmid using pCMV6 mammalian expression vector

C. DH5α Competent Cell Preparation Protocol

On day 1, glycerol stock of DH5α Competent Cell was streaked onto an LB Agar plate (without antibiotic) and the plate was incubated in a 37ºC incubator overnight. On day 2, a single colony was selected from the DH5α Competent cell-streaked agar plate and the colony was transferred into 10 mL LB broth medium in a 50 mL canonical centrifuge tube. The starter culture was incubated in the shaker incubator at 200 rpm for 8 hours at 37°C. Next, 4 mL of starter culture was transferred into a 500 mL Erlenmeyer flask containing 100 mL LB broth medium and incubated at 200 rpm overnight at 20 °C. On day 3, the optical density (OD_{600}) of competent cell culture was measured using an optical densitometer. When optical density reached 0.55, 100 mL culture was divided into two 50 mL conical centrifuge tube as 50 mL/tubes and centrifuged at 2500 g for 10 minutes at +4°C. After that, supernatants were discarded and bacteria pellets were resuspended in 8 mL ice-cold ITB buffer. They were centrifuged at 2500 g for 10 minutes at +4°C and supernatants were discarded again.

Next, bacteria pellets were resuspended in 2 mL ice-cold ITB buffer and two tubes were united. After that, 300 μL DMSO was added and they were incubated for 10 minutes on ice. Next, bacteria stock was aliquoted into 1.5 mL centrifuge tubes and snapped froze by liquid nitrogen. Aliquoted competent bacteria stocks were stored at -80°C until further use.

D. Cloning of pCMV6-IL18RAP plasmid

The human canonical *IL18RAP* cDNA (ENST00000687160.1, NM_001393487.1) open reading frame (ORF) was obtained from THP-1 cell line. From THP-1 cDNA, *IL18RAP* cDNA fragment was obtained using forward primer IL18RAP HindIII Fwd including a HindIII restriction site, together with the reverse primer IL18RAP XhoI Rev including a XhoI restriction site. PCR reactions, restriction digestion, ligation, transformation, screening of single colonies for the presence of plasmid with insert by colony PCR and isolation of generated plasmid was performed as indicated in the Methods part.

E. Copyright permission

SPRINGER NATURE LICENSE
TERMS AND CONDITIONS

Jun 30, 2023

This Agreement between Zeynep Güneş Tepe Demir ("You") and Springer Nature ("Springer Nature") consists of your license details and the terms and conditions provided by Springer Nature and Copyright Clearance Center.

License Number	5578960668812
License date	Jun 30, 2023
Licensed Content Publisher	Springer Nature
Licensed Content Publication	Journal of Clinical Immunology
Licensed Content Title	Inherited IRAK-4 Deficiency in Acute Human Herpesvirus-6 Encephalitis
Licensed Content Author	Zeynep Güneş Tepe et al
Licensed Content Date	Oct 7, 2022
Type of Use	Thesis/Dissertation
Requestor type	academic/university or research institute
Format	print and electronic
Portion	full article/chapter
Will you be translating?	no

Circulation/distribution	50000 or greater
Author of this Springer Nature content	yes
Title	CHARACTERIZATION OF INHERITED IRAK-4 DEFICIENCY IN A PATIENT WITH ACUTE HHV-6 ENCEPHALITIS
Institution name	Bilkent University
Expected presentation date	Jul 2023
Requestor Location	Zeynep Güneş Tepe Demir Bilkent Universitesi, Merkez Kampüs SB Binası Moleküler Bioyoloji ve Genetik Laboratuvarları, Kat 2 Çankaya Ankara, 06800 Turkey Attn: Zeynep Güneş Tepe Demir
Total	0.00 USD

Terms and Conditions

Springer Nature Customer Service Centre GmbH Terms and Conditions

The following terms and conditions ("Terms and Conditions") together with the terms specified in your [RightsLink] constitute the License ("License") between you as Licensee and Springer Nature Customer Service Centre GmbH as Licensor. By clicking 'accept' and completing the transaction for your use of the material ("Licensed Material"), you confirm your acceptance of and obligation to be bound by these Terms and Conditions.

1. Grant and Scope of License

1. 1. The Licensor grants you a personal, non-exclusive, non-transferable, non-sublicensable, revocable, world-wide License to reproduce, distribute, communicate to the public, make available, broadcast, electronically transmit or create derivative works using the Licensed Material for the purpose(s) specified in your RightsLink Licence Details only. Licenses are granted for the specific use requested in the order and for no other use, subject to these Terms and Conditions. You acknowledge and agree that the rights granted to you under this License do not include the right to modify, edit, translate, include in collective works, or create derivative works of the Licensed Material in whole or in part unless expressly stated in your RightsLink

Licence Details. You may use the Licensed Material only as permitted under this Agreement and will not reproduce, distribute, display, perform, or otherwise use or exploit any Licensed Material in any way, in whole or in part, except as expressly permitted by this License.

1. 2. You may only use the Licensed Content in the manner and to the extent permitted by these Terms and Conditions, by your RightsLink Licence Details and by any applicable laws.

1. 3. A separate license may be required for any additional use of the Licensed Material, e.g. where a license has been purchased for print use only, separate permission must be obtained for electronic re-use. Similarly, a License is only valid in the language selected and does not apply for editions in other languages unless additional translation rights have been granted separately in the License.

1. 4. Any content within the Licensed Material that is owned by third parties is expressly excluded from the License.

1. 5. Rights for additional reuses such as custom editions, computer/mobile applications, film or TV reuses and/or any other derivative rights requests require additional permission and may be subject to an additional fee. Please apply to journalpermissions@springernature.com or bookpermissions@springernature.com for these rights.

2. Reservation of Rights

Licensor reserves all rights not expressly granted to you under this License. You acknowledge and agree that nothing in this License limits or restricts Licensor's rights in or use of the Licensed Material in any way. Neither this License, nor any act, omission, or statement by Licensor or you, conveys any ownership right to you in any Licensed Material, or to any element or portion thereof. As between Licensor and you, Licensor owns and retains all right, title, and interest in and to the Licensed Material subject to the license granted in Section 1.1. Your permission to use the Licensed Material is expressly conditioned on you not impairing Licensor's or the applicable copyright owner's rights in the Licensed Material in any way.

3. Restrictions on use

3. 1. Minor editing privileges are allowed for adaptations for stylistic purposes or formatting purposes provided such alterations do not alter the original meaning or intention of the Licensed Material and the new figure(s) are still accurate and representative of the Licensed Material. Any other changes including but not limited to, cropping, adapting, and/or omitting material that affect the meaning, intention or moral rights of the author(s) are strictly prohibited.

3. 2. You must not use any Licensed Material as part of any design or trademark.

3. 3. Licensed Material may be used in Open Access Publications (OAP), but any such reuse must include a clear acknowledgment of this permission visible at the same time as the figures/tables/illustration or abstract and which must indicate that the Licensed Material is not part of the governing OA license but has been reproduced with permission. This may be indicated according to any standard referencing system but must include at a minimum 'Book/Journal title, Author, Journal Name (if applicable),

Volume (if applicable), Publisher, Year, reproduced with permission from SNCSC'.

4. STM Permission Guidelines

4. 1. An alternative scope of license may apply to signatories of the STM Permissions Guidelines ("STM PG") as amended from time to time and made available at https://www.stm-assoc.org/intellectual-property/permissions/permissions-guidelines/.

4. 2. For content reuse requests that qualify for permission under the STM PG, and which may be updated from time to time, the STM PG supersede the terms and conditions contained in this License.

4. 3. If a License has been granted under the STM PG, but the STM PG no longer apply at the time of publication, further permission must be sought from the Rightsholder. Contact journalpermissions@springernature.com or bookpermissions@springernature.com for these rights.

5. Duration of License

5. 1. Unless otherwise indicated on your License, a License is valid from the date of purchase ("License Date") until the end of the relevant period in the below table:

Reuse in a medical communications project	Reuse up to distribution or time period indicated in License
Reuse in a dissertation/thesis	Lifetime of thesis
Reuse in a journal/magazine	Lifetime of journal/magazine
Reuse in a book/textbook	Lifetime of edition
Reuse on a website	1 year unless otherwise specified in the License
Reuse in a presentation/slide kit/poster	Lifetime of presentation/slide kit/poster. Note: publication whether electronic or in print of presentation/slide kit/poster may require further permission.
Reuse in conference proceedings	Lifetime of conference proceedings
Reuse in an annual report	Lifetime of annual report
Reuse in training/CME materials	Reuse up to distribution or time period indicated in License
Reuse in newsmedia	Lifetime of newsmedia
Reuse in coursepack/classroom materials	Reuse up to distribution and/or time period indicated in license

6. Acknowledgement

6. 1. The Licensor's permission must be acknowledged next to the Licensed Material in print. In electronic form, this acknowledgement must be visible at the same time as the figures/tables/illustrations or abstract and must be hyperlinked to the journal/book's homepage.

6. 2. Acknowledgement may be provided according to any standard referencing system and at a minimum should include "Author, Article/Book Title, Journal name/Book imprint, volume, page number, year, Springer Nature".

7. Reuse in a dissertation or thesis

7. 1. Where 'reuse in a dissertation/thesis' has been selected, the following terms apply: Print rights of the Version of Record are provided for; electronic rights for use only on institutional repository as defined by the Sherpa guideline (www.sherpa.ac.uk/romeo/) and only up to what is required by the awarding institution.

7. 2. For theses published under an ISBN or ISSN, separate permission is required. Please contact journalpermissions@springernature.com or bookpermissions@springernature.com for these rights.

7. 3. Authors must properly cite the published manuscript in their thesis according to current citation standards and include the following acknowledgement: '*Reproduced with permission from Springer Nature*'.

8. License Fee

You must pay the fee set forth in the License Agreement (the "License Fees"). All amounts payable by you under this License are exclusive of any sales, use, withholding, value added or similar taxes, government fees or levies or other assessments. Collection and/or remittance of such taxes to the relevant tax authority shall be the responsibility of the party who has the legal obligation to do so.

9. Warranty

9. 1. The Licensor warrants that it has, to the best of its knowledge, the rights to license reuse of the Licensed Material. **You are solely responsible for ensuring that the material you wish to license is original to the Licensor and does not carry the copyright of another entity or third party (as credited in the published version).** If the credit line on any part of the Licensed Material indicates that it was reprinted or adapted with permission from another source, then you should seek additional permission from that source to reuse the material.

9. 2. EXCEPT FOR THE EXPRESS WARRANTY STATED HEREIN AND TO THE EXTENT PERMITTED BY APPLICABLE LAW, LICENSOR PROVIDES THE LICENSED MATERIAL "AS IS" AND MAKES NO OTHER REPRESENTATION OR WARRANTY. LICENSOR EXPRESSLY DISCLAIMS ANY LIABILITY FOR ANY CLAIM ARISING FROM OR OUT OF THE CONTENT, INCLUDING BUT NOT LIMITED TO ANY ERRORS, INACCURACIES, OMISSIONS, OR DEFECTS CONTAINED THEREIN, AND ANY IMPLIED OR EXPRESS WARRANTY AS TO MERCHANTABILITY OR FITNESS FOR A PARTICULAR PURPOSE. IN NO EVENT SHALL LICENSOR BE LIABLE TO YOU OR ANY OTHER PARTY OR ANY OTHER PERSON OR FOR ANY SPECIAL, CONSEQUENTIAL, INCIDENTAL, INDIRECT, PUNITIVE, OR EXEMPLARY DAMAGES, HOWEVER CAUSED, ARISING OUT OF OR IN CONNECTION WITH THE DOWNLOADING, VIEWING OR USE OF THE LICENSED MATERIAL REGARDLESS OF THE FORM OF ACTION, WHETHER FOR BREACH OF CONTRACT, BREACH OF WARRANTY, TORT, NEGLIGENCE, INFRINGEMENT OR OTHERWISE (INCLUDING, WITHOUT LIMITATION,

DAMAGES BASED ON LOSS OF PROFITS, DATA, FILES, USE, BUSINESS OPPORTUNITY OR CLAIMS OF THIRD PARTIES), AND WHETHER OR NOT THE PARTY HAS BEEN ADVISED OF THE POSSIBILITY OF SUCH DAMAGES. THIS LIMITATION APPLIES NOTWITHSTANDING ANY FAILURE OF ESSENTIAL PURPOSE OF ANY LIMITED REMEDY PROVIDED HEREIN.

10. Termination and Cancellation

10. 1. The License and all rights granted hereunder will continue until the end of the applicable period shown in Clause 5.1 above. Thereafter, this license will be terminated and all rights granted hereunder will cease.

10. 2. Licensor reserves the right to terminate the License in the event that payment is not received in full or if you breach the terms of this License.

11. General

11. 1. The License and the rights and obligations of the parties hereto shall be construed, interpreted and determined in accordance with the laws of the Federal Republic of Germany without reference to the stipulations of the CISG (United Nations Convention on Contracts for the International Sale of Goods) or to Germany's choice-of-law principle.

11. 2. The parties acknowledge and agree that any controversies and disputes arising out of this License shall be decided exclusively by the courts of or having jurisdiction for Heidelberg, Germany, as far as legally permissible.

11. 3. This License is solely for Licensor's and Licensee's benefit. It is not for the benefit of any other person or entity.

Questions? For questions on Copyright Clearance Center accounts or website issues please contact springernaturesupport@copyright.com or +1-855-239-3415 (toll free in the US) or +1-978-646-2777. For questions on Springer Nature licensing please visit https://www.springernature.com/gp/partners/rights-permissions-third-party-distribution

Other Conditions:

Version 1.4 - Dec 2022

Questions? customercare@copyright.com.